PHYSICAL ENHANCEMENT OF TRANSDERMAL DRUG DELIVERY: POLYSACCHARIDE DISSOLVING MICRONEEDLES AND MICRO THERMAL SKIN ABLATION

A Thesis
Presented to
The Academic Faculty

By

Jeong Woo Lee

In Partial Fulfillment
of the Requirements for the Degree
Doctor of Philosophy in the
School of Chemical & Biomolecular Engineering

Georgia Institute of Technology
May 2009

PHYSICAL ENHANCEMENT OF TRANSDERMAL DRUG DELIVERY: POLYSACCHARIDE DISSOLVING MICRONEEDLES AND MICRO THERMAL SKIN ABLATION

Approved by:

Dr. Mark R. Prausnitz, Advisor
School of Chemical & Biomolecular Engineering
Georgia Institute of Technology

Dr. Mark G. Allen
School of Electrical & Computer Engineering
Georgia Institute of Technology

Dr. Yulin Deng
School of Chemical & Biomolecular Engineering
Georgia Institute of Technology

Dr. Lakeshia J. Taite
School of Chemical & Biomolecular Engineering
Georgia Institute of Technology

MD. Eric Felner
School of Chemical & Biomolecular Engineering
Georgia Institute of Technology

Date Approved: Mar 27, 2009

To the memory of my son, Dabok

ACKNOWLEDGEMENTS (English)

I would like to thank everyone who helped me through the course of my PhD. First of all, my advisor, Dr. Mark R. Prausnitz, has guided me with the invaluable support and knowledge and has always encouraged me to challenge what I have explored for my thesis work. I would like to thank him for allowing me to expand my knowledge and realize my thesis work as one of references. I am proud that I joined Drug Delivery Lab and studied under Dr. Mark R. Prausnitz. I would also like to thank my committee, Dr. Mark G. Allen, Dr. Yulin Deng, Dr. Lakeshia J. Taite, and Dr. Eric Felner for helpful comment and advice throughout my research.

I met many people who were valuable for my study and life at Atlanta and owed them for many things. I would like to thank lab families. I could enjoy and complete my PhD research because they were with me. Especially, I thank Ms. Donna Bondy. I cannot forget her devotion and effort trying to assist our research. I also thank Dr. Jung-Hwan Park for teaching me how to approach to a new experiment. He was a mentor I asked whenever I got struck at some points of my study. I want to say a special thanks to Dr. Seong-O Choi. He was a coworker helping me for the fabrication of microneedles and in vivo animal study and an old friend cheering me and giving me advice always when I had hard time. I also thank cell group members, Dr. Robyn Schlicher, Dr. Prerona Chakravarty, Joshua Hutcheson, and Ying Liu for helping me about cell works. I thank Dr. Yeu-Chun Kim and Dr. Young Bin Choy for helping me about my study and life. I received many valuable comments about my study and learned how to communicate with people in conflict. I also thank Dr. Vladimir Zarnitsyn and Dr. Harvinder Gill for helpful answers about my questions, Jyoti Gupta for the study of skin resealing process,

Samirkumar Patel, Samantha Andrew, James Norman, Leonard Chu, Chris Ednes, and You-Chun Kim for the discussion at the group meeting. I also thank Dr. Wijaya Martanto, Dr. Jason Jiang and Dr. Daniel Hallow, and Dr. Sean Sullivan for valuable comments and help.

I would like to thank Dr. Priya Gadiraju for working together on the skin ablation work. It was a joyful experience to work with people in other fields. I also want to say a special thanks to Dr. Yeun-Ho Joung, Dr. Jin-Woo Park, and Dr. Seungkeun Choi for helping me about the fabrication works and the affectionate advice. I also thank Dr. Ajay K. Banga at Mercer University for training me on the rat bandaging method and Dr. Laura O'Farrell and Jaehyung Park for helping me about in vivo animal study.

ACKNOWLEDGEMENTS (Korean)

이제 또 새로운 시작을 하려고 합니다. 박사과정이라는 긴 여정을 시작할때 설레던 기억이 아직 생생한데 벌써 이렇게 긴 한 걸음을 마쳤습니다. 이 지면을 빌어, 유학생활 동안 가까이서 그리고 멀리서 도와주신 분들께 감사의 인사를 전하고 싶습니다.

우선, 유학을 나오기전 2 년여 동안 한국과학기술연구원 (KIST) 에서 인연을 맺고 유학생활 계획에 대해 소중한 조언과 연구에 임하는 자세의 기틀을 마련해 주신, 존경하는 이윤우 교수님께 (현, 서울대학교 화학공학과 재직) 감사의 말씀을 드리고 싶습니다. 박사과정 동안 어려움에 부딪혀, 어디로 가야할지 무엇을 해야 할지 자문할 때마다, 이윤우 교수님께서 보여주신 학문에 대한 열정과 공학자로서의 마음가짐은 제게 늘 방향타가 되었습니다.

유학생활 동안 늘 격려해준, 오랜 친구들, 김규범, 김현욱, 그리고 93 학번 친구들 김홍찬, 강현욱에게 고마움을 전합니다. 그리고 앞서 나간 조지아 공대 화공과 선배님들 그리고 아틀란타에서 같이 유학생활을 하고 있는 화공과 후배님들에게도 고마움을 전합니다. 특히, 미국생활 길잡이 역활을 해 준 인구, 재인이, 영수 형, 성호 형, 종민이 형, 세영이 형에게 고마움을 전합니다. 무엇보다도 무사히 박사과정을 마칠 수 있도록 항상 기도해주시고 유학생활 내내 힘이 되어주신 부모님, 형/형수님, 동생 그리고 장인/장모님, 처남, 처형께 감사드립니다. 힘든 일이 있을때 가족의 힘이 어떤 것인지를 깨달았습니다. 그리고 그동안 헌신해 준 사랑스런 제 아내, 김미경에게 감사드립니다. 그리고 미처 언급하지 못한 고마운 분들에게 죄송하게 생각하며, 모두에게 감사드립니다.

TABLE OF CONTENTS

LIST OF TABLES

LIST OF FIGURES

LIST OF SYMBOLS OR ABBREVIATIONS

Symbols

P_{cr}	Critical Buckling Load
R	Radius
J	Flux
k_p	Permeability coefficient
C_v	Concentration of drug in donor solution
E	Energy
C_p	Heat capacity
ΔH_{vap}	Heat of vaporization
m	Mass

Abbreviations

CMC	Carboxymethyl Cellulose
PLA	Polylactic acid
BSA	Bovine serum albumin
hGH	Human growth hormone
SubQ	Subcutaneous
MSA	Micro skin ablation
MN	Microneedle
MW	Molecular weight
BA	Bioavailability

SUMMARY

Transdermal drug delivery system has sought various methods to administer biopharmaceuticals with the development of the technologies for the production of biopharmaceuticals. Because skin has the intrinsic function to protect the body preventing entry of the external species into the body, the controlled removal of the skin barrier without losing the protection function is the key to the transdermal administration of biopharmaceuticals through the skin.

In this thesis, two physical methods were studied to overcome the skin barrier in the controlled breakage of the skin barrier and to deliver macromolecules-based drugs through the skin; (1) polysaccharide dissolving microneedles and (2) micro thermal skin ablation.

The previous generation of microneedles has demonstrated the enhanced skin permeability to molecules that cannot penetrate stratum corneum, which is the outmost layer of the skin, by breaking it in a micron size. However, many types of microneedles have focused on the controlled breakage of stratum corneum so microneedles material was selected with the good mechanical properties and the capability of the easy processability for the mass production. These criteria for the material limited the encapsulation of biopharmaceuticals within microneedles due to the incompatible properties of them with sensitive biopharmaceuticals. Thus, polysaccharide dissolving microneedles system was designed and developed in this study to encapsulate biopharmaceuticals without losing their integrity, to break the skin barrier in a minimized size with the mechanically poor material, to release them into skin with the dissolution of microneedles, and to deliver human growth hormone into the living hairless rats.

The skin ablation methods have been evolved to administer biopharmaceuticals because it is a simple method to overcome the skin barrier and deliver drugs. Many of them have already shown the effect of the removal of stratum corneum on the skin permeability to macromolecules, but they are somewhat subjective for the practical application or less controlled for the selective removal of the skin barrier leaving the possibility of the deeper skin tissue damage. Thus, micro thermal skin ablation was designed and developed to fabricate the device generating the energy impact with the basis of arc discharge, to transfer the energy impact on the skin, to remove stratum corneum selectively with three-dimensionally controlled manner, and to deliver hydrophilic macromolecules through skin.

1. Introduction

Molecular biology and genetic engineering have been instrumental in revealing the role of genes and proteins in human disease; therefore effective delivery of these compounds into the body has become a significant requirement for health treatments [1-3] This type of healthcare has also become the challenge for the pharmaceutical industry [4-6] to lower the cost of treating human disease and improving human health. However, biomolecules-based drugs are very sensitive and the oral delivery route is believed to be an impossible pathway for these methods due to the digestive and enzymatic environment of the gastrointestinal tract and the first-pass effect at the liver [7], which rapidly degrade biomolecules. Thus, most biopharmaceuticals have been administered by a parenteral method using hypodermic needle injection through skin to avoid these problems. However, many are fearful of needles [8, 9] and treatment by injection requires a visit to the hospital or clinic for the administration. In addition, hypodermic needles should be disposed of under specific protocols because reuse can be another path for disease infection. To resolve these problems, pharmaceutical companies are currently focused on the design of biopharmaceutical delivery by non-conventional routes [10-12] such as transdermal drug delivery systems.

The role of the integumentary system which is composed of the skin layers and accessory structures is the regulation of interactions between the body and the external environment for the purpose of protecting the body and maintaining biological functions. The protective function of the integumentary system resides in the outer layer of the skin, which prevents entry of noxious chemicals and dangerous microorganism and the dehydration of the body by controlling water loss. Therefore, it is generally believed that

transdermal administration of drugs is feasible for only low molecular weight and moderately lipophilic drugs and that it is almost impossible to deliver high molecular weight and hydrophilic biomolecules drugs into the body without using hypodermic needles.

Many scientists have studied these barrier properties of the skin [13-16] and the effect of skin disruption [17-22] on the absorption of external molecules into the body. It was discovered that the most superficial layer of the skin, the stratum corneum, is the important layer for blocking entry into the body. For example, using the tape-stripping method to disrupt stratum corneum demonstrated an increased absorption of cortisone and nicotinic acid [23]. Furthermore, skin disruption with a microenhancer array boosted luciferase gene delivery [24] comparable to intramuscular or intradermal needle injection.

However, these methods are limited due to subjective procedures in application; the degree of skin disruption is highly variable and cannot be easily controlled, thus causing significant differences in drug delivery amounts and/or adverse side effects. The key variable in developing a method for breaking stratum corneum to deliver drugs is achieving controlled disruption of the skin without losing protective function and thus causing unfavorable side effects. To achieve this, stratum corneum should be removed in a minimal size possible to allow drugs to be delivered at therapeutic rates without loss of protective function. Thus, the best method for making the small holes in the skin is one of the most important criteria for the design of transdermal drug delivery system based on the breakage of stratum corneum. In this work, we studied two physical methods to enable the transdermal delivery of biopharmaceuticals by controlling the disruption of

stratum corneum in micro scale: (1) dissolving microneedles and (2) micro skin ablation created by energy impact on the skin.

Microneedles were originally designed to make small holes in the skin [25], which can be passages for the diffusion of drugs into the body. Microneedles applications [20, 26-31] have already demonstrated increased permeability of drugs after micro-scale stratum corneum breakage. We were motivated to design the fabrication of dissolving microneedles made out of material dissolvable in the skin because these microneedles dissolve in the skin and releases drugs after insertion. It is almost impossible to create biohazardous sharps after usage. Moreover, biotherapeutics can be encapsulated in the microneedles, maintaining their integrity for long periods of time due to the limited mobility of molecules, while trapped in the solid phase [32].

To develop the second approach for making a delivery route in the micro-scale, we designed a micro skin ablation method based on generation of energy impact, which uses a rapid and intense energy transfer onto the skin to remove stratum corneum. The impact of thermal energy generated by the arc discharge phenomenon will quickly remove only stratum corneum because heat energy does not deeply penetrate into the skin, thus avoiding damage to the deeper skin tissue. Therefore, stratum corneum can be selectively removed in the micro-scale by guiding the thermal impact on the skin with a masking system.

These methods, dissolving microneedles and micro skin ablation, are expected to overcome the skin barrier by breaking or removing stratum corneum in a highly controlled manner and thereby deliver various kinds of biopharmaceuticals at therapeutic rates, which have not been achieved by traditional transdermal patch applications. We

expect these two methods to be a new platform for delivery of biopharmaceuticals that may bring better quality of life to patients suffering from diseases treatable with these means, for example, daily injection with hypodermic needles or delivery with bulky electrical equipments.

2. Background

2.1 Transdermal drug delivery system

2.1.1 Drug delivery

The pathway for drugs to achieve therapeutic effects comprises distinct phases of delivery in the body. The first is administration of the drug into the body which will be absorbed into the blood stream through absorption membranes, which serve as the gate connected to the circulation system. While the drugs circulate along the blood vessels, they can either act on the areas of disease or disappear by excretion and/or by catabolic metabolism depending upon the drugs. In addition to technical challenges with the administration methods [9], the poor absorption of drug [33, 34], the possible unfavorable side effects during the circulation [35, 36], etc. make engineering a drug delivery system to obtain the optimized therapeutic effect a challenge.

Since the biomolecules-based biotherapeutics market has been expanding [2, 3, 5] with the development of genetic engineering and proteomics, a number of techniques for delivering biotherapeutics [32] have been designed and developed to improve the pathway and the efficacy of these drugs. Among these techniques, the development of a transdermal drug delivery system has been of interest as one of the alternatives to conventional injection methods because (1) skin is the most easily accessible site for drug administration, (2) transdermal patches are easy and convenient to use, and (3) they would likely have better patient compliance than hypodermic needles.

2.1.2 The barrier properties of skin

Transdermal drug delivery systems have been investigated for a long time due to the advantages described above. However, the skin is exposed to external environments and has become evolved into an efficient barrier to prevent entry of harmful chemicals and microorganisms. These barrier properties of the skin result from the histological layers: the subcutaneous tissue, the dermis layer, and the epidermis layer as shown in Figure 2.1.

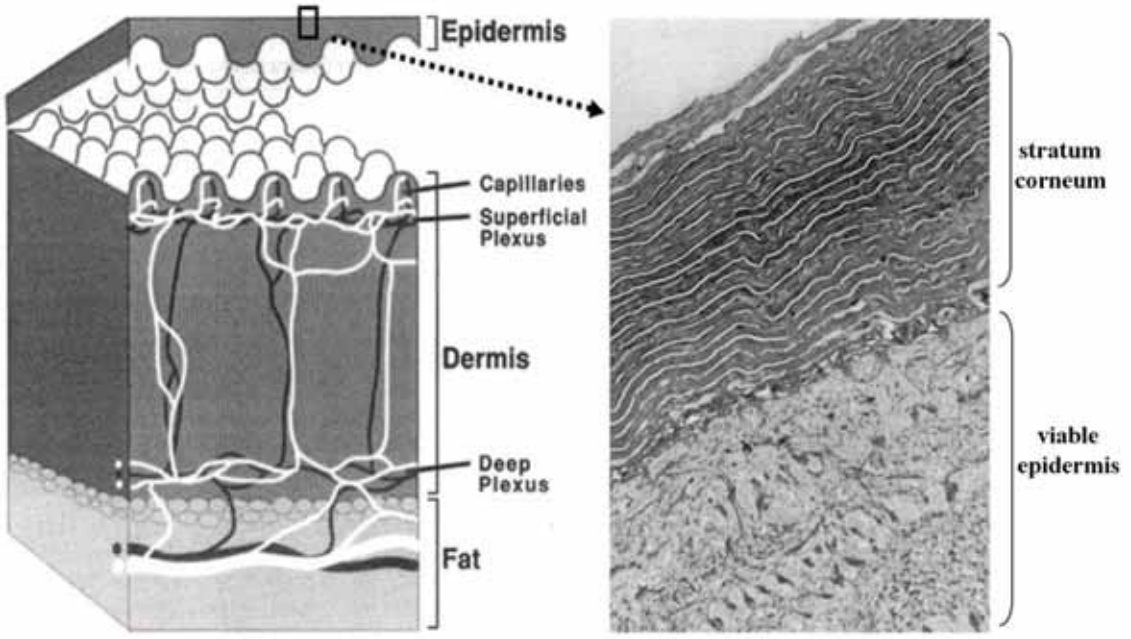

(a) (b)

Figure 2.1 Schematic illustrations of (a) skin and (b) stratum corneum and viable epidermis layer. [37, 38]

The skin consists of two main parts; the outermost layer, epidermis, and the inner connective tissue layer, dermis, as shown in Figure 2.1. The dermis layer is 3-5 mm thick and the major component of skin. It is composed of mostly collagen fibrous protein providing the mechanical properties of skin. The vascular structures, such as blood or lymphatic vessels, nerve endings, and various glands, are in this layer to perform nutrient/waste exchange, create sensation, regulate body temperature controlling, and so forth [37, 39]. From the standpoint of transdermal drug delivery, the vasculature elements in the dermis layer are the absorption sink causing the concentration gradient of drug diffusion from the exterior into skin and are the driving force for drug permeation.

The epidermis layer creates the barrier function against transdermal drug delivery. It has complex multiple layers of cells in the differentiation processes with the changes of structure and the lipid content of skin [40-42]. While cells in the lower layers of epidermis, the viable epidermis, contain typical organelles like mitochondria, the outermost epidermis layer, the stratum corneum, is a horny layer with approximately 10-15 μm thickness and composed of dead cells, which are the final product of the differentiation process. A typical horny cell has an amorphous structure, created by dead keratinized cells with approximately 30-40 μm of diameter encompassed by multiple lipid bilayers. This envelope structure, in which keratinized cell and lipids are continuously overlapped with each other, is shown in Figure 2.2. Because of this ʻbrick and mortarʻ structure of stratum corneum [41, 43], stratum corneum is the key layer of the skin barrier for regulating the flux of molecules from the inside to the outside of the body and vice versa. Due to the stratum corneum barrier, only small molecular weight and moderately lipophilic drugs are able to diffuse through the skin at a therapeutic rate [44, 45]. Consequently, various

transdermal methods [46, 47] have been designed for enhanced transdermal delivery of hydrophilic or large molecular weight drugs by modulating the barrier properties of stratum corneum [48] or disrupting it [24] or breaking it [20] or removing it [19].

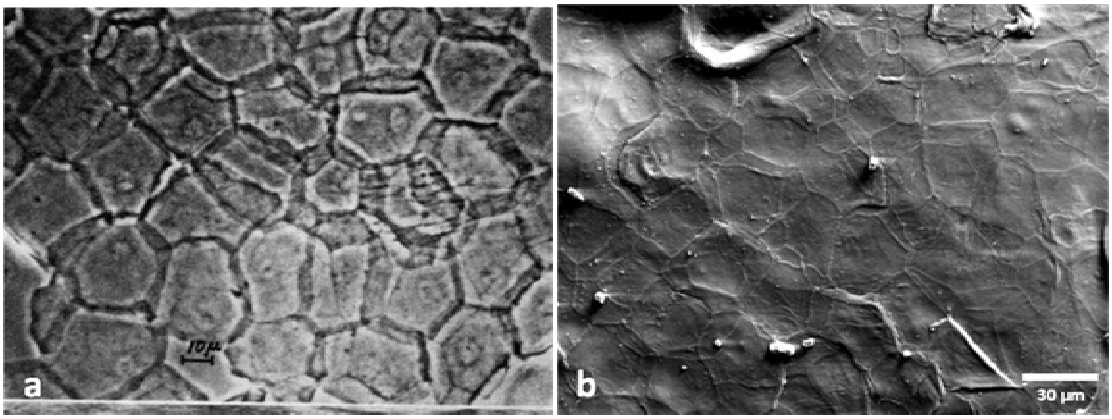

Figure 2.2 The surface of the overlapped structure of stratum corneum; Images (a) by phase contrast [49] and (b) by scanning electron microscopy.

2.2 Transdermal drug delivery system with patches

Historically, a primitive type of transdermal drug patch was used in the form of a medicated plaster in China several hundred years ago [49]. This prototype of a transdermal drug patch (Figure 2.3) simply contained herb extracts composed of small molecules such as menthol and methyl salicylate used to soothe inflammation in muscle or to help healing of bone fractures by inducing a local analgesic effect.

While the barrier properties of skin have been a subject of scientific debate since the early 1900's, it was shown that these properties reside in stratum corneum [50-52] and drugs can or cannot permeate stratum corneum depending on their water/oil partition coefficient [16, 43, 53] around 1950's. These scientific findings triggered development of transdermal drug delivery systems for systemic therapy. In early 1970's, the first transdermal drug delivery system for 3 days of systemic effect of scopolamine against motion sickness [47], Transderm-Scop® was developed by Alza and approved for the USA market in 1979. Since then, various types of transdermal drug patches have been designed for systemic effect at controlled rates, as shown in Table 2.1 [49].

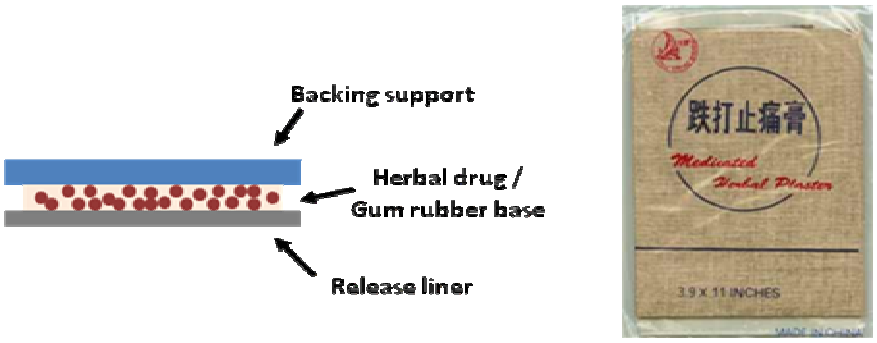

(a) (b)

Figure 2.3 Cross-sectional view (a) of the medicated plaster (b) available over the counter (OTC) currently (from www. itmonline.org/jintu).

For patch types of drug formulations, it has been suggested that transdermal administration for systemic effects might be limited to small and moderately lipophilic

drugs because patches are based on the passive diffusion of drugs from the reservoir of a patch to skin. Thus, an active transdermal drug delivery system has been sought to deliver hydrophilic or large size drugs which are biotherapeutics that cannot permeate through intact stratum corneum [54, 55]. These active delivery systems have utilized an integrity change of stratum corneum or the physical removal and breakage of stratum corneum to increase the permeability of the skin.

To create an integrity change in stratum corneum, chemical treatment of the skin surface or the use of energy application was studied such as chemical enhancement [56, 57] with various chemicals, sonophoresis [22, 58] with ultrasound, and iontophoresis [18, 59] or electroporation [60, 61] with electrical energy. For the removal or breakage of stratum corneum, minimally invasive methods were designed, such as the jet injector [62, 63], microneedle [20, 27, 28, 31], and skin ablation treatment [19, 21, 64].

Chemical enhancement for altering stratum corneum was the early approach and has been long studied [57] for almost 50 years using various chemicals such as: dimethylsulfoxide, azone, pyrrolidone, alcohol, surfactant, and terpenes. The potential mechanisms of these enhancers [39] are (1) to act on intracellular keratin and modify its conformation to cause swelling of stratum corneum, (2) to affect the desmosomes connecting corneocytes, (3) to modify lipid domains surpassing corneocytes, and (4) to alter the solvent nature of the stratum corneum. However, the use of chemical enhancers has been limited due to skin irritation and the inability to deliver large size drugs. Recently, the small peptide identified via phase display could be an enhancer as the co-administration of the short synthetic peptide and target protein drug was reported with the facilitated delivery of the protein drug [65], suggesting that the synthetic peptide creates a

transient pathway in the skin to enable transdermal delivery of macromolecular drugs for the systemic circulation.

Table 2.1 The classification of rate-controlling transdermal drug delivery systems [49].

Polymer membrane permeation-controlled system • Transderm-Scop® (Scopolamine) • Transderm-Nitro® (Nitroglycerin) • Catapres-TTS® (Clonidine) • Estraderm® (Estradiol)	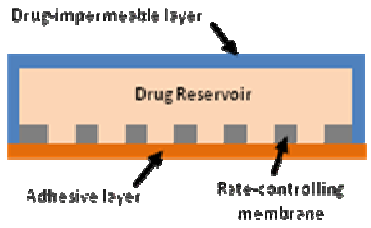
Adhesive polymer dispersion system • Deponit® (Nitroglycerin) • Frandol® (Isosorbide dinitrate) • Minitran® (Nitroglycerin) • Nitro-Dur II® (Nitroglycerin)	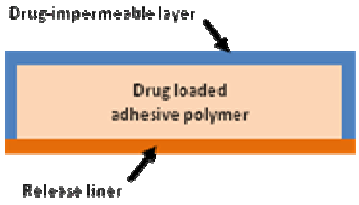
Nonadhesive polymer dispersion system • Nitro-Dur® (Nitroglycerin) • NTS® (Nitroglycerin)	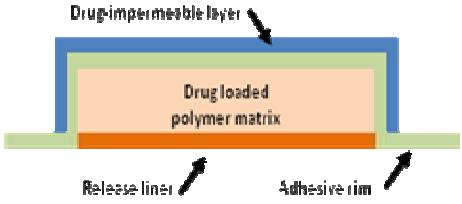
Microreservoir dissolution-controlled system • Nitrodisc® (Nitroglycerin)	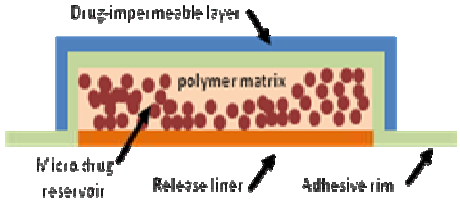

Sonophoresis uses ultrasonic energy to increase the permeation of drugs through skin. Although the mechanism of enhanced drug flux by ultrasound has not been fully elucidated yet, it has been suggested that sonophoresis has promoting effects for both hydrophilic and lipophilic drug delivery. The potential mechanisms of sonophoresis are (1) thermal effects causing the increase of molecular diffusivity or fluidity of stratum corneum lipids [66], (2) radiation pressure related to the force driving molecules through membrane [67, 68], (3) cavitational activity inducing the perturbation of stratum corneum lipids [69, 70], and (4) microstreaming by the removal of the unstirred water layer [71].

Encapsulations systems, Inc. designed an active transdermal drug delivery system using ultrasound in conjunction with an insulin patch operated by a programmable controller as shown in Figure 2.4 (a). This is designed to deliver both a basal and bolus dose of insulin to both Type-1 and Type-2 diabetics. Currently, this device is in Phase-2 clinical trials and is not yet approved for human use by the FDA. As another example, SonoPrep® marketed by Echo Therapeutics (Figure 2.4 (b)) was invented by Massachusetts Institute of Technology and was FDA-approved for increasing local dermal anesthesia effects with lidocaine. The delivery of a high molecular weight drug such as insulin or vaccine with SonoPrep® will be investigated in the future.

Iontophoresis uses an electrical gradient for the transport of charged drugs like peptides or small proteins. Drugs with either a positive or negative charge are dissolved in an electrolyte solution, then the drug is repelled from the same polarity electrode and attracted to the opposite polarity electrode, thus driving drug into the skin. Two primary mechanisms explaining iontophoresis [39, 72] are electromigration and the disruption of skin lipids by the density of current flow.

(a) (b)

Figure 2.4 (a) Transdermal delivery with a programmable ultrasound device, U-strip®. (Revised images from www.encsys.com) and (b) the SonoPrep® transdermal drug delivery device powered by ultrasound (www.medgadget.com and www.onemedplace.com)

Iontocaine® produced by IOMED, Inc. was FDA approved in May 1996 as the first drug (lidocaine) combined with device, in which drug is transferred by an iontophoresis controlling device, Numby® as shown in Figure 2.5. An integrated lidocaine device, Lidosite® (Figure 2.6 (a)) was desgined by Vyteris as the first FDA-approved pre-filled active anesthetic patch. The iontophoresis of analgesics has been studied for a long time [73, 74] and fentanyl iontophoretic transdermal system, IONSYS™ produced by Alza Corp. was FDA approved in May 2006 (Figure 2.6 (b)). This is a more effective treatment for acute pain than passive transdermal patch and provides patients with an on-demand dose

of fentanyl. The use of iontophoresis for transdermal delivery of large molecules like peptides has been reported [75-77] but they are still at the investigation level.

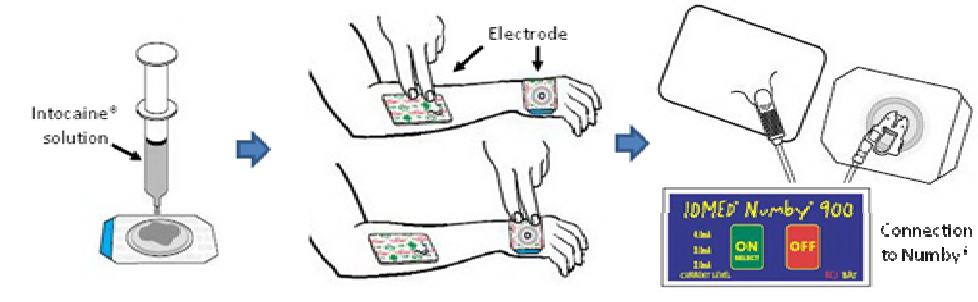

Figure 2.5 Lidocaine delivery with iontophoresis (Revised images from www.iomed.com).

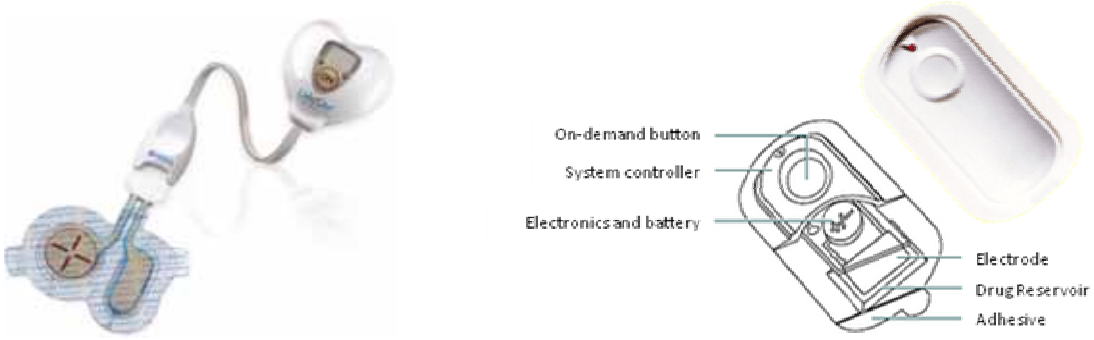

(a) (b)

Figure 2.6 (a) Lidosite®, the drug-device integrated iontophoresis system (www.vyteris.com), and (b) iontophoretic fentanyl delivery, IONSYS™ (www.pallimed.org).

Electroporation applies a relatively higher voltage (~100 V) pulse to skin than iontophoresis does, but the electric field lasts for a shorter time, usually, 10 μs –10 ms. The increased flux of hydrophilic drugs by electroporation is believed to occur by the creation of aqueous pathways within stratum corneum [60, 78, 79] or thermal effects of locally heated stratum corneum [80, 81]. However, the efficiency of electroporation in a single bilayer such as cell membranes or microbial membranes is higher than with stratum corneum, which containes multiple lipid bilayers in human skin. Thus, most electroporation devices are based on invasive needles inserted into dermis or epidermis for administration of large-size molecule therapeutics, allowing the intracellular delivery to cells in the skin.

2.3 Transdermal drug delivery by the breakage of stratum corneum

Microneedles were conceptualized in the early 1970's [25] as a simple idea to enhance the skin permeability of hydrophilic and large size molecules therapeutics by breaking the skin barrier layer physically. Since the first generation of microneedles was fabricated out of silicon [20] using micro-electro mechanical systems (MEMS) in 1998 as shown in Figure 2.8, various types of microneedles have been designed and evolved with improved features; such as solid metal microneedles [27], hollow metal microneedles [31], hollow glass microneedles [82], solid biodegradable polymer [28], and so forth. These microneedles enabled various types of transdermal drug delivery [26]. Transdermal drug delivery with microneedles has been extensively investigated with various drugs [83, 84], most of which have hydrophilic properties that are not applicable to passive diffusion-based transdermal patch systems.

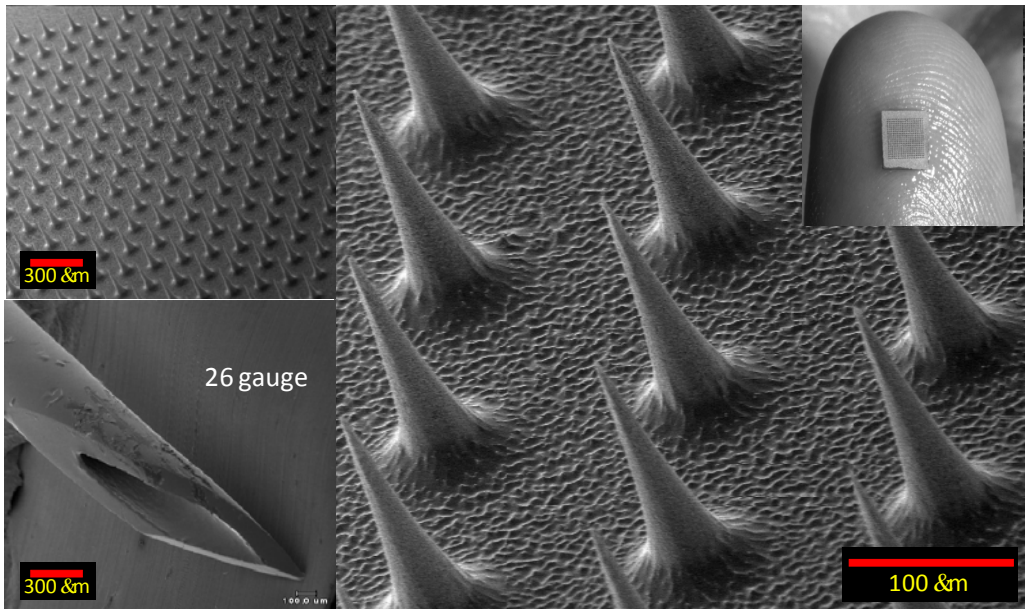

Figure 2.7 Silicon microneedles fabricated using etching techniques [20]

Alza Corp. designed the drug coated microprojection array system, Macroflux® as shown in Figure 2.8. They fabricated a titanium microprojection array which is inserted with coated drug into skin. Zosano Pharma™, Inc. developed a parathyroid hormone (PTH) transdermal delivery system with Macroflux® technology for osteoporosis and Phase II clinical trials have been complted.

For hollow microneedle applications, Nanopass Technologies LTD developed MicronJet, an intradermal system for proteins and vaccines requiring minimal expertise for administration. As shown in Figure 2.9, the device consists of MicroPyramids made of pure silicon crystals which are mounted on a standard syringe for the replacement of a

conventional hypodermic needle. Currently, two pilot clinical studies have been completed to assess the safety and efficacy of MicronJet.

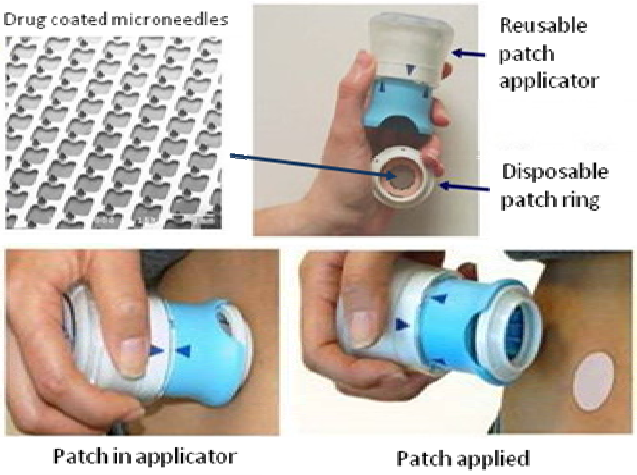

Figure 2.8 Transdermal drug delivery with Macroflux® technology using drug coated microneedles (Revised images from www.zosanopharma.com).

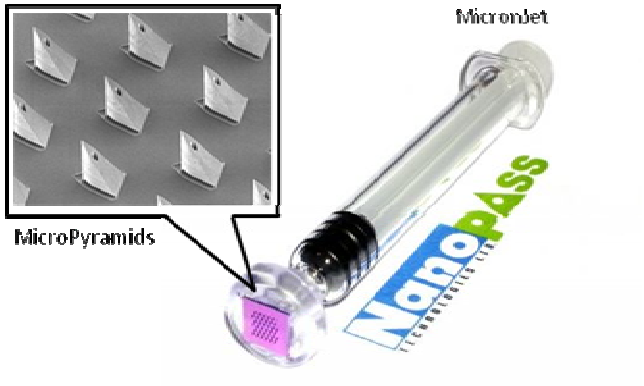

Figure 2.9 MicronJet intradermal self-administration system (Revised images from www.nanopass.com).

Recently, 3M has developed two types of microstructured transdermal systems (MTS): solid microneedles for drug coating (sMTS) and hollow microneedles for liquid drug formulation (hMTS) as shown in Figure 2.10. They performed pre-clinical study [85] of human growth hormone and Naloxone for macromolecules and small hydrophilic drugs, respectively, using a hollow type of microstructured transdermal system in a pig animal model.

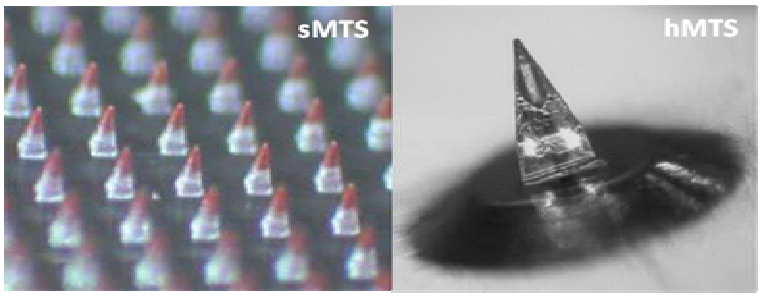

Figure 2.10 Microstructured transdermal system: solid type (left) and hollow type (right) (Revised images from www.3m.com).

Hypodermic jet injection was patented in the 1950's [86] and has been developed to accelerate drug penetration of skin as shown in Figure 2.11. The early generation of jet injection focused only on delivery of drugs into skin such as mass vaccination in the military and it caused problems like bruising or bleeding [87]. Due to low patient compliance with the painful administration of this technique, jet injection system needs to be engineered in such a manner to ensure that it is more patient-friendly and convenient to use. Currently, many companies are developing this type of system for insulin, growth

hormone, vaccine, and so forth [87]. Anesiva designed Zingo™ to deliver lidocaine as a topical anesthetic and it was FDA approved in 2007. Antares Pharma has developed a transdermal delivery platform for insulin called Medi-Jector VISION®.

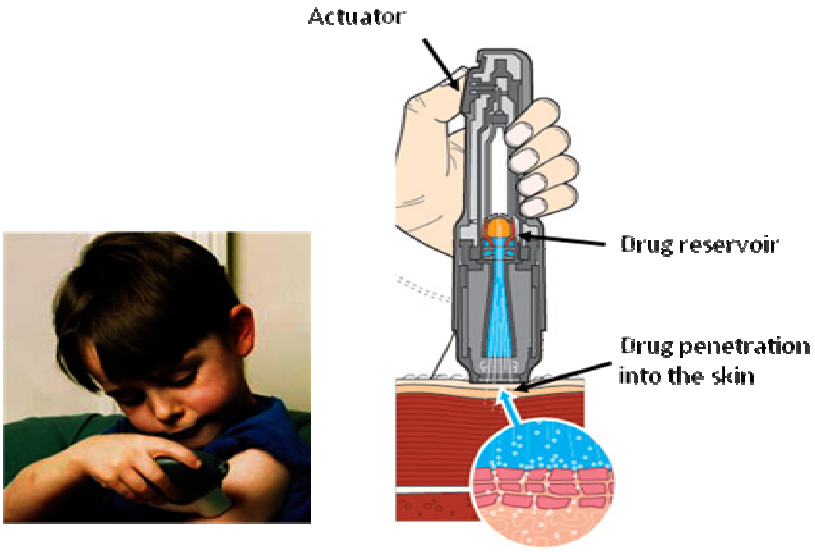

Figure 2.11 Jet injection device (Revised images from www.popsci.com and PowderJect technology).

2.4 Transdermal drug delivery by removal of stratum corneum

While microneedles are used to break stratum corneum, another approach for overcoming the barrier properties of skin is to remove stratum corneum in a controlled manner. The enhanced flux and therapeutic effects of hydrophilic or large size drugs after

removal of stratum corneum have been demonstrated by various methods using mechanical disruption like tape-stripping [88, 89] or the microenhancer array (MEA, BD technology) and the more controlled methods [24] using additional energy, such as laser assisted drug delivery by Norwood Abbey [90], thermal ablation by Altea Therapeutics [91], and radio-frequency ablation by TransPharma Medical [92, 93].

The tape-stripping method is a simple way to remove stratum corneum, but is a subjective method meaning that the stratum corneum ablation cannot be controlled consistently and thus, its effect on the skin permeability of a drug will have significant variability. To achieve more controlled skin ablation, BD Technology designed a microenhancer array (MEA) system (Figure 2.12), the shape of which is similar to the structure of microneedles. The compnay has demonstrated the effect of the MEA system on transdermal vaccine delivery [24]; however, the technology using the MEA system is not under active study at this time.

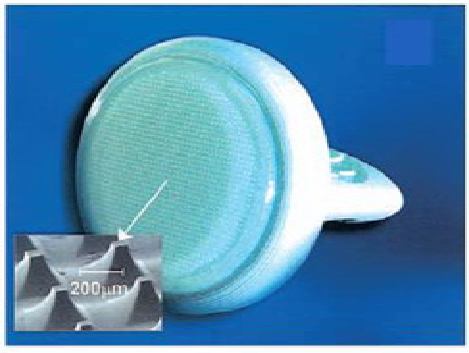

Figure 2.12 Microenhancer array (MEA) fabricated by BD technology for the skin abrasion (Revised image from www.bd.com). The inset is a SEM image of MEA.

Skin ablation technology requires highly controlled depth of ablation to prevent damage of deeper skin tissue. To achieve this, most energy applications for ablation should be applied onto the skin for short periods of time; therefore skin ablation using laser technologies [19, 64] has been investigated due to the property of laser energy enabling rapid energy transfer to skin. Norwood Abbey developed a portable skin ablation device with 3.6 V DC rechargeable batteries, Epiture Easytouch™, to create laser light for transdermal drug delivery as shown in Figure 2.13. The laser for this device is Er:YAG (2940 nm) and performs with single laser pulse, which transfers 1 J ±20% of energy to skin within 600 μs ±20%. Norwood Abbey is currently performing clinical studies with lidocaine for local anesthesia [90].

Figure 2.13 (a) Epiture Easytouch™, laser assisted drug delivery (LAD) system developed by Norwood Abbey and (b) the demonstration of LAD on hands (Revised images from www.epitureeasytouch.com)

Similar to this approach using laser energy, TransPharma Medical designed the portable skin ablation device, ViaDerm patch system (Figure 2.14), operated by radio-frequency (100-500 kHz), which generates electrical energy that passes through cells in the upper skin layers via an array of electrodes, which then induces ionic vibrations in the skin cells resulting in local heating, liquid evaporation, and the creation of microchannels [21, 92, 93] to the inner skin within around 100 ms of the total operation time. TransPharma Medical is studying transdermal delivery of various molecules such as Granisetron HCl, PTH hormone, insulin, and DNA.

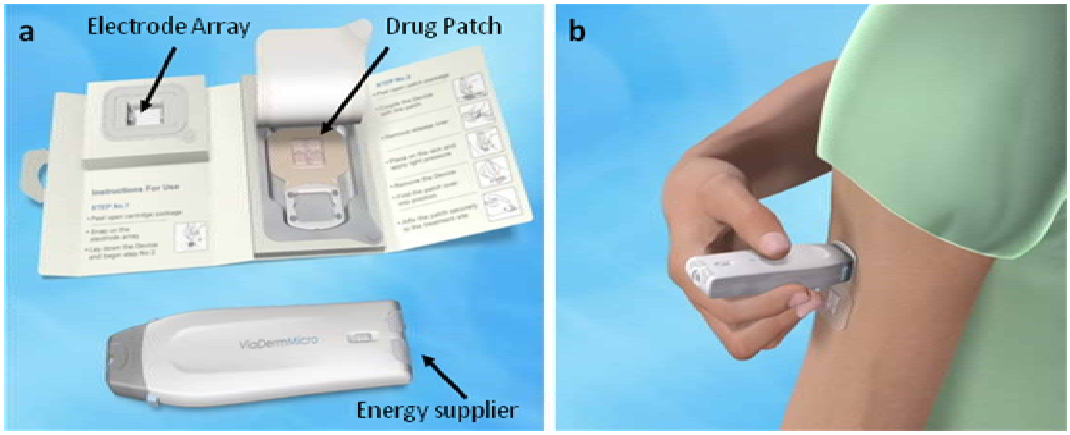

Figure 2.14 Radio-frequency assisted transdermal drug delivery system. (a) ViaDerm patch and (b) the demonstration of ViaDerm on skin (Revised images from www.transpharma-medical.com)

As another approach based on electrical energy, Altea Therapeutics developed the PassPort® patch system, in which an electric device (Figure 2.15 (b)) supplies electrical energy to a micron size heating element (Figure 2.15 (a)). The heating element then generates thermal ablation energy to make micro size pores [91] in the skin on the basis of ohmic heating of electrically conductive material. The skin ablation depth by PassPort® will be determined by the duration of current flow through the heating elements and the electrical properties of material used for heating elements. Altea Therapeutics began Phase I clinical study of insulin and hydromorphone patch in 2003 and completed Phase II clinical studies with hydromorphone in 2005.

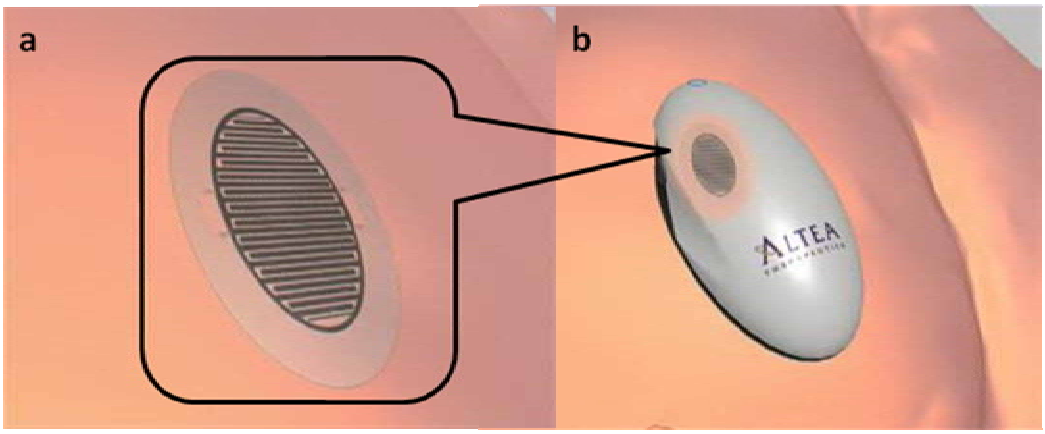

Figure 2.15 Passport® patch designed by Altea Theapeutics. (a) Ohmic heating element to remove stratum corneum and (b) skin ablation using an electrical energy supplying device.

2.5 Summary of transdermal delivery technologies

The transdermal administration of small size drugs has been used in conjunction with the diffusion mechanism of skin for many years and stratum corneum has been known as the main barrier of skin for the delivery of the large molecules, including biopharmaceuticals. These barrier properties have been of interest in developing technologies for the enhanced transdermal drug delivery using mechanisms such as disruption of stratum corneum integrity, breakage of stratum corneum, and removal of stratum corneum.

Methods that disrupt stratum corneum integrity like chemical enhancers, sonophoresis, and iontophoresis, make a pathway for drug diffusion through stratum corneum after its barrier properties are changed. However, stratum corneum is still present in these methods, so delivery of large molecules remains a challenge even though they are successful for fast delivery of small molecules and local treatments. Methods that break or remove stratum corneum, such as microneedles, jet injection, mechanical microenhancer, and laser/RF/heat ablation, overcome the skin barrier simply by the physical breakage of stratum corneum, allowing delivery of large molecules with these techniques. Therefore, various biopharmaceuticals are in the clinical trials currently using these types of methods for enhanced transdermal delivery.

However, these methods for the breakage or removal of stratum corneum have focused mainly on the stratum corneum alterations, thus the efficient delivery of biopharmaceuticals is still in the development stage. Since most biopharmaceuticals are sensitive molecules, they can lose integrity during the process of combining them with these delivery technologies. For example, microneedles have successfully shown the

controlled breakage of stratum corneum, but the amount of dose available, due to the small size of the system and the stability of biomolecules may create problems in the future. In the case of ablation of the skin with external energy to remove stratum corneum, the highly controlled removal of the skin barrier would be necessary to prevent deeper skin tissue damage.

3. Methods

3.1 Dissolving microneedles

3.1.1 Fabrication of microneedles

3.1.1.1 Molding

Micromolds were fabricated using photolithography and molding processes described in the previous study [94]. A female microneedle master-mold was structured in SU-8 photoresist (SU-8 2025, Microchem, Newton, MA) by UV exposure to create conical (circular cross section) or pyramidal (square cross section) microneedles tapering from a base measuring 300 μm in width to a tip measuring 25 μm in diameter over a microneedle length of 600-800 μm. A male microneedle master-structure made of polydimethylsiloxane (PDMS, Sylgard 184, Dow Corning, Midland, MI) was created using this mold. The male PDMS master-structure was sputter-coated (601 Sputtering System, CVC Products, Rochester, NY) with 100 nm of gold to prevent adhesion with a second PDMS layer cured onto the male master-structure to create a female PDMS replicate-mold. To modify the master-structure, a replicate of master-structure was made out of PLA polymer with the melting technique [28], and then the PLA replicate was electroplated with nickel after coating with gold. This thickened structure was replicated with PLA again after PDMS molding and the tip of PLA replicates of thickened microneedle structure was sharpened with reactive ion etching techniques [28].

With the male master-structure made of PDMS or PLA, a female PDMS mold was fabricated. Excess PDMS on the female replicate-mold was trimmed so that the mold fit within the 27-mm inner diameter of a 50 ml conical tube (Corning Inc., Corning, NY) or

the bottom area of the rectangular swing bucket (FL400, Eppendorf, Westbury, NY). The metal-coated male master-structure was repeatedly used to make replicate-molds that were repeatedly used to make microneedle devices.

3.1.1.2 Preparation of microneedle matrix

To serve as microneedle matrix materials, ultra-low viscosity carboxymethylcellulose (CMC, Cat No. 360384, Aldrich, Milwaukee, WI), amylopectin (Cat No. 10120, Fluka, Steinheim, Germany) and bovine serum albumin (BSA, Sigma, St. Louis, MO) were dissolved in deionized water. For the mixture matrix of microneedles, trehalose (Cat No. T9531, Sigma, St. Louis, MO) was dissolved with CMC together in deionized water.

Water was then evaporated off until the concentration of solute (e.g., CMC) was approximately 27 wt%, which resulted in a viscous hydrogel. CMC was concentrated by heating at 60-70^{o}C at ambient pressure or vacuuming at -50 kPa at room temperature. Amylopectin and BSA were concentrated only by the heating method at 60-70^{o}C or 37^{o}C, respectively. Solute concentration was determined by measuring solution mass before and after evaporation. Viscosity of concentrated hydrogels was measured using a Couette viscometer (Physica MCR300, Anton Paar Physica, Ostfildem, Germany).

In some cases, a model drug was added by hand mixing to solubilize or suspend the compound in the concentrated hydrogel. Three model drugs were added at final concentrations of 0.15-30 wt% sulforhodamine B (Molecular Probes, Eugene, OR), 20 wt% BSA (Sigma), or 5 wt% lysozyme (Sigma). The term “model drug” is used to indicate that these compounds have physicochemical and transport properties

representative of certain classes of drugs, but not to suggest that these compounds have pharmacological activity representative of drugs. For human growth hormone delivery, recombinant human growth hormone, hGH (Genotropin®, Pfizer, Groton, CT) was provided from Division of Pediatric Endocrinology in Emory University School of Medicine. Human growth hormone was added to the concentrated hydrogel of CMC or mixture of CMC and trehalose (50:50) at final concentrations of 2-10 wt%.

3.1.1.3 Casting

To mold microneedles from concentrated hydrogels, 100-300 mg of hydrogel was placed on a female PDMS mold in a conical centrifuge tube (Corning) and centrifuged in a 45^{o} angled rotor (GS-15R, Beckman, Fullerton, CA) or on the bottom of swing bucket (Eppendorf) and centrifuged in a swing-bucket rotor (A-4-38, Eppendorf, Westbury, NY) at 3000×g and 25-37^{o}C for up to 2 h to fill the microneedle mold cavities and dry the hydrogel.

To prepare microneedles with model drug encapsulated only within the microneedles and not in the backing layer, 8-10 mg of hydrogel mixed with model drug was filled just into the microneedle cavities in the mold and then dried under centrifugation for up to 30 min. Residual hydrogel on the surface of the mold was removed with dry tissue paper (Kimwipes, Kimberly-Clark, Roswell, GA) and 100-200 mg pure hydrogel without drug was then applied and dried onto the mold to form the backing layer. To prepare microneedles with model drug encapsulated only in the backing layer and not within the microneedles, the same two-step process was followed, except pure hydrogel was filled into the microneedle mold cavities and a hydrogel mixed

with model drug was used to form the backing layer. The fabrication process from the preparation of microneedle matrix to the casting is summarized in Figure 3.1.

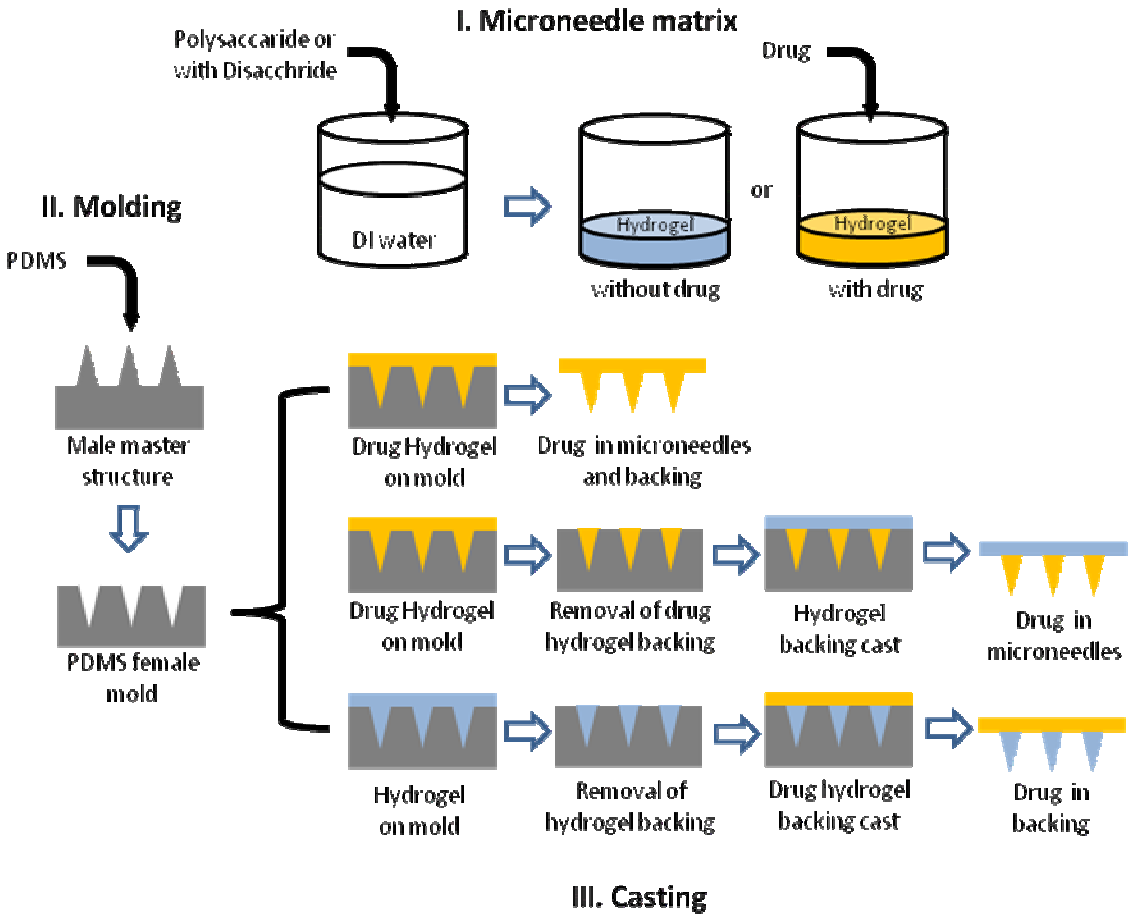

Figure 3.1 The fabrication processes of dissolving microneedles (I: Preparation of microneedle matrix, II: molding fabrication, and III: microneedle casting).

3.1.2 Microneedle mechanics

3.1.2.1 Microneedle failure

Mechanical failure tests were performed with a displacement-force test station (Model 921A, Tricor Systems Inc., Elgin, IL, USA), as described in previous study [95]. A 3×3 array containing 9 microneedles was attached to the mount of a moving sensor and an axial force was applied to move the mount at a speed of 1.1 mm/s. The mount pressed the microneedles against a flat, rigid surface of stainless steel oriented perpendicularly to the axis of mount movement. The test station recorded the force required to move the mount as a function of distance as shown in Figure 3.2.

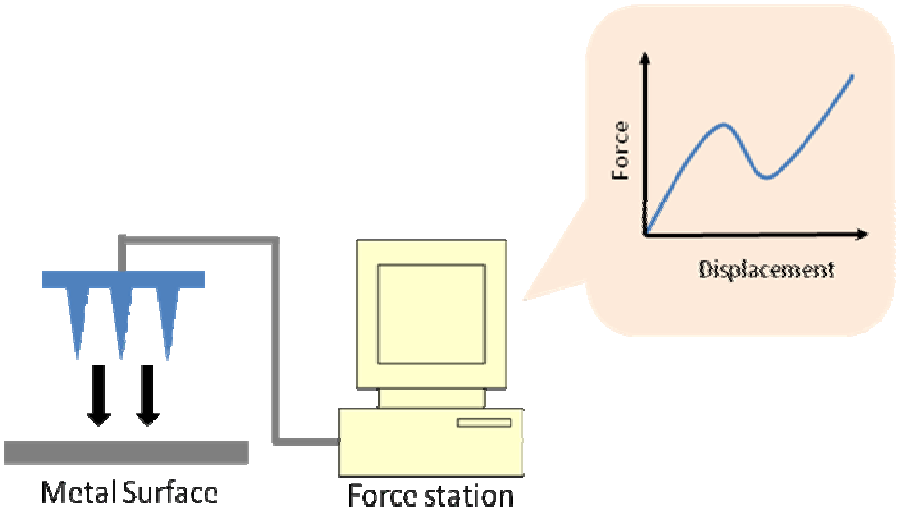

Figure 3.2 Schematic of microneedle failure measurement.

3.1.2.2 Microneedle skin insertion

To determine if microneedles insert into skin, CMC pyramidal microneedles (600 μm height, 300 μm base width, and 600 μm center-to-center spacing) in a 10×10 array were inserted with IACUC approval into full-thickness cadaver pig skin without subcutaneous fat that was shaved (series 8900, WHAL, Sterling, IL) and affixed under mild tension to a wooden plate using 1 cm long screws. Microneedles were inserted by pressing against the microneedle backing layer with a thumb using a force of approximately 1.5 N and then removed immediately after the insertion. The site of microneedle insertion on the skin surface was exposed for 10 min to a red tissue-marking dye (Shandon, Pittsburgh, PA, USA) that selectively stains sites of stratum corneum perforation. After wiping residual dye from the skin surface with dry tissue paper, skin was viewed by brightfield microscopy (SZX12, Olympus).

Skin samples were prepared for histology by freezing in histology mounting compound (Tissue-Tek, Sakura Finetek, Torrance, CA) and slicing into 20-μm thick sections (Cryo-star HM 560MV, Microm, Waldorf, Germany) and then viewed by brightfield microscopy (E600, Nikon, Tokyo, Japan).

3.1.2.3 Simulation of microneedle critical buckling load

Critical buckling load, P_{cr}, of microneedles was simulated during axial loading using analytical methods of Smith (ref). For the fixed-free case, where the microneedle base was fixed in position and the microneedle tip could move freely, the square-based

pyramidal and circle-based conical geometries were modeled using the equations for P_{cr5} of case 3 and P_{cr7} of case 5 in Appendix A of Smith [96], respectively:

$$P_{cr5} = E\ (120(H_2(H_2^2(H_2-2H_1)+2H_1^3)-H_1^4) + \pi^2(20(H_2(H_2^2(-H_2+H_1)-H_1^3)+H_1^4) + \pi^2(H_2(H_2(H_2(H_2+H_1)+H_1^2)+H_1^3)+H_1^4)))/(240\pi^2L^2) \quad \text{(pyramidal geometry)} \quad (1)$$

$$P_{cr7} = E\ (120(R_2(R_2^2(R_2-2R_1)+2R_1^3)-R_1^4) + \pi^2(20(R_2(R_2^2(-R_2+R_1)-R_1^3)+R_1^4) + \pi^2(R_2(R_2(R_2(R_2+R_1)+R_1^2)+R_1^3)+R_1^4)))/(80\pi L^2) \quad \text{(conical geometry)} \quad (2)$$

Here, E is Young's modulus; L is microneedle length; $H_1$and H_2 are microneedle widths at the base and tip of pyramidal microneedles, respectively; and R_1 and R_2 are radii at the base and tip of conical microneedles, respectively. Young's modulus of CMC microneedles was determined to be 1 GPa by direct measurement (MicroTester, Instron 5548, Norwood, MA) using bulk CMC prepared using the same casting process used to make microneedles. Young's modulus of PLA microneedles was previously determined to be 5 GPa [28]. Tip width and diameter of pyramidal and conical microneedles, respectively, were estimated both to be 25 μm based on microscopic examination.

3.1.3 Drug release from microneedles

3.1.3.1 Imaging bolus release from dissolving microneedles

CMC pyramidal microneedles (600 μm height, 300 μm base width, and 600 μm center-to-center spacing) in a 6×6 array were inserted by hand into pig cadaver skin. Just

the microneedles, and not the backing layer, contained sulforhodamine B at 0.15 wt% on a dry basis, such that each microneedle contained 0.04 μg of sulforhodamine and the 36-needle array contained 1.44 μg of sulforhodamine. After 5 min, the microneedles were removed from skin and the skin sample was examined histologically. In a separate set of experiments, the shape of microneedles was also observed after 10 s, 1 min, 15 min, and 60 min insertion into the skin by light microscopy (SZX12, Olympus).

3.1.3.2 Imaging and quantification of sustained release from microneedle patches

To image long-term release from dissolving microneedles into skin, sulforhodamine B was encapsulated within the needles and the backing layer at 0.15 wt% in a 6×6 array of CMC pyramidal microneedles (600 μm height, 300 μm base width, and 600 μm center-to-center spacing). The microneedle device contained 15 μg of sulforhodamine. The microneedles were inserted into pig cadaver skin by hand, covered with dermal tape (Blenderm, 3M Health Care, St. Paul, MN), and kept at room temperature for up to 12 h. Next, the microneedle device was removed and skin was examined histologically.

To quantify sulforhodamine release, a 7×7 array of CMC or amylopectin pyramidal microneedles (600 μm height, 300 μm base width, and 600 μm center-to-center spacing) was prepared with a backing layer of approximately 300 μm thickness. Sulforhodamine B was encapsulated within the needles and the backing layer at 10 wt%, which corresponded to 1 mg of sulforhodamine in the microneedle device weighing 10 mg. Alternatively, sulforhodamine was encapsulated only within the backing layer at 10 wt% and 30 wt%, which corresponded to almost 1 mg and 3 mg of model drug per device,

respectively. Microneedles were inserted by hand into heat-stripped human cadaver epidermis [97] (Emory University Body Donor Program, Atlanta, GA) with IRB approval. Microneedles were secured to skin with dermal tape and the microneedle-skin assembly was placed in a Franz diffusion chamber (Permegear, Hellertown, PA) at 32^{o}C. Phosphate-buffered saline (PBS) in the receptor compartment of the Franz chamber contained 0.01 M sodium azide as an anti-bacterial agent and was sampled periodically for up to 7 days to determine sulforhodamine flux by spectrofluorimetry (QM-1, Photon Technology International, South Brunswick, NJ).

3.1.4 Protein stability and activity

3.1.4.1 Circular dichroism

The secondary structure of lysozyme was examined by spectropolarimetry (JASCO, J-810, Tokyo, Japan) after encapsulation and release from dissolving microneedles. CMC pyramidal microneedle devices weighing 5 mg that encapsulated lysozyme at a mass fraction of 5 wt% were completely dissolved in 50 ml PBS at room temperature for 10 min and filtered by centrifugal filtration (Centricon YM-50, Millipore, Bedford, MA, USA) at 1000×g and room temperature for 10 min to isolate lysozyme (14.3 kDa) from the dissolved CMC matrix material (90 kDa average molecular mass). After determining lysozyme concentration by Lowry protein assay [98], PBS was added to dilute to lysozyme to 20 μg/ml. CD spectra were taken for (1) untreated lysozyme, (2) lysozyme encapsulated in microneedles that were dissolved 1 h after fabrication, (3) lysozyme encapsulated in microneedles that were dissolved after 60 days of storage at ambient

conditions (23±2^{o}C and 38±5% relative humidity), and (4) lysozyme thermally treated at 80^{o}C for 30 min to cause irreversible denaturation [99].

3.1.4.2 Lysozyme activity

Enzymatic activity of lysozyme encapsulated within CMC microneedle devices was tested with EnzCheck lysozyme assay kit (Molecular Probes). Microneedle devices weighing 5 mg that contained lysozyme encapsulated at a concentration of 5 wt% were completely dissolved in PBS at room temperature for 10 min. PBS was added to dilute each sample to 0.05 μg/ml lysozyme and 0.95 μg/ml CMC. Lysozyme activity was assayed using 1 ml solution samples for: (1) untreated lysozyme, (2) untreated lysozyme (0.05 μg) and CMC hydrogel (0.95 μg) mixed, and dissolved together, (3) lysozyme encapsulated in microneedles that were dissolved 1 h after fabrication, and (4) lysozyme encapsulated in microneedles that were dissolved after 60 days of storage at ambient conditions.

3.2 Human growth hormone delivery

3.2.1 Animal model

For in vivo delivery of human growth hormone, wild-type male hairless rat (CD® Hairless Rat, Charles River) was selected as an animal model and this study was approved by the Institutional Animal Care and Use Committee of Georgia Tech. All rats at 10-11 weeks after the birth were purchased from Charles River and weighed at 280-340 g and they were kept freely with water and food for at least 48 hours after they were

transferred from Charles River to Georgia Tech facility. They were anesthetized with isoflurane, ISOTHESIA™ (Butler Animal Health Supply, Dublin, OH) for the insertion of microneedles or the skin bandaging and anesthesia was maintained during the measurement of skin impedance for the skin resealing study and the blood draw for the pharmacokinetics study. After the measurement of skin impedance and the blood draw, they were euthanized with carbon dioxide gas. For the study of skin reaction after the insertion of microneedles, the skin inserted with microneedles was cut off, fixed by using formalin, embedded with paraffin, and sectioned for histology to investigate the skin reaction. See the section 3.2.5 for the detail.

3.2.2 Skin Resealing

3.2.2.1 Skin Bandaging

The animal skin was covered with the bandaging, which is necessary to secure the microneedles system on the animal skin to maintain the occlusion state as well as to prevent the reach of animal's limbs and any artifact. In some cases, a rodent e-collar (404 ¼VS, Webster Veterinary, Sterling, MA) was placed around the animal neck for maximally 24 hours. Microneedles were inserted into the skin on the torso of the animal with the same method used in described in the section 3.1.2.2 and they were covered with a dressing, Tegaderm™ (3M Health Care, St. Paul, MN), and then the torso of the animal was bandaged with self-adherent wrap, Coban™ (3M Health Care, St. Paul, MN) and fixed with porous adhesive tape, Zonas (Johnson and Johnson, Skillman, NJ) as shown

Figure 3.3. This was performed with the training from Prof. Ajay K. Banga at Mercer University in Atlanta, GA.

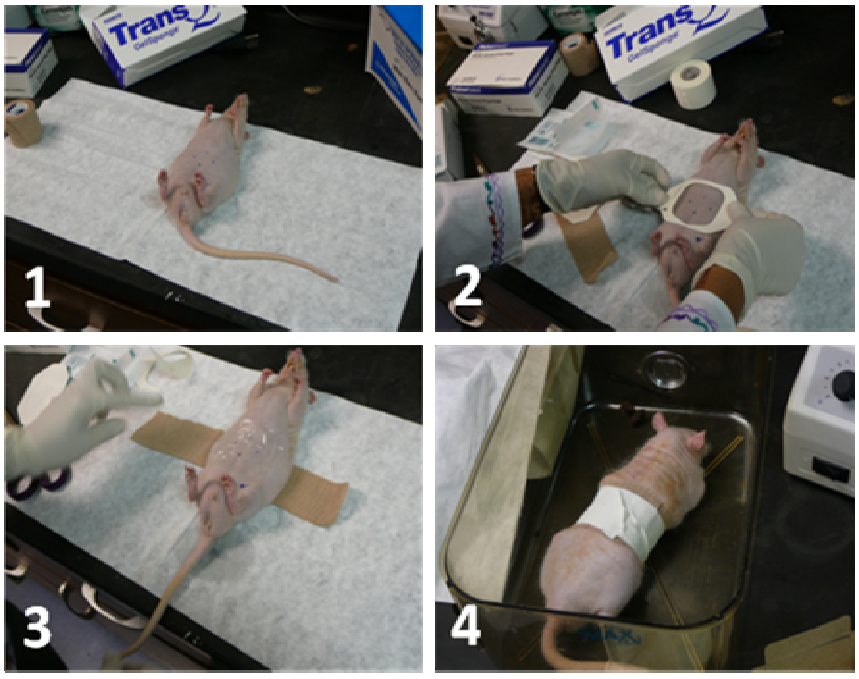

Figure 3.3 Hairless rat bandaging processes (1: Determination of site, 2: Application of dressing, 3: Wrapping, and 4: Fixing with tape).

3.2.2.2 Measurement of skin impedance

The skin resealing after the insertion of CMC microneedles was estimated with the skin impedance measurement by using an electrode impedance meter, Prep-Check (EIM-105, General Devices, Ridgefield, NJ) applying 30 Hz AC current modified with a 200 kΩ resistor (Ack Electronics, Atlanta, GA) in parallel to enable the measurement of skin

impedance greater than 200 kΩ. The reference electrode coated with highly conductive gel, Superior Silver® Electrode with PermaGel™, (Uni-Patch, Wabasha, MN) was attached to the rat skin and a disposable Ag/AgCl dry electrode (T3404, Thought Technology, Montreal, Quebec, Canada) for each category was covered on the site of the microneedles insertion with the same distance from the reference electrode. The measurement of skin impedance was performed by connecting the reference electrode and a dry electrode for each category to the impedance meter, Prep-Check.

The skin impedance was measured for 4 categories; (A) CMC microneedles were inserted for 24 hours without the measurement. (B) CMC microneedles were inserted and immediately removed at 0 h. Then the skin impedance was measured for 24 h. (C) The impedance of intact skin with no treatment was measured for 24 h. (D) CMC microneedles were inserted, immediately removed, and covered with the CMC backing for 24 h without the measurement. The skin was occluded for the first 24 h and unoccluded for the second 24 h. In category (A) and (D), the skin impedance was measured only for the second 24 h after the system was removed at 24 h. In category (B) and (C), it was measured for the first 24 h with the occlusion and for the second 24 h without the occlusion.

3.2.3 Human growth hormone activity

3.2.3.1 SDS-PAGE

To check the change of the primary structure of hGH encapsulated in CMC microneedles, the electrophoresis with unprocessed and processed hGH was performed

by using a SDS-PAGE device, Owl mini-vertical Electrophoresis (P8DS, Thermo Scientific, Waltham, MA). The unprocessed hGH is hGH before the fabrication of dissolving microneedles and the processed hGH is hGH encapsulated in CMC microneedles. The hGH solution at the concentration of 1 mg/ml was made with unprocessed and processed hGH by using sample loading buffer (Tris-Glycine SDS, Pierce, Rockford, IL). Then 20 μg hGH of each solution (20 μl) and the unstained standard solution (20 μl), Mark 12™ (Invitrogen, San Diego, CA) were pipetted into each well of a pre-cast gel with a cassette, Precise™ Protein Gel (25204, Pierce, Rockford, IL), which was inserted into the SDA-PAGE device running with running buffer, BupH™ (Tris-HEPES-SDA, Pierce, Rockford, IL) and 120 V of the power supply (FB300, Fischer Scientific, Dubuque, IA) for approximately 40 min . After running, the gel was washed three times for 5 min each in 200 ml of deionized water and stained with commassie blue, SimplyBlue™ (Invitrogen, San Diego, CA).

3.2.3.2 Nb2 Cell growth

The functional activity of hGH was estimated with the hGH-stimulated growth of Nb2 rat lymphoma cells [100, 101], purchased from Sigma-Aldrich (Cat. No. 97041101, Sigma-Aldrich). The basic steps of this study are composed of three phases; (I) the cell growth with bovine serum based culture medium for verifying the normal growth rate of Nb2 cell (3 days), (II) the transfer of Nb2 cell to horse serum based culture medium to ensure stationary cell growth (1 day), and (III) the addition of hGH solution to Nb2 cell culture based on solely horse serum and no bovine serum for checking the growth-promoting activity of hGH inducing to resume the cell growth (3 days). The number of

viable Nb2 cell at each phase was measured using a cell viability analyzer, Vi-CELL™ (Beckman coulter, Miami, FL).

The culture medium for phase I was prepared with Fischer's medium (Quality Biological Inc., Gaithersburg, MD) supplemented with 10% fetal bovine serum (FBS, Atlanta Biologicals, Atlanta, GA) and 10^{-4} M 2-mercaptoethanol (Sigma-Aldrich, Milwaukee, WI). The culture medium for phase II was prepared with Fischer's medium supplemented with 1 % FBS, 10% horse serum (HS, Mediatech Inc., Herndon, VA), and 10^{-4} M 2-mercaptoethanol. For phase III, the culture medium was prepared without FBS; Fischer's medium, 10% HS, and 10^{-4} M 2-mercaptoethanol only. Nb2 cells were cultured as suspension in a humidified atmosphere of 95% air and 5% CO_2 at 37^{o}C. The hGH solution was prepared with the culture medium used for phase III and added to Nb2 cell culture with the designated concentration ranging from 1 pg/ml to 3000 pg/ml of hGH after Nb2 cell in phase II was transferred to the culture medium of phase III.

When Nb2 cells were transferred to the next phase medium, they were centrifuged for 3 min at 300×g with a centrifuge (GS-15R, Beckman, Fullerton, CA) and supernatants were aspirated using a vacuuming flask. Then, Nb2 cells were rinsed with deionized water twice to prevent the previous medium from mixing with the next phase medium when they were transferred to the next phase medium. The increased population of Nb2 cell due to the addition of hGH solution was calculated with the comparison of two populations of Nb2 cell at the beginning of phase III before the addition of hGH solution and at the third day of phase III. The processes are summarized in Figure 3.4.

The five different groups of hGH solutions were added to Nb2 cell culture in phase III; (1) Placebo solution having only processed CMC, (2) unprocessed hGH solution

(negative control), (3) unprocessed hGH solution mixed with processed CMC, (4) processed hGH and CMC solution (reconstitution of hGH encapsulating CMC microneedles), and (5) processed hGH and CMC solution (reconstitution of hGH encapsulating CMC microneedles after 3 months storage at ambient conditions (23±2^{o}C and 38±5% relative humidity)). For all groups, the mass ratio of hGH to CMC is 5 to 95, which means that 5 wt% hGH was loaded in CMC microneedles. The processed CMC is the solidified CMC hydrogel cast by using the same method used to fabricate CMC dissolving microneedles described in the section 3.1.1.3.

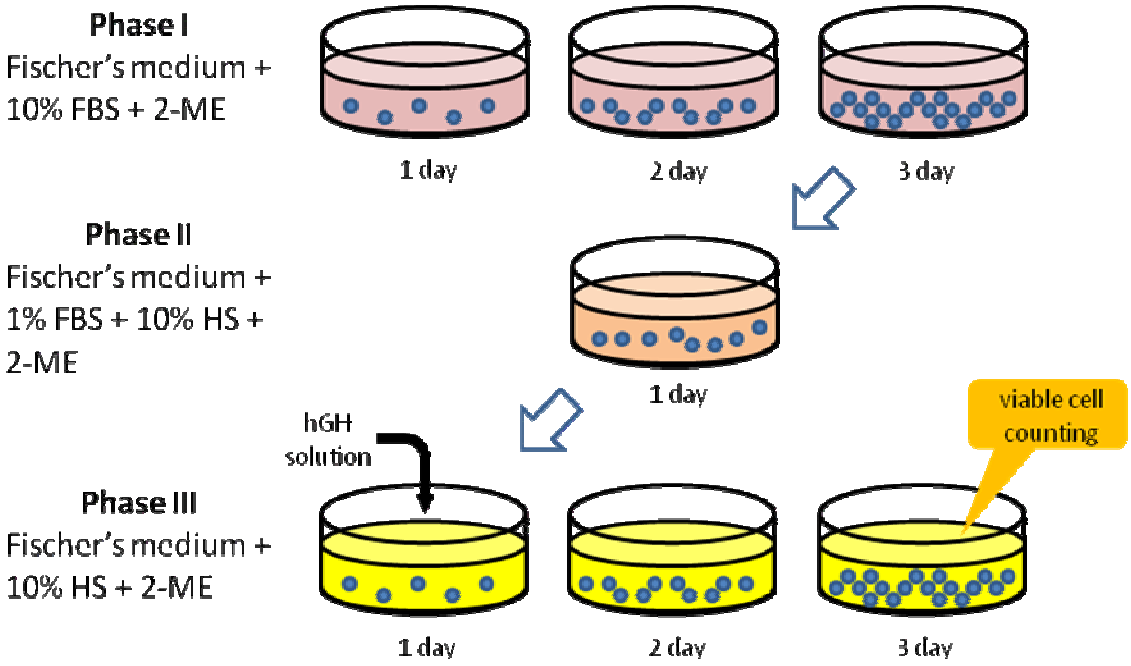

Figure 3.4 hGH activity measurement with the population of Nb2 cell.

3.2.4 Pharmacokinetics

3.2.4.1 Administration of hGH

hGH encapsulating microneedles were fabricated with the method described in the section 3.1.1.2 and 3.1.1.3. For the matrix material of microneedles, CMC only or CMC/trehalose mixture hydrogels were prepared. To administer hGH to hairless rats, 5 groups were designed; (Group 0) – the subcutaneous injection of the reconstitution of unprocessed hGH (negative control group), (Group 1) – the insertion of hGH encapsulating CMC microneedles, (Group 2) – the subcutaneous injection of the reconstitution of hGH encapsulating CMC microneedles after 15 months storage at ambient conditions (23±2^{o}C and 38±5% relative humidity), (Group 3) – the insertion of hGH encapsulating CMC/trehalose microneedles, and (Group 4) – the subcutaneous injection of the reconstitution of hGH encapsulating CMC/trehalose microneedles. The subcutaneous injection for group 0, 2, and 4 was performed by using a 27G hypodermic needle (Becton Dickinson, Franklin Lakes, NJ) and dissolving microneedles encapsulating hGH for group 1 and 3 were inserted with a thumb push method describe in the section 3.1.2.2.

3.2.4.1 Analysis of plasma concentration hGH (ELISA)

Blood of hairless rat was drawn at 0, 0.5, 1, 2, 4, 6, 8, 12, and 24 h after hGH of each group was administered by hypodermic needle injection or microneedles insertion and the volume of each blood collection was determined as 120 μl in order to obtain the minimum volume (60 μl) of serum for ELISA and not to exceed the maximum volume of

1.2 ml blood over 24 h. Blood was drawn from the saphenous vein in the tail by cutting it slightly with a surgical blade (Butler Animal Health Supply, Dublin, OH) and collected with a small tube, CAPIJECT® (T-MG, Trumo Medical Corp., Elkton, MD) with gel barrier inside it used for the separation of serum and blood cells. The blood collected with a CAPIJECT® tube was left at the room temperature for 2 h, the necessary time for blood to clot, and then it was spun at 1200×g for 10 min with a centrifuge (5415 R, Eppendorf, Westbury, NY) to obtain the rat serum. The rat serum was transferred into a safe-lock 0.5 ml conical tube (Eppendorf) and stored at -70^{o}C until ELISA analysis.

The concentration of hGH in rat serum was measured with an enzyme-linked immunosorbent assay kit, ACTIVE® human growth hormone ELISA (DSL-10-1900, Diagnostic Systems Laboratories Inc., Webster, TX). This kit is specific for human growth hormone without detecting endogenous rat growth hormone. Areas under the concentration curves (AUCs) were computed with the area of trapezoid formed between data points. The color intensity of samples at the final step of ELISA was measured with a microplate reader, iMark™ (Bio-Rad, Hercules, CA).

3.2.5 Skin reaction

To study skin reactions that may occur after the insertion of hGH dissolving microneedles, the insertion site was imaged by a digital camera (FZ50, Panasonic, Tokyo, Japan) at 24, 27, 30, 36, and 48 h for the first 24 hours and every day for the week. After euthanasia, the treated skin samples were prepared for histology by tissue fixing with 10% neutral buffered formalin, PROTOCOL™ (Fisher Healthcare, Swedesboro, NJ), paraffin embedding with tissue embedding system (Histocentre 2, Shandon), slicing into

1 μm thick sections with rotary microtome (HM355S, Microm, Waldorf, Germany), and staining with hematoxylin and eosin (H&E). Then, they were viewed by brightfield microscopy (E600, Nikon, Tokyo, Japan) to check visually the skin reaction such as erythema and edema with focusing on the area near the insertion site by using the subjective rating method [102].

3.3 Micro skin ablation

3.3.1 Micro skin ablation (MSA) device

3.3.1.1 Design and fabrication of MSA

To create the energy impact required for selective ablation of skin, an arc discharge phenomenon was believed to be a good model for the energy source. The key points of the design of MSA device were: (1) the rapid generation and extinction of arc discharge in the minimized scale and (2) the controlled utilization of arc energy. This design was enabled by the modification of the laminated gas generator actuators system [103] developed by the MicroSensors and MicroActuators (MSMA) research group in the School of Electrical and Computer Engineering of Georgia Tech. All fabrication and device characterization for the MSA system were performed in collaboration with the MSMA group.

The MSA system has two major parts: the MSA device and a power supplying system. The MSA device was designed to have two basic elements; a microchamber where arc discharge occurs and a nozzle by which the energy medium ejected from microchamber is guided to drive the energy impact to the skin surface. Two methods

were employed to fabricate the MSA device: laser micromachining to pattern layers and lamination technologies to integrate the layers. For the laser micromachining, two kinds of lasers were used to pattern all the layers of the micro skin ablation device: A CO_2 gas laser (LS500 Laser Engraving System, New Hermes-Gravograph, Duluth, GA), which was used to cut polymer-based material and a solid state infrared laser (Nd:YLF, Resonetics Maestro, Nashua, NH) which was used to process metals. The microchamber was made by patterning and integrating 5 layers; a chamber layer (Biaxially-oriented polyethylene terephthalate, BoPET), two electrode layers (Metal), and two backing layers (Polymethylmethacrylate, PMMA). The geometry for the microchamber and the nozzle was patterned on 250 μm thick BoPET film, Mylar sheet (Goodfellow, Oakdale, PA). The electrode layers to supply the energy for creating arc discharge were made using a 25-50 μm thick metal sheet (McMaster-Carr, Elmhurst, IL) such as brass, nickel and titanium. For backing layers to maintain structural integrity of the device during arc discharge phenomenon, a 1.5 mm thick PMMA sheet (Goodfellow, Oakdale, PA) was used.

To provide electrical energy to the MSA device for skin ablation energy, a circuit (Figure 3.5) was designed with three main components; a high voltage DC power supply (Kiethley Instruments, Cleveland, OH) to provide the electrical energy, a capacitor (Digi-key, Thief River Falls, MN) to store the electrical energy with the maximum of 250 V and provide it to the MSA microchamber, and a MOSFET (IRG4P254, International Rectifier, El Segundo, CA) connected to a pulse generator to control the flow of the electrical energy.

All details of the fabrication work and the optimization of parameters in MSA function are described in Chapters 3 and 4 of the dissertation "Laminated chemical and physical micro-jet actuators based on conductive media" [104] (Gadiraju, Priya, School of Chemical and Biomolecular Engineering, Georgia Institute of Technology).

3.3.1.2 Design of MSA function

The MSA system is based on the rapid generation and extinction of energy caused by the arc discharge phenomenon. The energy medium is ejected from the microchamber in the form of thermal and mechanical energy [104] so that the MSA function is based on thermal or mechanical effects. To utilize this energy impact for controlled skin ablation, four different MSA scenarios were designed in combination with the masking system, as shown in Table 3.1. Three different types of metal sheets (25 μm thickness); tungsten (3N8), titanium (3N7), and nickel (3N, ESPI metals, Ashland, OR) were tested as materials for the masking system to obtain the localized and selective removal of stratum corneum. The fabrication of the masking system was performed by using the same methods described in the section 3.3.1.1.

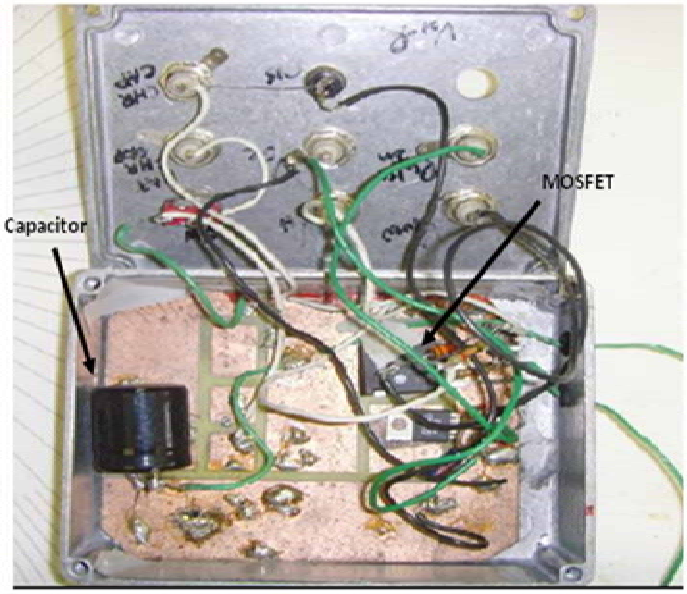

(a)

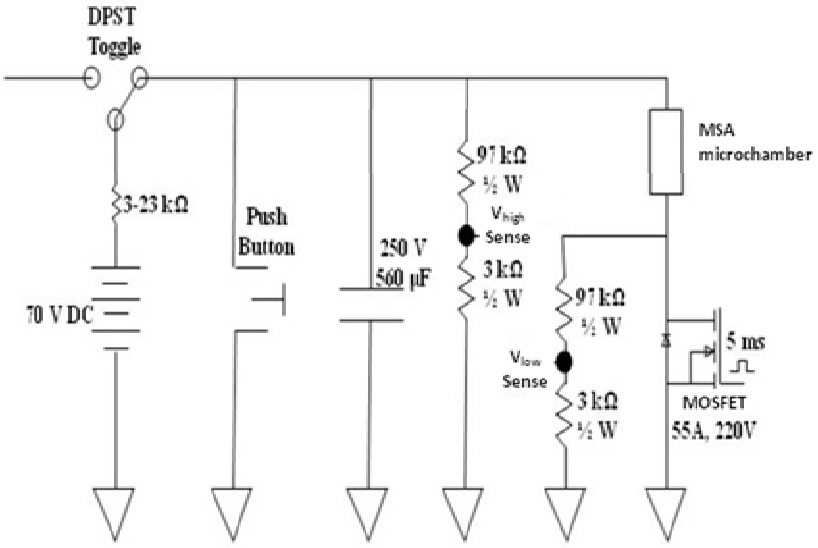

(b)

Figure 3.5 (a) Power supply for controlling the electrical energy and (b) schematic of power supply circuit combined with MSA microchamber [104].

Table 3.1 Micro skin ablation using the energy impact from arc discharge

Group	1	2	3	4
Schematic Description	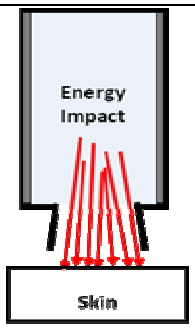	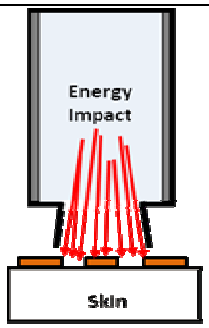	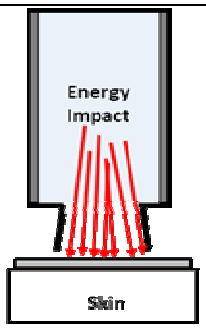	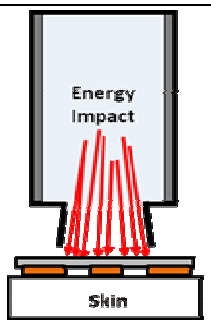
Localization	Non-localized	localized	Non-localized	localized
Mask	No mask	Windows	Solid	Solid and Windows
Ablation Effect	Thermal + Mechanical		Thermal	

3.3.2 Characterization of thermal ablation function

3.3.2.1 Measurement of thermal energy temperature

The temperature of the energy impact triggered by arc discharge occurring in the MSA device was measured using irreversible temperature indicating paper, THERMAX® (Thermographic Measurements Ltd., Glenview, IL). This paper is coated with a heat sensitive white polymer, that melts at specific temperature when in contact with a hot medium, allowing the black background to appear. For the thermal and mechanical

ablation scenario, temperature indicating papers were exposed to the medium as it escapted from the microchamber so that the temperature of the ejected medium was measured. In the thermal ablation scenario, the papers were placed under a solid mask and the temperature of the thermal energy transferred through the solid mask was measured. The detectable range of temperature by THERMAX® was from 30°C up to 290°C, which is the available maximum value.

3.3.2.2 Simulation of thermal energy temperature

The temperature of the energy released from the MSA microchamber and the temperature profile in the skin layer were simulated by conversion of the electrical energy to the thermal energy using a semi-infinite model of heat transfer in the skin.

The consumed energy of the MSA device was estimated with Joule's law ($P = V \cdot I$) by the change of voltage and current in the device during operation. The operating voltage in the power supply circuit was adjusted, at a range from 100 V to 200 V, and the length of the 5 V pulse applied to MOSFET was 1.5 ms. The voltage change across the microchamber was measured by two voltage divider circuits placed on either side of the microchamber (Figure 3.5 (b)). The current was estimated by the measured voltage drop across MOSFET and the technical data sheet of MOSFET supplied from the manufacturer (International Rectifier, El Segundo, CA). The voltage drop across the microchamber and MOSFET was measured by using a 12-bit data acquisition board (DAQ MIO-16E, National Instruments, Austin, TX) and a junction box (BNC-2090, National Instruments, Austin, TX) and recorded with LabVIEW software (National Instruments, Austin, TX).

The heat transfer from the ejected medium to the skin layers was computed with simulation software, ANSYS® (ANSYS Inc., Canonsburg, PA), by using a transient semi-infinite model with the boundary condition that the temperature at the outer surface of the solid mask is constant and the same as the temperature of the ejected medium during MSA operation. The heat conductivity, heat capacity, and density of the solid mask, the windows mask, stratum corneum, and epidermis were assumed to be constant over the entire temperature range. All thermal properties of each layer are in Table 3.2.

Table 3.2 Thermal conductivity, heat capacity, density, and thickness of tungsten, titanium, stratum corneum, and viable epidermis [105, 106] used for the simulation of the temperature profile during the operation.

	Tungsten	Titanium	Stratum Corneum	Viable Epidermis
Thermal conductivity (W/m·K)	174	21.9	0.123	0.42
Density (kg/m^3)	19300	4500	1280	1090
Heat Capacity (J/kg·K)	132	522	1880	3350
Thickness (μm)	25	25	15	100

3.3.3. Skin ablation

3.3.3.1 Thermo mechanical or thermal ablation

The skin ablation system was operated in the following order. First, the microchambers were filled with an electrically conductive medium, PBS. Then, the assembled circular disk unit with multiple microchambers was combined with the piezoelectric force sensor (9144A21, Kistler Instruments, Amherst, NY) to measure the mechanical energy exerted by the arc discharge phenomenon. Finally, two electrodes in the microchamber were connected to the power supplying circuit as shown in Figure 3.6.

The full-thickness cadaver pig skin without subcutaneous fat was shaved (series 8900, WHAL, Sterling, IL) with IACUC approval and trimmed to fit the size of the nozzle exit hole. The pig skin sample was placed on the nozzle of the microchamber and pushed slightly by using a cotton swab, Critical Swab® (VWR, West Chester, PA) to prevent the skin sample from moving out of place. Then the pig skin was treated with the arc discharge ablation system.

As described in Table 3.1, the pig skin samples were exposed to the medium ejected from the microchamber without (Group 1) or with the window mask (Group 2) to study the thermal and mechanical skin ablation effect. For the thermal ablation effect, the solid mask was placed on the surface of the pig skin (Group 3) and the combined masking system of solid and window masks (Group 4) were tested to investigate both localized and selective removal of stratum corneum by arc discharge phenomenon.

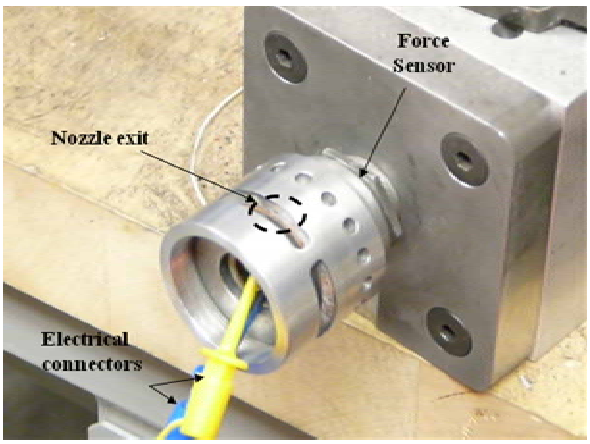

Figure 3.6 Micro skin ablation device combined with a power supply circuit and a force sensor [104].

3.3.3.2 Imaging micro skin ablation

To visualize the ablation effect of the energy impact on stratum corneum, the surface of the pig skin samples were viewed by brightfield microcopy (SZX12, Olympus). To verify the removal of stratum corneum, the delivery of a hydrophilic model drug, sulforhodamine was performed. The drug formulation of transdermal delivery consisted of 30 mg of sulforhodamine and 970 µl of viscous solution made with 10% CMC and deionized water, which was applied to the ablated pig skin samples for 12 hours. For visualization of the localized removal of stratum corneum, the delivery time was reduced to 30 min to image the skin surface with the distinct ablation sites. After the brightfield observation of the pig skin surface, each pig skin sample was prepared for histology and sectioned to determine the selective removal of stratum corneum by histological methods.

Skin samples were prepared by freezing in histology mounting compound (Tissue-Tek, Sakura Finetek, Torrance, CA) and slicing into 20-μm thick sections (Cryo-star HM 560MV, Microm, Waldorf, Germany) which were mounted and viewed by brightfield and fluorescent microscopy (E600, Nikon, Tokyo, Japan).

3.3.4 Skin permeability and transdermal flux

This experiment was designed to study how efficiently the MSA device can deliver hydrophilic or large size drug through the skin. The skin permeability of two different molecular weight compounds, sulforhodamine (Molecular Probes, Eugene, OR) and Texas Red BSA (Molecular Probes, Eugene, OR) was measured using a Franz diffusion chamber (Permegear, Hellertown, PA) and human skin with IRB approval.

First, heat-stripped human cadaver epidermis [97] was used as the skin membrane. The untreated epidermis and epidermis treated with the MSA system were prepared and placed between the donor and the receptor compartment of Franz diffusion cell. The donor compartment was filled with the solution of sulforhodamine (10^{-3} M) or Texas Red BSA (10^{-4} M) with PBS as models of low and high molecular weight model drugs, respectively, and the receptor compartment was filled with PBS. Assuming that the steady state of flux from the donor compartment to the receptor compartment is within three hours, the content in the receptor compartment was sampled after 1 hour and the concentration of model drug was analyzed by using a spectrofluorimetry (QM-1, Photon Technology International, South Brunswick, NJ). The skin permeability experiment was performed with human full thickness skin to have better approximation to the in-vivo situation. With the exception of the type of skin membrane, all protocols were the same

as those performed with epidermis layer alone. The diffusion process of each model drug through human full thickness skin, ablated full thickness skin, and epidermis-striped skin (dermis only) was visualized using histological skin images, which were prepared by the same methods described in the section 3.3.3.2.

4. Results

4.1 Dissolving microneedles results

Four materials-related criteria were determined for the design of microneedles suitable for self-administration of biotherapeutics from a minimally invasive patch: (1) gentle fabrication to avoid damaging sensitive biomolecules, (2) sufficient mechanical strength for insertion into the skin, (3) controlled release for bolus and sustained drug delivery, and (4) rapid dissolution of microneedles made of safe materials. Guided by these criteria, two polysaccharides, carboxymethylcellulose and amylopectin were selected because they are biocompatible materials with a history of use in FDA-approval parenteral formulations [107, 108], are expected to be mechanically strong due to their relatively high Young's modulus [109, 110], and are highly water soluble for rapid dissolution in the skin [111]. These polysaccharides are degraded by a number of glycosidases, which are distributed in all of cell territories: nucleus, cytosol, endoplasmic reticulum, plasma membrane, and lysosomes [111] through the endocytosis mechanism with macrophages [112]. Additionally, disaccharide, trehalose was used for the microneedle matrix material for the dissolution enhancer because it has higher solubility in water than high molecular weight polysaccharides. A fabrication method for gentle encapsulation of biomolecules was also developed with the casting using an aqueous solution that is evaporated at 37^{o}C during centrifugation.

4.1.1 Fabrication of dissolving microneedles

As the successor to the previous microneedle fabrication methods [28, 94], a method to fabricate dissolving microneedles was developed using a micromolding approach that faithfully reproduces microneedle structures in an economical manner suitable for scale up to mass production. Female master-molds were first prepared out of SU-8 photoresist by lithography and reactive ion etching techniques used to create PDMS male master-structures, shown in Figure 4.1 (a) and (e). These master-structures were then molded to make PDMS female molds. PDMS was chosen as the material for master- structures and molds because of its ability to conformally coat microstructures and fill micromolds; its poor adhesion and flexibility to facilitate separation of microstructures from micromolds; and its low cost.

These micromolds were then used to prepare dissolving microneedles by solvent casting with aqueous solutions of CMC and amylopectin or the mixture with trehalose. However, simply filling molds with a polysaccharide solution and then drying produced weak needles, probably due to structural voids left within the microneedle matrix after water evaporation. To avoid this problem, we developed a modified casting method in which the CMC solution was first concentrated by evaporation under vacuum (i.e., -50 kPa) or heating (i.e., 60-70^{o}C) to produce a highly viscous solution that minimized water content, but was still fluid enough to fill the mold. We found that an aqueous CMC solution with a viscosity of $4.5x10^{5}$ cP (measured with a Couette viscometer at 1/s shear rate at 23^{o}C) met these criteria. In case of amylopectin, the initial solvent removal was carried out at elevated temperature (i.e., 60-70^{o}C) rather than just under vacuum, because amylopectin has poor water solubility at room temperature.

Concentrated polysaccharide solution was then cast into micromolds and dried completely by centrifugation at 37^{o}C. The elevated temperature increased the speed of evaporation and the centrifugation continuously compressed the mold contents, which minimized void formation during drying. This modified casting method was effective to reproduce polysaccharide microneedles having the same dimensions as their master-structures, as shown in Figure 4.1 (b), 4.1 (C), and 4.1 (f) for CMC, amylopectin, and CMC/trehalose microneedles, respectively. A similar approach was used to make microneedles out of BSA in Figure 4.1 (d), which is a model for making needles out of pure drug, rather than encapsulating drug within a polysaccharide matrix.

As an alternative approach, we tried using high viscosity CMC (1.5 – 3 x 10^3 cP for a 1% aqueous solution at 25^{o}C) as the matrix material, but found that it required much more water to be solubilized compared to the ultra-low viscosity CMC used above. As a result, the high viscosity CMC took longer to dry and produced deformed microneedles that shrank substantially during drying and were mechanically weak.

Different drug delivery scenarios were addressed by selectively encapsulating drug within microneedles, within the microneedle device backing layer, or within both. To encapsulate drugs within the polysaccharide matrix, we simply mixed the drug into the polysaccharide solution before casting into the molds. To selectively encapsulate within the microneedles and not in the backing layer, a smaller volume of drug-polysaccharide solution was cast into the holes of the micromold to form the microneedles. After wiping off excess solution from the micromold surface, a polysaccharide solution without drug was cast onto the micromold and dried.

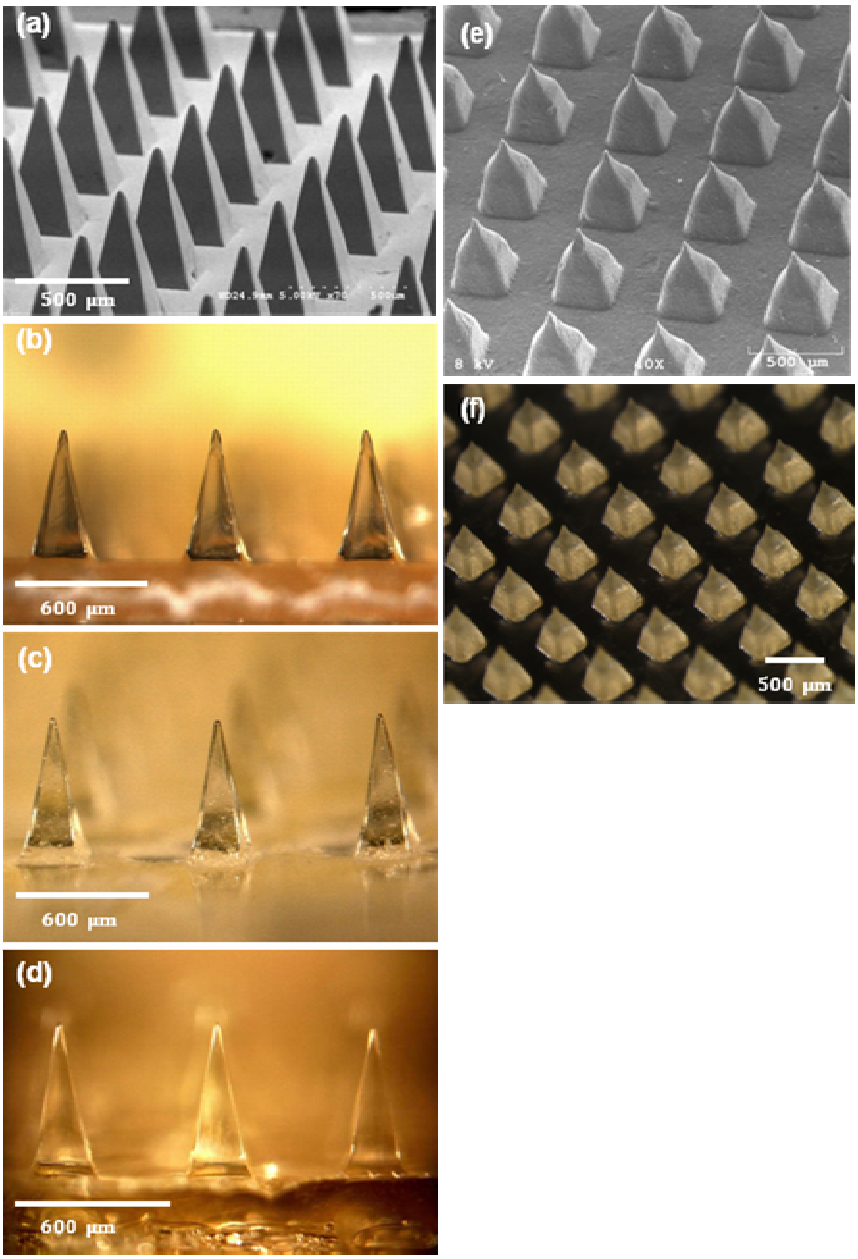

Figure 4.1 Microneedles for transdermal drug delivery. (a) Microneedle master-structure (600 µm in height and 300 µm wide at base). Dissolving microneedle made out of (b) CMC, (c) amylopectin and (d) BSA with (a) master-structure; (e) Modified microneedle master-structure. (f) Dissolving microneedle made out of CMC, Trehalose, and human growth hormone (hGH).

To selectively encapsulate within the backing layer and not in the microneedles, a similar two-step process was carried out, in which the drug was only added to the polysaccharide solution applied to the micromold during the second step. Drying of the complete, integrated system or just the backing layer during the second step required 1 to 2 h, whereas drying of just the microneedles during the first step took approximately 30 min. These process times varied depending on materials and processing conditions.

4.1.2 Mechanical properties of dissolving microneedles

The design of dissolving microneedles is governed by a number of interdependent materials and fabrication constraints, one of which is the need for microneedles to have sufficient strength to insert into the skin without mechanical failure. For this question, microneedle mechanical properties were therefore measured and simulated as a function of microneedle material composition and geometry, and then insertion of optimized microneedles into skin was visualized.

4.1.2.1 Measurement of microneedle failure force

The mechanical behavior of CMC microneedles with a conical shape was first measured. As shown in Figure 4.2 (a) by the black circle data points, the force-displacement curve (which is analogous to a stress-strain curve) exhibited an initial increase in force with displacement, followed by a discontinuity at a force of approximately 0.1 N/needle. This is interpreted as the point of microneedle failure, which is consistent with previous studies [28]. Moreover, microscopic examination of the

microneedles showed little deformation before this failure point and showed microneedles bent up to 90º starting approximately half way up the shaft after this failure point, which is consistent with failure by buckling.

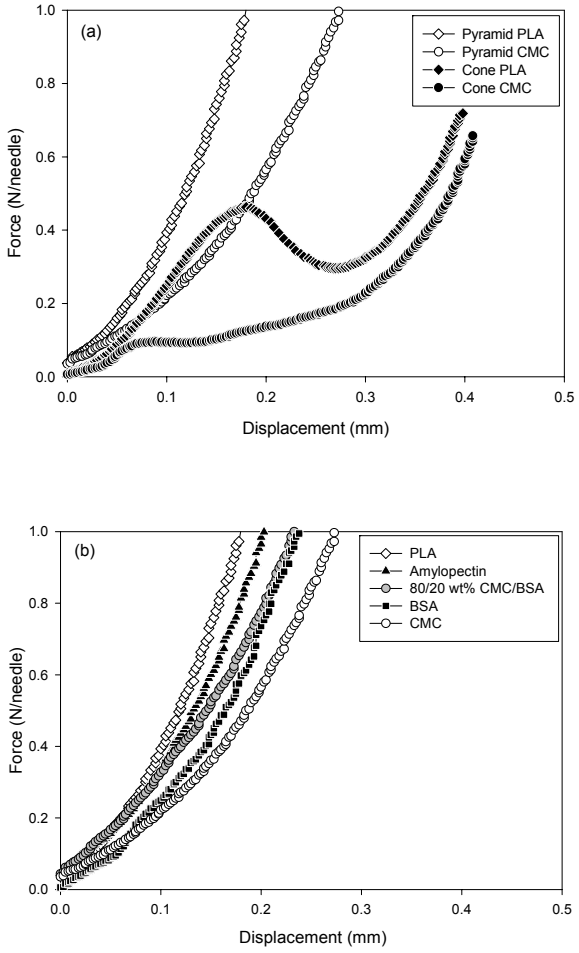

Figure 4.2 Mechanical behavior of dissolving microneedles. Force measured as a function of microneedle displacement while pressing against a rigid surface. (a) CMC and PLA microneedles having conical and pyramidal geometries and (b) pyramidal microneedles made of PLA, amylopectin, BSA, CMC and a mixture of CMC/BSA.

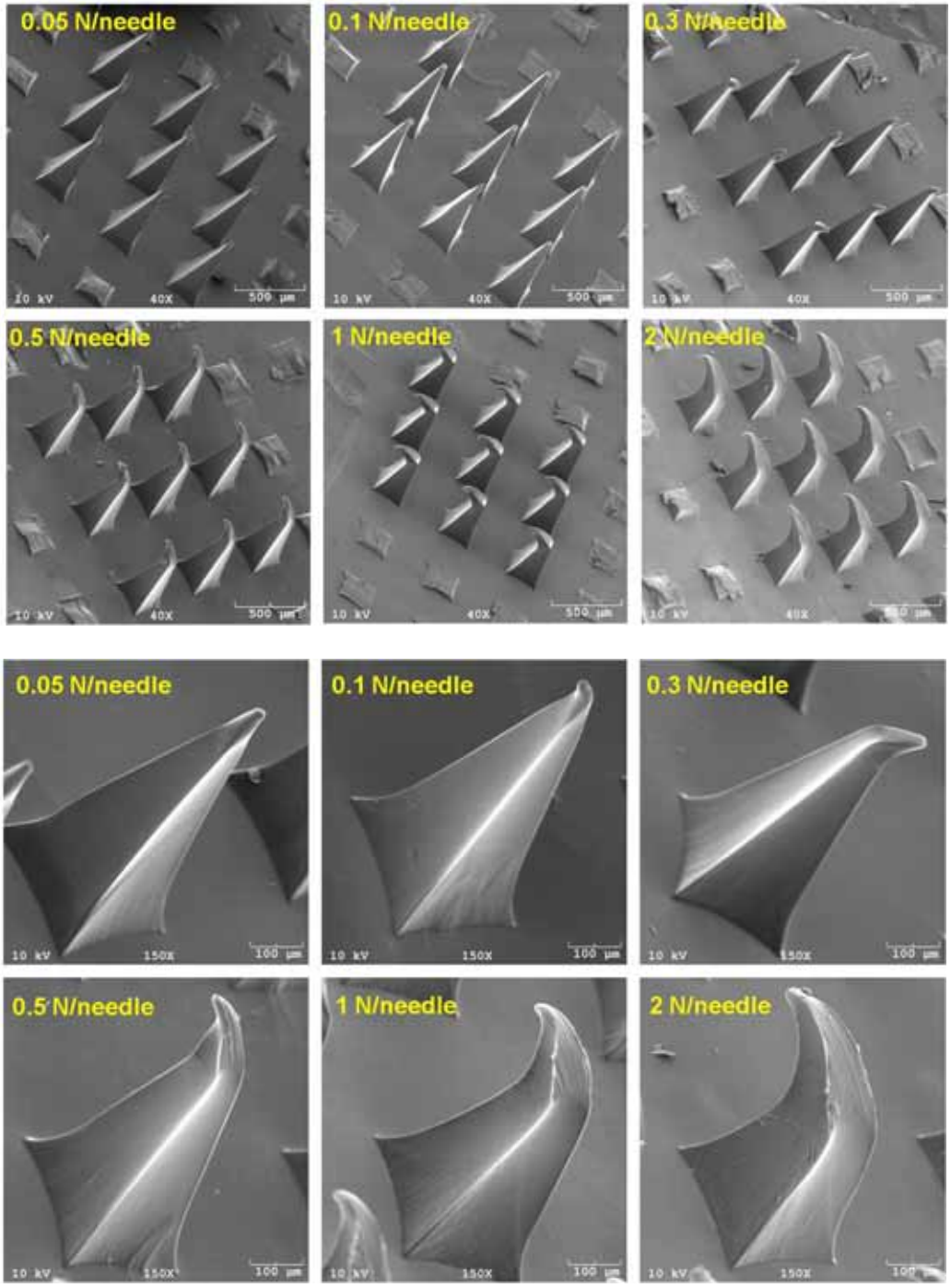

Figure 4.3 SEM images of the deformation of CMC pyramidal microneedles loaded with each maximum force of 0.05, 0.1, 0.3, 0.5, 1, and 2 N/needle.

For comparison, PLA microneedles having the same geometry showed a similar curve but demonstrated a five-fold greater failure force of 0.5 N/needle (black diamonds in Figure 4.2 (a)). Previous work [28] has shown that conical PLA microneedles similar to those used in this study have a failure force more than 3 times greater that the force needed for insertion into the skin, which indicates that these conical PLA microneedles are suitable for skin insertion without breaking [28]. Given that the conical CMC microneedles are 5 times weaker than their PLA counterparts, this analysis suggests that the conical CMC microneedles are too weak to insert into the skin.

Because microneedle geometry affects mechanical strength, pyramidal microneedles made of CMC and PLA were examined to investigate the difference from the different geomtery. In contrast to conical microneedles, pyramidal microneedles did not show a distinct transition point indicating failure over the range of conditions tested. Microscopic examination of pyramidal microneedles showed a progressive deformation of the microneedles, starting near the tip and moving downward with increasing force as shown in Figure 4.3, but never showed a catastrophic buckling event at a single point of failure. This progressive deformation is consistent with the continuous force-displacement curve shown in Figure 4.2. The reason for the different behaviors of conical and pyramidal microneedles may have to do with the larger aspect ratio and the smaller cross-sectional area of conical microneedles.

To further study the effect of microneedle composition on mechanical strength, the mechanical behavior of pyramidal microneedles having the same geometry was measured for microneedles made of CMC, PLA, amylopectin, a 20/80 wt% mixture of BSA and CMC, and 100% BSA. As shown in Figure 4.2 (b), these five pyramidal microneedles all

showed similar mechanical behavior, although the choice of material influenced the microneedle strength (i.e., amount of deformation). The materials can be ranked from strongest to weakest as: PLA, amylopectin, CMC/BSA, BSA, and CMC. Amylopectin microneedles were stronger than CMC microneedles, which can be explained by the higher Young's modulus of amylopectin (4.5 GPa, ref) compared to CMC (1 GPa). CMC and CMC/BSA microneedles were designed to simulate a CMC microneedle encapsulating a model protein and a microneedle made completely of a model protein, respectively. These two microneedles designs had similar mechanical strength, both of which were greater than for pure CMC microneedles. In this case, encapsulation of a model protein increased microneedle mechanical strength, but this is unlikely to be true in all cases. Other encapsulated drugs may decrease microneedle strength.

4.1.2.2 Simulation of microneedle failure force

To better interpret these experimental results, the mechanical behavior of microneedles was simulated to predict the critical buckling load. As shown in Table 4.1, the CMC microneedles with a conical geometry (800 μm length and 200 μm base diameter) have a predicted failure force of 0.10 N and the PLA microneedles with the same geometry have a predicted failure force of 0.51 N, which is in excellent agreement with experimental measurements shown in Figure 4.2 (a). The pyramidal microneedles (600 μm length and 300 μm base width) made of CMC and PLA have predicted failure forces of 1.8 N and 8.9 N, respectively (Table 4.1). The 18-fold increase in critical buckling load for these pyramidal microneedles compared to the conical microneedles is also consistent with experimental measurements. However, this model accounts only for

buckling and does not account for the progressive deformation observed experimentally at smaller forces.

Table 4.1 Simulated critical buckling load, P_{cr} of CMC and PLA microneedles as a function of microneedle shape, length and base width/diameter.

Conical (800 μm Length)			Pyramidal (600 μm Length)			Conical (600 μm Length)		
Diameter (μm)	P_{cri} (N)		Base (μm)	P_{cri} (N)		Diameter (μm)	P_{cri} (N)	
	CMC	PLA		CMC	PLA		CMC	PLA
50	0.0004	0.0020	50	0.0020	0.0102	50	0.0007	0.0035
75	0.0019	0.0096	75	0.0087	0.0435	75	0.0034	0.0171
100	0.0061	0.0307	100	0.0255	0.1271	100	0.0109	0.0546
200	**0.1021**	**0.5105**	200	0.3639	1.8194	200	0.1815	0.9076
300	0.5266	2.6329	300	**1.7798**	**8.8899**	300	**0.9362**	**4.6808**
400	1.6813	8.4064	400	5.5223	27.6113	400	2.9889	14.9447
600	8.6032	43.0158	500	13.3433	66.7164	500	7.3438	36.7191
800	27.3415	136.7075	600	27.4795	137.3976	600	15.2945	76.4725

The above comparison involved longer and thinner conical microneedles versus shorter and wider pyramidal microneedles. To make a comparison that isolates the effect just of microneedle shape, failure force for microneedles of 600 μm length and 300 μm base width/diameter was predicted to be 0.93 N and 4.7 N for conical microneedle made

of CMC and PLA, respectively, which is almost two-fold smaller than the corresponding predictions for pyramidal microneedles (Table 4.1). It is therefore concluded that pyramidal microneedles are stronger, probably due to their larger cross-sectional area at the same base width/diameter.

Examination of Table 4.1 for each microneedle design as a function of base width/diameter also shows that increasing base dimensions (i.e., decreasing aspect ratio) increases needle strength. Thus, using pyramidal microneedles with a small aspect ratio can provide added mechanical strength for mechanically weak biomaterials like CMC. However, microneedles with an aspect ratio that is too small will also have poor insertion due to fabrication difficulties to make a sharp tip and insertion difficulties to force the rapidly widening needle shaft into the small hole made in the skin by the needle tip.

4.1.2.3 Microneedle insertion into skin

Guided by the expectation that pyramidal CMC microneedles with an aspect ratio of two should be strong, arrays of these needles were inserted into pig cadaver skin and it was found that 100-needle arrays of microneedles were inserted reliably into the skin using the gentle force of a thumb. The back side of a representative microneedle array made of transparent CMC is shown in Figure 4.4 (a), with its microneedles embedded in the skin. After removing the microneedles from the skin after just 3 s, the tips had already begun to dissolve (Figure 4.4 (b)), indicating the onset of rapid dissolution in the skin. Next the skin was treated with a dye that selectively marks sites of skin penetration and it was found that typically all microneedles in the array inserted into the skin, as shown in Figure 4.4 (c).

Histological examination of skin pierced with microneedles showed penetration depths of approximately 150 – 200 μm, which corresponded to insertion across the stratum corneum and viable epidermis and into the superficial dermis of the skin, as shown in Figure 4.4 (d). The microneedles used in this experiment measured 600 μm in length, which means that just one-fourth to one-third of the microneedle shaft penetrated into the skin. This can be explained by deformation of the skin's surface that is known to occur during microneedle insertion due to the skin's viscoelasticity [113]. The relatively wide base (i.e., 300 μm) and small aspect ratio (i.e., 2) of the pyramidal microneedles contributed to this incomplete insertion. Further optimization of microneedle geometry, such as aspect ratio, tip sharpness, and spacing between microneedles, and microneedle material may increase the depth of insertion. However, partial microneedle insertion should be adequate for the drug delivery strategies presented in this study.

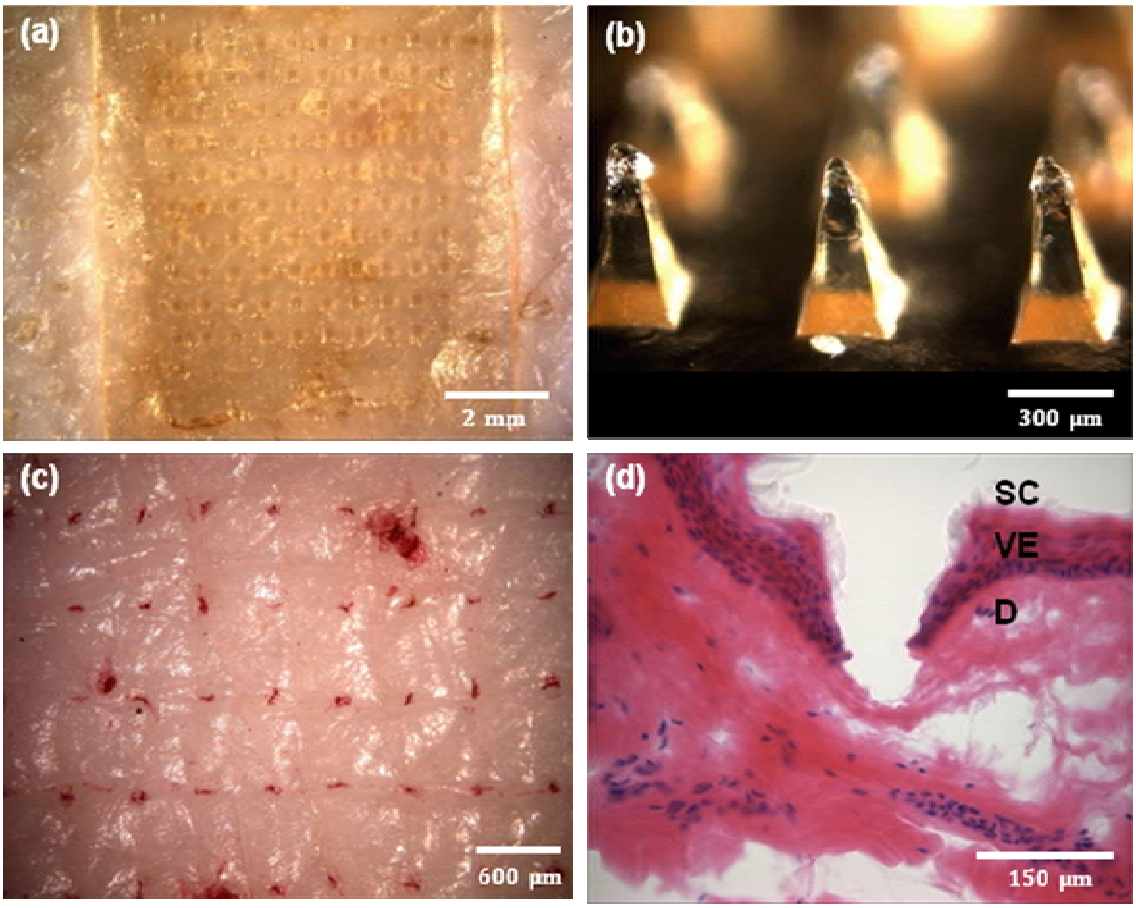

Figure 4.4 Imaging microneedle insertion into pig cadaver skin. (a) View of the backside of a CMC microneedle patch onto the surface of the skin. (b) CMC pyramidal microneedles after insertion into the skin for 3 s. (c) Skin stained with red tissue-marking dye to identify the sites of needle penetration after insertion of CMC pyramidal microneedles. (d) Cross-sectional image of H&E-stained skin at a site of microneedle penetration (SC: stratum corneum, VE: viable epidermis, and D: dermis).

4.1.3 Release of model drugs from dissolving microneedle patches

By loading drug into dissolving microneedles in different ways, we were able to design systems that can achieve either bolus or extended drug release from a microneedle patch. To achieve bolus release, drug was selectively incorporated into the microneedles themselves and not into the backing layer. In this way, it was hypothesized that microneedles can be inserted into the skin and release the encapsulated drug during their rapid dissolution. The rate of release in this scenario is controlled largely by the microneedle dissolution rate. A limitation is that the total dose that can be administered is small, because microneedles each contain on the order of 25-60 μg of matrix material and typically just a fraction of the microneedle matrix can made of drug in order to maintain microneedle mechanical strength. Thus, bolus delivery from a microneedle patch containing a few hundred microneedles is likely to be limited to less than 1 mg of drug.

To administer larger drug doses as an extended release over at least hours of time, drugs are incorporated into both the microneedles and the backing layer or, alternatively, just the backing layer. This permits much larger doses to be administered, because the backing layer can be large (e.g., 10 - 100 mg) and can be loaded with larger fractions of drug, because backing layer mechanical properties have fewer constraints. In this scenario, it was hypothesized that drug can diffuse over time from the drug reservoir in the backing layer and into the skin through the transdermal pathways created by the dissolving microneedles. In this way, the backing layer acts as a drug source similar to a conventional matrix-design transdermal patch.

4.1.3.1Boluse release

To test hypothesis regarding bolus release from drug-loaded, dissolving microneedles, a model drug, sulforhodamine B was selectively encapsulated, in pyramidal CMC microneedles. As shown in Figure 4.5 (a), red-colored sulforhodamine was encapsulated within each microneedle, but the bottom portion of each microneedle and the backing layer did not contain sulforhodamine. After inserting sulforhodamine-loaded microneedles into pig cadaver skin and then removing them after 5 min, inspection of the skin surface showed an array of red spots corresponding to the sites of each microneedle insertion, as shown in Figure 4.5 (b). These spots could not be wiped off by cleaning the surface of the skin and are therefore interpreted as sulforhodamine deposited within the skin after microneedle dissolution.

This interpretation is confirmed by histological sections shown in Figure 4.5 (c), which show deposition of sulforhodamine within the skin at the sites of microneedle penetration after 5 min. The microneedle insertion depth was approximately 150 to 200 μm, which is in agreement with Figure 4.4 (d). The width of each hole was approximately 100 μm (Figure 4.5 (b)), which is similar to the microneedle width at a distance of 150 to 200 μm up the shaft from the tip. To supplement this information, Figure 4.5 (d) shows a lower-magnification histological section of skin 1 h after insertion of bolus-delivery microneedles. In this case sulforhodamine is not located just at the sites of microneedle insertion, but has diffused more extensively within the skin.

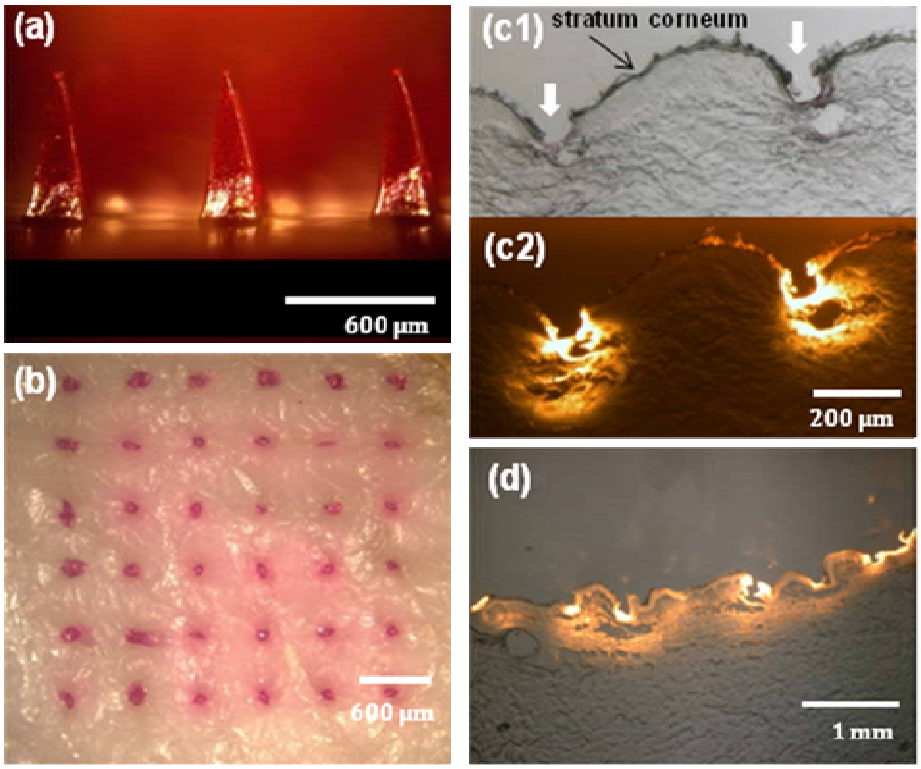

Figure 4.5 Dissolving microneedles of bolus delivery into skin. (a) CMC pyramidal microneedles encapsulating sulforhodamine B within the microneedle shafts, but not in the backing layer. (b) Skin surface showing sulforhodamine delivered into the skin by insertion of the microneedles shown in part (a) for 5 min imaged by brightfiled microscopy. (c) Cross-sectional histological image of skin at the penetration site of 2 adjacent microneedles shown in part (a) inserted for 5 min and imaged by brightfield (c1) and fluorescence (c2) microscopy. (d) Cross-sectional histological image of skin pierced by an array of sulforhodamine-containing microneedles for 1 h and imaged by an overlay of brightfield and fluorescence microscopy. Pig cadaver skin was used.

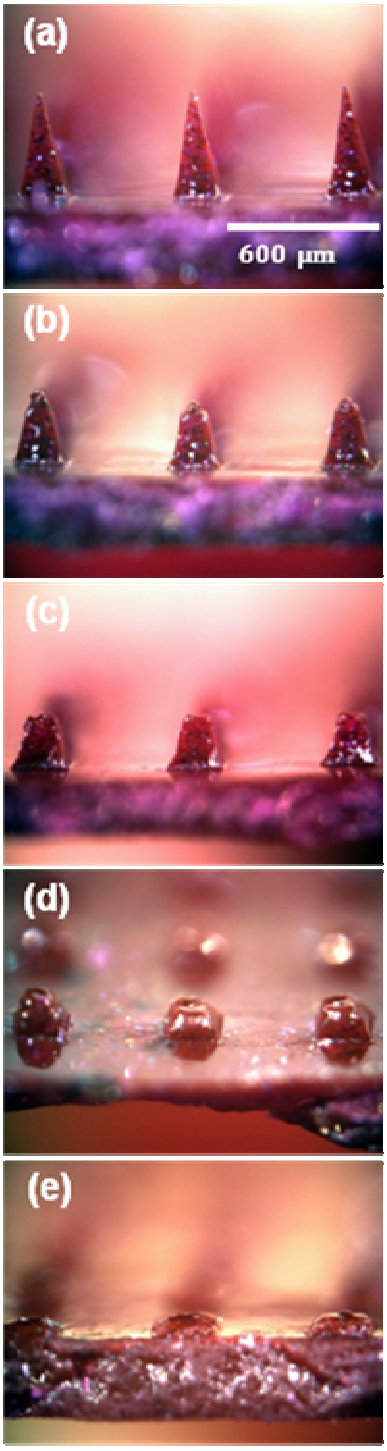

Figure 4.6 Dissolution kinetics of microneedles after insertion into skin. (a) CMC pyramidal microneedles before insertion and (b) 10 sec, (c) 1 min, (d) 15 min, and (e) 1 h after insertion into pig cadaver skin.

To generate a better understanding of the kinetics of bolus release from dissolving microneedles, we imaged the microneedle dissolution process after insertion into skin for different lengths of time. As shown in Figure 4.6, the tips of microneedles dissolved within 10 s (Figure 4.6 (b)), half of the microneedle height disappeared within 1 min (Figure 4.6 (c)) and two-thirds disappeared within 15 min (Figure 4.6 (d)). After 1 h, the microneedles were fully dissolved (Figure 4.6 (e)). These kinetics could be altered by changing microneedle geometry and matrix material. It is also worth noting that even though microneedles did not penetrate to their full length into the skin, they were nonetheless able to fully dissolve, probably due to transport of interstitial fluid from the skin up the needle shaft, as discussed below.

4.1.3.2 Sustained release

To test the hypothesis regarding sustained release, sulforhodamine was encapsulated in the backing layer and shafts of pyramidal CMC microneedles (Figure 4.7 (a)). The microneedle device contained 1 mg of sulforhodamine at a concentration of 10 wt% (on a dry basis). These microneedles designed for sustained release could be inserted into skin (Figure 4.7 (b)) and histological examination showed release of sulforhodamine throughout the skin (Figure 4.7 (c)).

To quantify sustained release properties in greater detail, we inserted microneedle patches into human cadaver skin and measured transdermal flux. Sulforhodamine release from CMC microneedle patches exhibited an initial lag time of a few hours, followed by steady release for approximately one day (Figure 4.8 (a)). Similar behavior was seen for

microneedle patches made of amylopectin, but with slower kinetics. In this case, lag time was longer and release took place over a few days (Figure 4.8 (a)).

These data validate the hypothesis that drug encapsulated within the backing layer of a microneedle patch can diffuse out of the patch and into skin. Moreover, they show that changing microneedle patch matrix material can alter release kinetics. It is important to be able to vary release kinetics based on patch design, because different drugs administered for different indications require different release patterns.

Release rate should also depend on sulforhodamine concentration in the patch. Consistent with this expectation, the drug release rate from a patch containing 30 wt% sulforhodamine was approximately three times greater than a patch containing 10 wt% sulforhodamine (Figure 4.7 (b)).

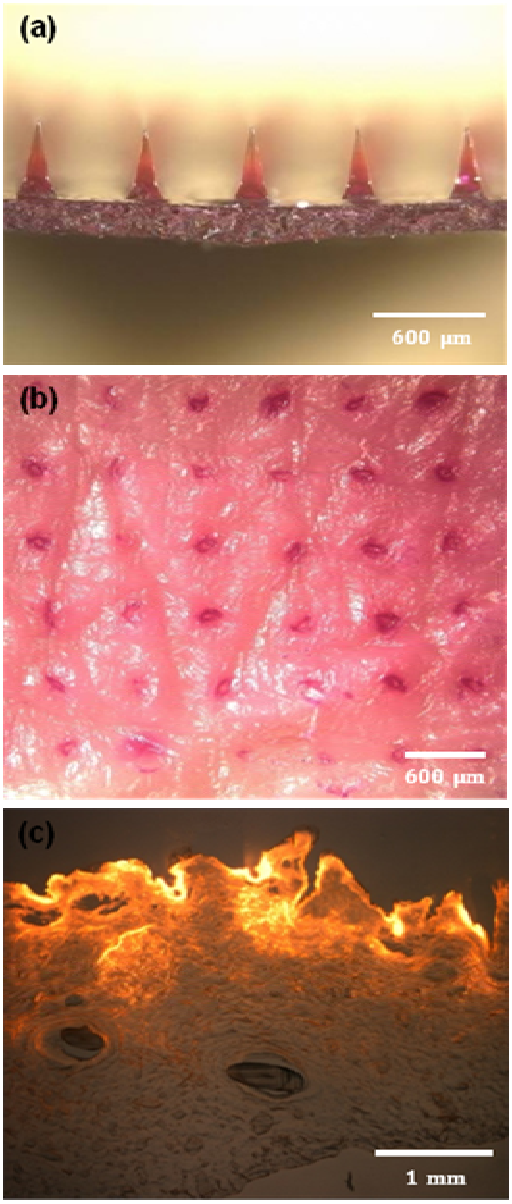

Figure 4.7 Dissolving microneedles for sustained release. (a) CMC pyramidal microneedles encapsulating sulforhodamine only in the backing layer. (b) Skin surface showing sulforhodamine delivered into the skin by insertion of the microneedles shown in part (a) for 12 h. (c) Cross-sectional histological image of skin pierced by the microneedles shown in part (a) for 12 h and imaged by an overlay of brightfield and fluorescence microscopy. Pig cadaver skin was used.

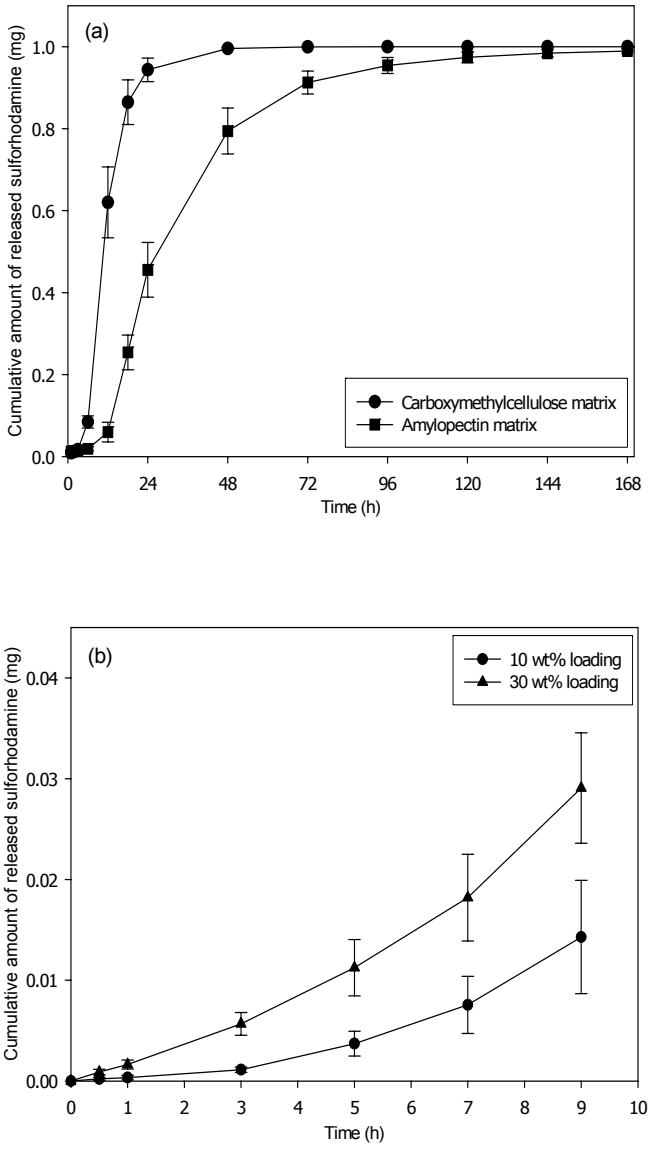

Figure 4.8 Transdermal release profile from dissolving microneedle patches. (a) Cumulative release of sulforhodamine encapsulated at 10wt% in the pyramidal microneedles and the backing layer of patches made of CMC and amylopectin. (b) Cumulative release during the initial release period of sulforhodamine encapsulated at 10 wt% or 30 wt% only in the backing layer of CMC patches. Human cadaver epidermis was used. Average values are shown with standard error bars based on 3 replicate measurements.

4.1.4 Drug stability after encapsulation in dissolving microneedles

Dissolving microneedles were designed to encapsulate sensitive biomolecules using a gentle fabrication process. Lysozyme was used as a model protein to assess success of this design and the integrity of lysozyme was studied with the measurement of changes in secondary structure and enzymatic activity after encapsulation and storage in CMC microneedle patches.

Circular dichroism (CD) analysis of untreated lysozyme compared to lysozyme encapsulated within a microneedle patch and then released by dissolution in water showed no detectable change in protein secondary structure (Figure 4.9 (a)). Even after storage of microneedle patches containing lysozyme for 2 months at room temperature, protein structure was unchanged (Figure 4.9 (a)). As a positive control, the CD spectrum showed extensive degradation of secondary structure after thermal denaturation (Figure 4.9 (a)).

To further test lysozyme integrity, enzymatic activity of lysozyme was measured (Figure 4.9 (b)). To make sure that the presence of dissolved CMC after microneedle dissolution did not create an artifact, a CMC microneedle containing no lysozyme was dissolved in PBS and then mixed with untreated lysozyme. This resulted in no change in lysozyme activity (Student's t-test, $p=0.51$). To test the effect of encapsulation, microneedles containing encapsulated lysozyme were dissolved in PBS and found to have no loss of enzymatic activity compared to untreated enzyme (Student's t-test, $p=0.28$). After two months of storage, lysozyme released from microneedles retained 96% enzymatic activity, indicating a small loss of activity (Student's t-test, $p=0.03$).

From the results of CD and enzymatic activity test, a model enzyme, lysozyme, encapsulated in CMC microneedles was not substantially degraded after two months storage at room temperature. This stability may be explained by the limited molecular mobility in the solid sate that is known to enhance protein stability [87]. Additional studies are needed to determine if other proteins are similarly stable. For this, the study of human growth hormone (hGH) delivery with the dissolving microneedles system was designed to assess the efficiency of the dissolving microneedles system as the platform of transdermal administration of biopharmaceuticals.

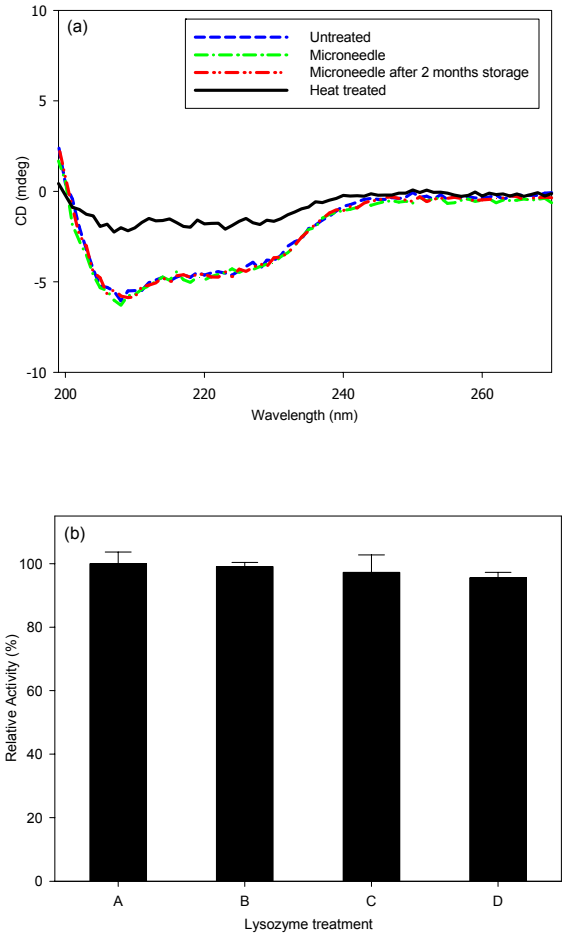

Figure 4.9 Protein stability after encapsulation and release from dissolving microneedles. (a) Circular Dichroism spectrum of untreated lysozyme (negative control); lysozyme encapsulated in CMC microneedles and released by dissolution in PBS; lysozyme encapsulated in CMC microneedles and released by dissolution in PBS after 2 months storage at room temperature; and lysozyme denatured at 80^{o}C for 30 min (positive control). (b) Enzymatic activity of untreated lysozyme (A, negative control); lysozyme mixed with dissolved placebo CMC microneedles (B, negative control); lysozyme encapsulated in CMC microneedles and released by dissolution in PBS (C); lysozyme encapsulated in CMC microneedles and released by dissolution in PBS after 2 months storage at room temperature (D).

4.2 Human growth hormone delivery results

Since recombinant gene engineering techniques have enabled the synthesis of human growth hormone (hGH), hGH deficient patients have been able to maintain required physiologic level of hGH by injection of recombinant hGH. However, they must be injected almost daily by trained personnel. Thus, hGH formulated and fabricated in dissolving microneedle patches are expected to minimize the need for injections by providing an easy and convenient administration technology without the fear and inconvenience of needles. Therefore, hGH was selected as a model drug in the study of dissolving microneedles for delivering biopharmaceuticals.

Guided by previous work with dissolving microneedles, the study of human growth hormone delivery was designed by examining some questions that must be answered for the delivery of hGH. (1) What is the amount of proper time for the administration of the microneedle-based patch application? The recovery of skin barrier properties is a critical consideration for microneedles patch application, because drug delivery is based on skin barrier removal. The microneedle application time will be contingent on the recovery of the disrupted stratum corneum. (2) How will the integrity of human growth hormone encapsulated in the microneedles be changed during the fabrication process and storage? The stability of biopharmaceuticals is directly related to the manufacturing cost of the amount of drug required to achieve therapeutic effects. Moreover, the stability time will also guide the storage of biopharmaceuticals while they are being transferred from the manufacturer to the patients. (3) What is the bioavailability of hGH encapsulated in microneedles compared to normal injection methods with hypodermic needles? Similar to the question number two, bioavailability is a consideration when determining the choice

of the biotherapeutic delivery platform as well as the most important factor in terms of the manufacturing cost. (4) Will there be the unfavorable skin reactions when the dissolving microneedles system is applied to skin? Contrary to the conventional injection method using hypodermic needles, dissolving microneedles leave the drug and the matrix material within the upper layer of skin where a responsive reaction might develope when the material comes through the skin. This safety problem should be also clearly assessed.

4.2.1 Skin resealing

As described above, transdermal drug delivery with microneedles is based on the removal of the skin barrier; therefore, the skin resealing time must be estimated. The kinetics of skin resealing after the insertion of dissolving microneedles was studied using a skin impedance measurement. The stratum corneum is a medium of weak electrical conduction, because it is a good electrical insulator with almost 10^6 $\Omega \cdot cm^2$ of resistivity [114]. Depending upon the degree of dehydration of stratum corneum or the amount of brakeage of the stratum corneum, the impedance between two sites of normal skin and disrupted skin will be dramatically changed. Generally, the impedance between the two sites decreases sharply with the removal or breakage of the stratum corneum and then increases gradually as a function of the recovery of the skin as shown in Figure 4.10.

The group C (green dots) in Figure 4.10 is the control group representing normal skin without the insertion of microneedles. When the skin was occluded at 0 hour, skin impedance decreased rapidly and stayed unchanged until the occlusion system was removed. After the skin was unoccluded at 24 hour, the impedance increased quickly and returned to the normal state before the occlusion. In the group B (red dots), dissolving

microneedles were inserted and immediately removed from the skin, and then the skin was occluded. In group B, the skin impedance was almost 10 folds lower than the control group (group C) at 1 hour after the insertion and the immediate removal of dissolving microneedles. After the removal of the occlusion system at 24 h, the impedance of the group B and C increased and returned to normal within 6 hours.

Unlike group B, group A, in which dissolving microneedles were inserted and applied for 24 hours, showed the different behavior in the impedance after 24 h. After the removal of the occlusion system at 24 h, group B showed rapid increase in impedance, but group A showed a gradual increase 100 folds lower in range than the impedance of group B.

It is possible that group C became hydrated by the occlusion system, causing the skin to become more electrically conductive by the addition of strongly dipolar water molecules [114], while group B experienced a break in the main electrical insulation layer of the skin, stratum corneum, causing the decrease in impedance. Therefore, it is highly probable that the lower value of group B impedance compared to group C is the effect of the stratum corneum breakage. While the impedance of the group C stayed unchanged until the removal of the occlusion system at 24 hour, the impedance of group B increased gradually, thus implying recovery of the skin barrier with time.

However, skin resealing of group A occurred slowly in comparison to the impedance measured in group B. It is likely that the dissolved microneedles material, CMC remained in the skin and retarded the recovery of the skin barrier. Another result also supporting this observation was seen in group D, where dissolving microneedles were inserted and immediately removed from the skin in a similar manner to group B.

The treated skin was then covered with the backing made of the same matrix material as that used in group A, CMC. While this treatment caused material to remain in the skin like in group A, the backing in group D was much less dissolved in the skin and a higher increase in impedance than group A was measured.

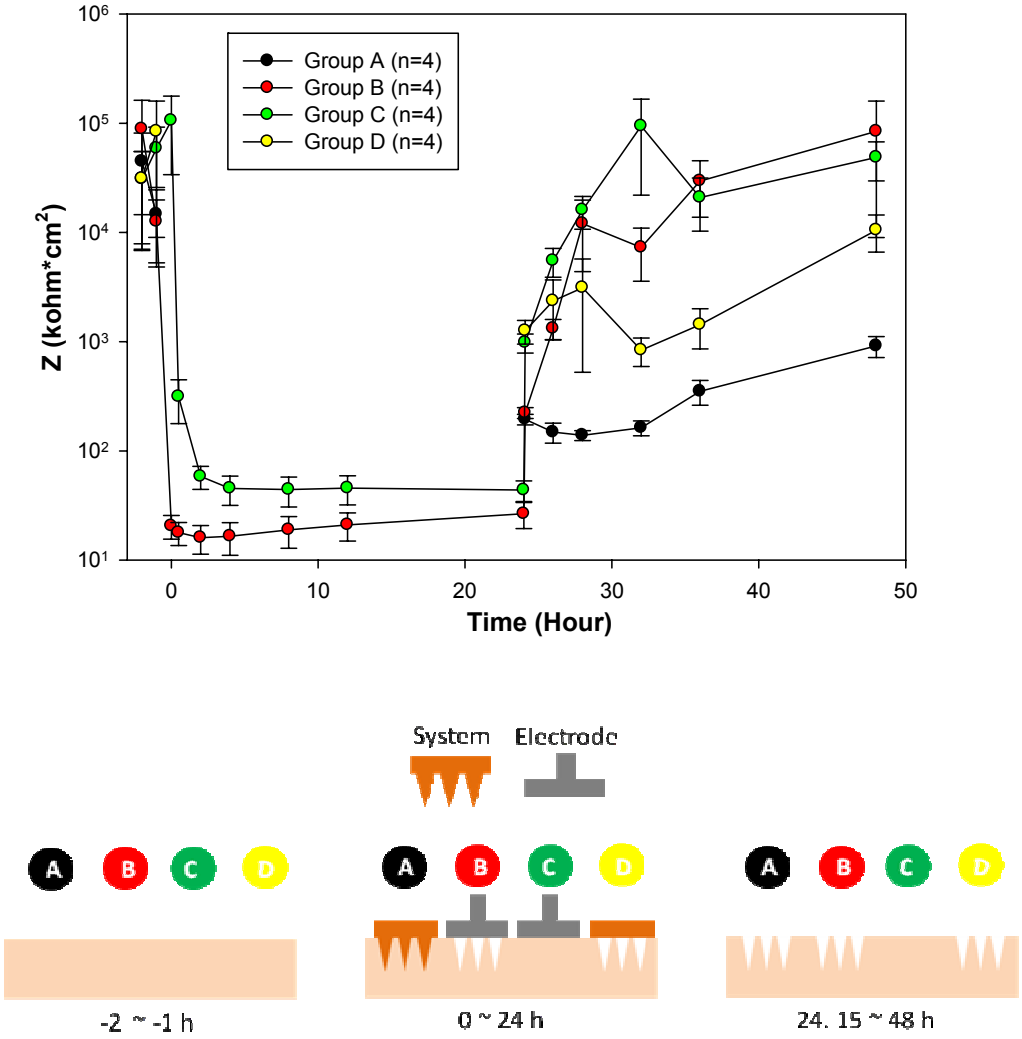

Figure 4.10 The impedance measurement of the skin after the insertion of dissolving microneedles.

These differences in the way that skin impedance changes after each treatment implies that skin inserted and covered with the dissolving microneedle patch may recover stratum corneum slowly and that the dissolving microneedle patch system can be applied at least for one day, which may be extended to two days unless side effects such as the skin irritation occur. However, this is only the possible application time as estimated by the skin resealing time; this does not necessarily mean that microneedle patches should be applied for long periods of time due to the fact that microneedles can dissolve within a few hours, as estimated in section 4.1.3. Thus, bolus release of drugs with dissolving microneedles can likely be completed within a few hours regardless of the skin resealing process.

The delayed resealing process of the treated skin might enable sustained delivery using dissolving microneedles. If the backing material of the microneedles is swollen with the interstitial fluid from the skin or fluid from the external device, drugs in the backing material can diffuse faster, thus allowing transdermal drug administration with the dissolving microneedle patch to probably achieve a controlled therapeutic effect of the drug for the prolonged time.

On the other hand, the result shown in Figure 4.10 may be used to prevent infection that might occur due to the incompletely sealed skin. Based on the observed changes of the impedance, it is believed that the dissolving microneedle patch for bolus release can be applied to skin for less than a few hours and then the skin might need to be covered for several hours to block entry of the external dangerous species that can cause infections in the skin.

4.2.2. Human growth hormone activity

We next sought to determine if the processes required for hGH encapsulation in microneedles would damage the integrity of hGH. Depending on the process conditions used for the formulation of protein biotherapeutics, drugs can exist as various forms (ref) such as: covalently or non-covalently linked dimers, higher-order aggregates, and clipped forms by degradation due to deamidation. These deteriorated forms of hGH might also occur in the fabrication process of dissolving microneedles and would decrease the bioavailability of dissolving microneedles encapsulating hGH. Thus, the integrity of hGH was investigated with two methods: (1) SDS-PAGE, used widely to identify proteins on the basis of molecular weight and (2) Nb2 cell growth analysis for the functional structure of hGH, which is relevant to the biological activity of hGH.

4.2.2.1 Electrophoresis (SDS-PAGE)

SDS-PAGE is used to obtain protein size information. If proteins are cleaved due to the reaction in the degradation pathway or if dimeric proteins are formed by the reduction of the disulfide bonds, they would appear at a position different from the original molecular weight position of the protein.

Figure 4.11 shows the electrophoresis result of the non-processed and processed human growth hormone. The processed hGH is hGH encapsulated with CMC dissolving microneedles fabricated using the same process as described in section 4.1 and the non-processed hGH is the hGH prior to the fabrication process. In Figure 4.11, both non-processed and processed hGH appeared at the molecular weight position of 22 kDa and

the intensity of the bands were almost the same. This shows that the original structure of hGH was not damaged by processing, therefore, the centrifugally modified solvent casting process used to make hGH microneedles may be compatible with the formulation of other protein drugs.

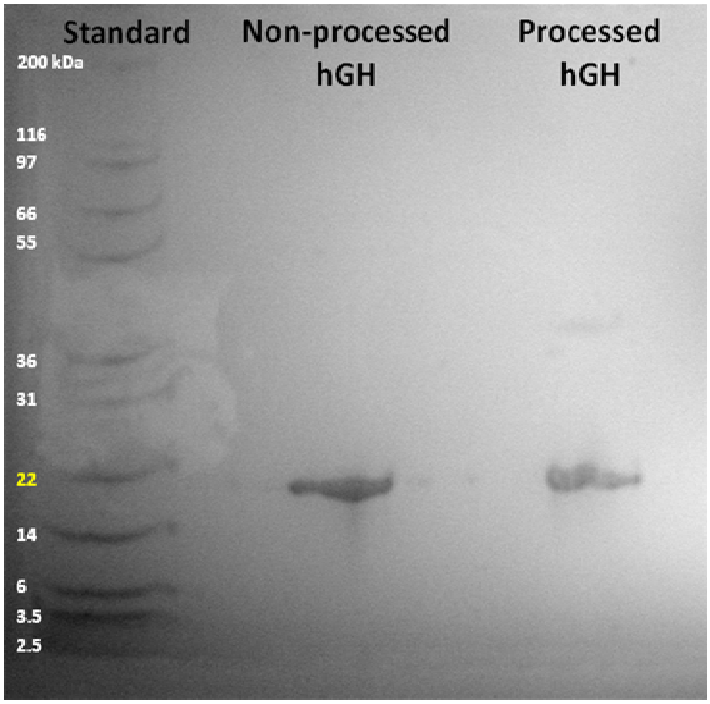

Figure 4.11 SDS-PAGE result of non-processed hGH and processed hGH encapsulated within CMC dissolving microneedles.

However, a very vague band in the column of the processed hGH was found at the molecular weight of the dimer form (44 kDa) of hGH, implying the possibility of forming

dimer during the fabrication process. Biosynthetic 22 kDa hGH can exist as the noncovalent dimer mediated by the Zn ion [115], or the covalent dimer with disulfide bond induced by reducing agents [116]. Even though noncovalent dimer is presumed to be the major storage form of 22 kDa hGH in the pituitary and was found to be more stable form compared to monomeric hGH denaturation in guanidine-HCl [115], it is known to have less somatogenic activity than monomeric hGH, e.g. almost one third the potency of momomeric 22 kDa hGH [117]. Also, the covalent dimer was reported to have about 10% of the growth promoting activity of a monomer [117]. Thus, the dimeric form of hGH should be controlled in the fabrication process, but the result in Figure 4.11 shows that the band intensity of the dimer seems to be insignificant. Additional tests such as functional activity or pharmacokinetics of hGH should be examined to obtain an overall conclusion about the integrity of hGH encapsulated in CMC dissolving microneedles.

4.2.2.2 Analysis of functional activity of hGH

The next step for examining the integrity of hGH encapsulated in CMC dissolving microneedles was the use of an analytical method to assess the functional activity of hGH. The Nb2 cell population method [100, 101], originally used to measure the concentration of hGH, was employed to estimate the biological activity of processed hGH.

Nb2 tumor cells are derived from estrogenized rat lymphoma. While originally cultivated in bovine serum-based culture medium, Nb2 cells stop growing and end proliferation when transferred to horse serum-based culture medium. Nb2 cells in horse serum culture medium resume cell growth upon addition of hGH, and the concentration of cells depends on the concentration of hGH added to the medium. Thus, the biological

activity of hGH encapsulated in CMC dissolving microneedles can be assessed by comparison of the Nb2 cell concentration after the stimulatory treatment with hGH.

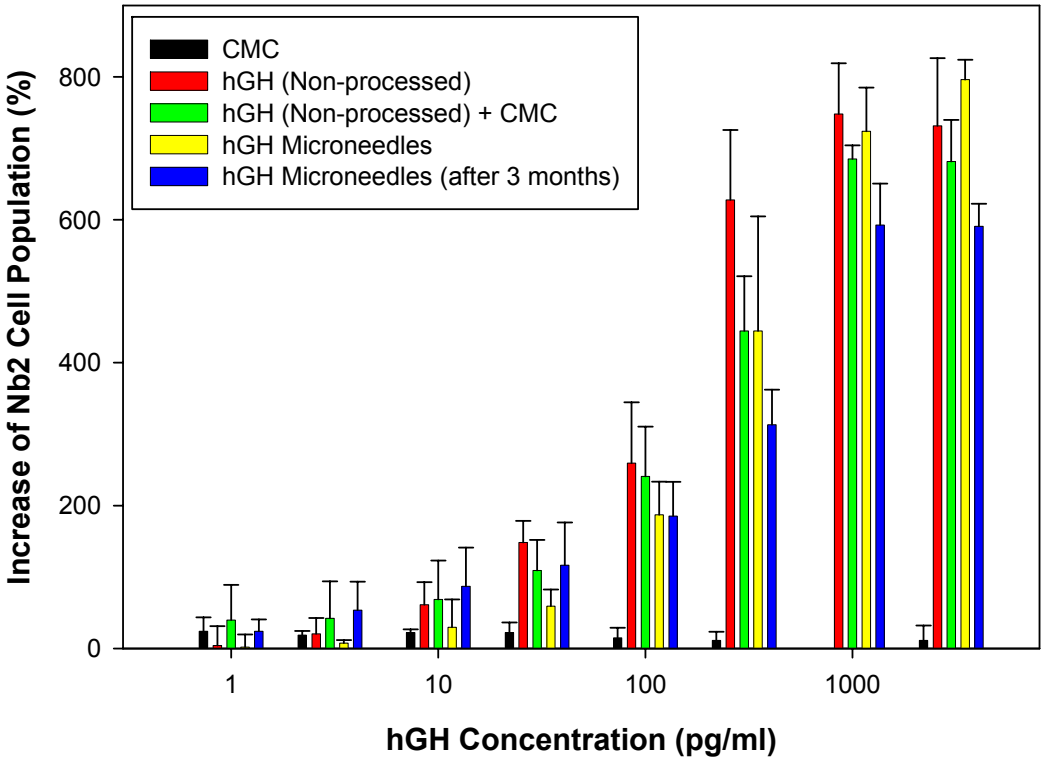

Figure 4.12 The increase of Nb2 cell population after the treatment with hGH solution made with the reconstitution of hGH encapsulated in CMC dissolving microneedles (Yellow group), hGH encapsulated in CMC dissolving microneedle for 3 months without controlling humidity or temperature (Blue group), non-processed hGH (Red group), non-processed hGH mixed with CMC processed with the same fabrication method (Green group), and no hGH solution having only processed CMC (Black group). With exception of the red group, all groups have the same mass proportion of CMC at each hGH concentration (1 hGH: 95 CMC).

Figure 4.12 shows the increase in Nb2 cell population stimulated by adding various types of hGH solution. Typically, it has been known that the concentration of hGH from 1 pg/ml to 1 ng/ml has the proportionality to the increase of cell population and the hGH concentration higher than 1 ng/ml has the saturation effect of the cell growth [100, 101]. The red group, the negative control showed the almost 750% population increase due to the cell growth stimulation effect of hGH (ANOVA with the replicates at all concentration, $p=3.85\times10^{-16}$) and the range of the increased population corresponded well to the value in other references [100, 101]. However, the black group treated with a solution of only reconstituted processed CMC but not hGH, which is used as placebo, showed no effect of cell growth, meaning the same population over all concentrations (ANOVA with the replicates at all concentration, P=0.29), thus excluding the possibility of growth stimulation by CMC.

The cell populations at each hGH concentration were compared for all groups with hGH using the two-factor ANOVA (95% significance) statistical method; (1) Red group (non-processed hGH), (2) Green group, in which non-processed hGH is mixed simply with the processed CMC, (3) Yellow group, in which hGH is encapsulated in CMC dissolving microneedles, and (4) Blue group, in which hGH is encapsulated in CMC microneedles for 3 months. According to the two-factor ANOVA result (ANOVA for the type of hGH solution, $p=9.71\times10^{-6}$ and ANOVA for the hGH concentration, $p=2.05\times10^{-67}$), the cell population based on each hGH type was not the same over all concentrations. The three ANOVA p values for the two-group comparison of red/green, red/yellow, and red/blue over all concentration were 0.02, 0.01, and 9.55×10^{-7}, respectively. Additionally, the p value of red/green comparison over all concentration was 0.31 (except 300 pg/ml)

meaning that the mixed CMC does not have any stimulation or inhibition effect on the cell growth. The p value of red/yellow comparison over all concentrations was 0.0503 (except 30 pg/ml) meaning that hGH encapsulated in CMC dissolving microneedles cause the same increase in population in the red group. Using this statistical analysis and the result of Figure 4.12, the integrity of hGH in the blue group (3 months storage) may be significantly different from that in the red, green, and yellow groups.

To determine this, single ANOVA analyses of these 4 groups at the highest concentration were performed. At each of 300, 1000, and 3000 pg/ml, red/green/yellow group showed the same increase of population ($p=0.09$, 0.31, and 0.1, respectively). However, the comparison of red/green/yellow/blue at each of 300, 1000, and 3000 pg/ml suggested that they had different cell population ($p=0.0089$, 0.0099, and 0.0027). Therefore, it is suggested that the processes used to fabricate hGH encapsulating microneedles did not damage the integrity of hGH.

Based on the result of the activity test with Nb2 cells, hGH encapsulated in CMC dissolving microneedles still maintained its integrity and biological activity, but an approximately 15% reduction of the maximum increase in cell population was found at the saturation range, 1000 and 3000 pg/ml, of hGH concentration. Thus, it is highly probable that hGH in CMC microneedles loses its integrity partially after 3 months storage. However, hGH encapsulating CMC dissolving microneedles in the blue group was exposed to air (21% oxygen) with 21-25^{o}C and 35-45% relative humidity conditions without controlling these variables. It is expected that the activity loss of hGH encapsulated in CMC dissolving microneedles could be lessened using a controlled storage protocol, with lower temperature or by vacuum packaging to control humidity. In

conclusion, hGH encapsulated in CMC dissolving microneedles did not lose its biological activity and it is possible that the processes used to fabricate CMC dissolving microneedles may be compatible with the formulation of other sensitive biopharmaceuticals.

4.2.3 Pharmacokinetics of human growth hormone

Dissolving microneedles were designed to replace the administration of drugs using hypodermic needles with a painless, sharps-free, and self-administered delivery tool. However, these advantages over hypodermic needles can be highlighted when the dissolving microneedles system is able to achieve a similar level of bioavailability or pharmaceutical effect of the injection method by hypodermic needles. This work hypothesized that CMC dissolving microneedles can deliver drugs without loss of integrity by breaking the skin barrier and releasing drugs upon the dissolution of the microneedles matrix. To verify this hypothesis, it was demonstrated that hGH can be encapsulated in CMC dissolving microneedles without integrity loss as shown in Figure 4.11 and 4.12. Guided by this result, the pharmacokinetics of hGH were studies to assess how effectively CMC dissolving microneedles can deliver hGH to the body and to determine any difference from the injection method.

The preliminary result of in vivo delivery of hGH encapsulated in CMC dissolving microneedles showed less than 10% of the bioavailability of the subcutaneous injection delivery method (data not shown). The reason for this was thought to be the limited amount of interstitial fluid available to dissolve microneedle matrix material. To increase the dissolution rate, the microneedles matrix material can be formulated with a mixture of

polysaccharide and disaccharides. Polysaccharide is the mechanical support material for the insertion into the skin and disaccharide is used as the dissolution enhancer, lowering the required amount of water for dissolution of microneedles.

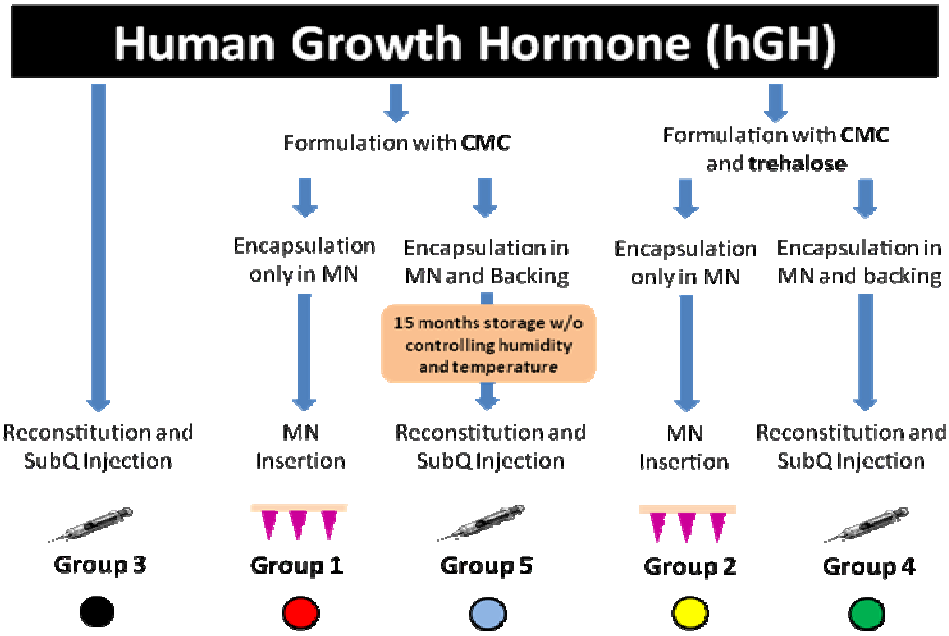

Figure 4.13 Summary of hGH formulation and administration. The subcutaneous injection of hGH as the positive control (Group 3, Black), hGH formulated with only polysaccharide CMC (Group 1, Red for the microneedle administration and group 5, Blue for subcutaneous injection of the reconstitution), hGH formulated with the mixture of polysaccharide, CMC and disaccharide, trehalose (Group 2, Yellow for the microneedle administration and Group 4, Green for subcutaneous injection of the reconstitution). Especially, hGH in group 5 was stored for 15 months without controlling humidity and temperature after the encapsulation in CMC matrix material.

It was hypothesized that CMC/trehalose microneedles have higher bioavailability than CMC microneedles because CMC/trehalose microneedles dissolve faster in the skin and thereby release more hGH during the same period of time. Based on this assumption, hGH was formulated with two types of microneedle matrix, CMC and CMC/trehalose mixture. The summarized description of hGH formulation and administration in each group is shown in Figure 4.13.

The pharmacokinetics profile of each group is shown in Figure 4.14. The group 1 in Figure 4.14 represents the originally designed dissolving microneedles which are made of only CMC polysaccharide, which releases hGH by the dissolution of CMC microneedles. As shown in Figure 4.14, the serum concentration of hGH of group 1 at the peak time between 0.5 and 1 hour was 6 fold lower than one of the subcutaneously injected unprocessed-hGH (group 3) (student's t-test, 95% significance, $p=2.258\times10^{-6}$) and the area under the profile of group 1 was approximately 9 fold lower than one of group 3 (student's t-test, 95% significance, $p=1.41\times10^{-6}$). Contrary to group 1, hGH in group 2 fabricated with the mixture matrix of CMC and trehalose showed almost the same but just 1.3 fold lower serum concentration than one of group 3 at peak time (student's t-test, 95% significance, p=0.15) and the area under the profile of group 2 was 1.5 fold lower than that of group 3 (student's t-test, 95% significance, p=0.0143). For the comparison of group 1 and 2, hGH in group 2 showed almost 5 fold higher serum concentration than group 1 at peak time (student's t-test, 95% significance, p=0.0003) and the area under the profile of group 2 was 6 fold higher than group 1 (student's t-test, 95% significance, $p=1.23\times10^{-5}$). The area under the profile and bioavailability of all groups are summarized in Table 3.1.

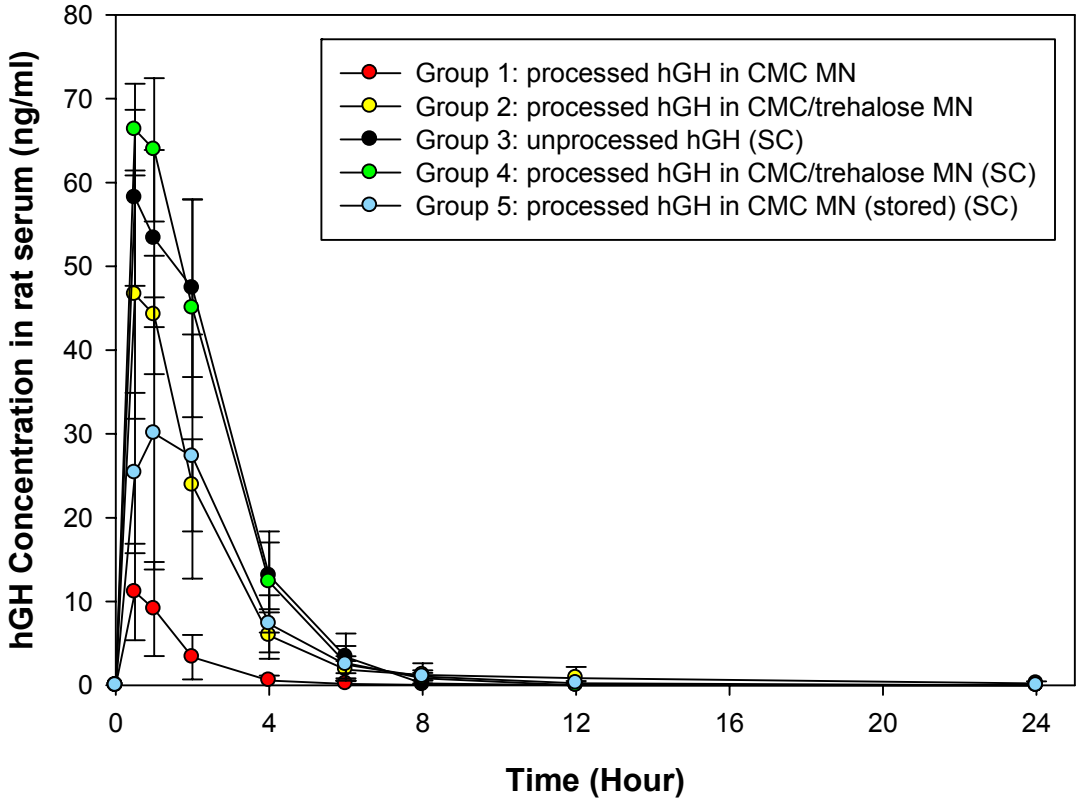

Figure 4.14 Pharmcokinetics profile of hGH in rat serum. Microneedle administration of hGH in CMC microneedles (Group 1, n=6), Microneedle administration of hGH in CMC/trehalose microneedles (Group 2, n=6), Subcutaneous injection of hGH as the positive control (Group 3, n=6), Subcutaneous injection of the reconstitution of hGH in CMC/trehalose microneedles (Group 4, n=6), and Subcutaneous injection of the reconstitution of hGH in CMC microneedles stored for 15 months after the fabrication (Group 5, n=3). MN and SC represents microneedles and subcutaneous injection, respectively.

Table 4.2 The applied dose (μg), area under curve (*AUC in hr·ng/ml), and bioavailability (BA in %) of samples from each group in Figure 4.14.**

Group		Group 1 (n=6)	Group 2 (n=6)	Group 3 (n=6)	Group 4 (n=6)	Group 5 (n=3)
Dose (± SE)		148 ± 3	164 ± 13	169 ± 6	167 ± 19	162***
Avg.	AUC (±SE)	**20 ± 5**	**120 ± 11**	**174 ± 14**	**181 ± 11**	**101 ± 28**
	BA (±SE)	**13 ± 3**	**71 ± 7**	**100 ± 8**	**106 ± 6**	**61 ± 17**

*AUC was calculated with trapezoid area formula. **BA = $(AUC_{group}/Dose_{group})/(AUC_{group\ 0\ avg.}/Dose_{group\ 0\ avg.})$
*** Based on the formulation value

The difference between the pharmacokinetics profiles of groups 1 and 2 is probably a result of the different microneedles matrix materials. To verify this hypothesis, two things were examined; (1) microscopic images of the microneedles surface after 24 h application and (2) the measurement of the remaining hGH in the system after 24 h application.

The surfaces of CMC microneedles (group 1) and CMC/trehalose microneedles (group 2) were imaged using scanning electron microscopy as shown in Figure 4.15. While CMC microneedles retained the blunt upper part of the original microneedle shape, CMC/Trehalose microneedles almost disappeared, leaving a small amount of bumpy surface. Due to the relatively higher solubility property of trehalose over CMC, it is probable that the CMC/trehalose mixture matrix could more easily dissolve and thus release encapsulated hGH faster than the CMC alone matrix.

The remaining hGH in group 1 was 69 ± 3 % (±SE) of total amount of hGH before application while group 2 was 17 ± 3 % (±SE) of total amount of hGH before the

application. Using the bioavailability (BA) information in Table 3.1 and measuring the amount of hGH remaining in the system, groups 1 and 2 had 82 % (13 % BA + 69 % remaining hGH) and 88 % (71 % BA + 17 % remaining of hGH) of total amount of hGH in the system before the insertion. The uncounted part of hGH (18 % for group 1 and 12 % of group 2) can be explained by the comparison of group 3. In group 3, the total hGH dose that was administered rapidly by a hypodermic needle can circulate almost immediately to the blood vessels; therefore the drug infusion time is shorter than that of group 1 where hGH is released relatively slowly from the microneedle matrix resulting in a lower infusion rate. Thus, blood from group 3 will have a more rapid increase of hGH concentration while blood from groups 1 and 2 will increase hGH concentration more slowly. On the other hand, blood with a lower concentration of hGH will clear hGH more effectively and easily; therefore, groups 1 and 2 may have cleared hGH from the body, explaining why there is some hGH unaccounted for thin the measurements described above.

Regarding the bioavailability of hGH formulation, another interesting result was observed that may also support this finding. When reconstituted CMC/trehalose encapsulating hGH was injected subcutaneously (group 4), the pharmacokinetic profile over time of this group 4 was almost the same as that of group 3 (two-factor ANOVA, 95% significance, $p=0.15$) and the bioavailability of hGH in both groups was almost the same (Student's t-test, 95% significance, $p=0.61$). This implies that if the dissolving microneedles had less drug remaining in the system after insertion, it may be a successful replacement for hGH administration. However, this must be achieved by a perfect insertion of dissolving microneedles made out of the mixture of polysaccharide and

disaccharide, thus creating high bioavailability comparable to subcutaneous injection. It is therefore worth examining this by designing a new geometry of dissolving microneedles to be inserted more perfectly into skin, thus enhancing the rate of dissolution and minimizing the amount of drug remaining in the system.

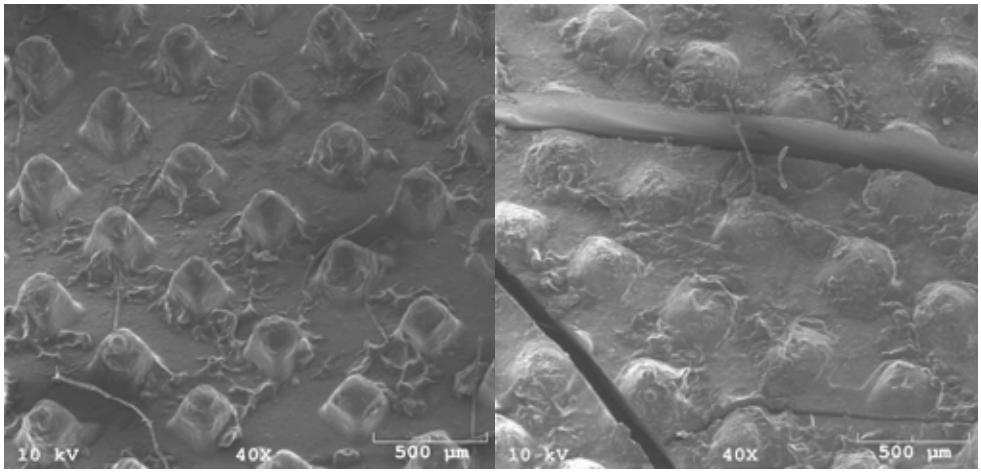

(a) (b)

Figure 4.15 SEM images of dissolving microneedles after 24 hours of insertion; (a) CMC microneedles and (b) CMC/Trehalose microneedles.

It was also hypothesized that encapsulating drugs in the solid form of dissolving microneedles can assist in manufacturing biotherapeutics for extended periods of time due to the limited mobility of the molecules when stored in this from [32]. To determine how long hGH will maintain integrity in dissolving microneedles, hGH encapsulated in CMC microneedles was stored for 15 months (group 5) without humidity or temperature

control to simulate the storage of normal drugs in the home. hGH in group 5 was subcutaneously injected after reconstitution.

As shown in Figure 4.14, the bioavailability of hGH in group 5 was estimated as approximately 60% compared to bioavailability of hGH in group 3. In a previous study using SDS-PAGE (section 4.2.2.1) and Nb2 cell population (section 4.2.2.2) to examine the integrity of the processed hGH and the pharmacokinetics of hGH, it was seen that hGH processed for the fabrication of dissolving microneedles did not lose its integrity, and showed that it was similar levels or insignificant changes in parameters from the non-processed hGH.

However, after 3 months (Nb2 cell assay) and 15 months of storage (Pharmacokinetics), hGH assayed for these showed the lower levels, 85% and 60%, respectively. However, since the hGH studied in this work was stored without control over the storage conditions, it is highly probable that dissolving microneedles can encapsulate biotherapeutics and maintain their integrity for a long periods of time when storage conditions are controlled at low temperature and/or low humidity.

Regarding the stability of the commercialized recombinant hGH, the suggested shelf life for freeze-dried hGH is around 2 years with the storage at 2-8^{o}C and the reconstituted solution can be stored for around 2 weeks at 2-8^{o}C [118]. However, the major degradation reactions; deamidation, oxidation, and aggregation were found after the storage of freeze-dried hGH in 5 ml vial with a nominal nitrogen headspace (~0.75% O_2) at room temperature (25^{o}C) over 6 months [119]. The freeze-dried hGH with no excipients stored under these condition showed around 12% decomposition of hGH by oxidation. It was found that even small increase (from 0.4% to 0.75%) of oxygen concenration

resulted in almost 2 fold higher degree of oxidation (the molar ratio of oxygen to hGH at 0.4% oxygen is around 10, which is more than sufficient from a stoichiometric viewpoint). Comparing this with hGH encapsulated in microneedles, microneedles system, which is exposed to 21% oxygen (air), seems to be able to reduce the oxidation by limiting the approach of oxygen molecules to hGH molecules in microneedles. Thus, it is probable that the stability of hGH for the long term storage can be improved by considering these.

4.2.4 Skin reaction

Organ systems used for the drug administration will show some functional responses to the artificial methods in which some treatments are applied for the enhancement of the drug absorption, recognizing those as the invaders and trying to regain the normal [38, 120]. Because the mechanism of dissolving microneedles is to break the skin barrier, stratum corneum, to be dissolved in the skin leaving microneedles matrix material, and then to release drug into the body, it is believed that the skin will react against the breakage of the skin or the material left inside. To assess the skin reaction caused by the insertion of dissolving microneedles, erythema was measured (Figure 4.16) by using 0-4 scale with half-point ratings [102] and the surfaces of the skin inserted with microneedles were examined as shown in Figure 4.17.

As expected, the surface of the skin inserted by a hypodermic needle (group 3 and 4 in Figure 4.16) did not show any symptom suspected for the skin reaction at 24 h when the system was removed. The skin of group 3 and 4 was rated as normal over the whole time. However, group 1 and 3 inserted with microneedles showed only more reddish

color on the surface of the applied skin, but edema (skin swelling) was not identified as shown in Figure 4.17.

In Figure 4.17, the erythema symptom shown in group 1 and 2 decreased rapidly for the first 3 hours after the removal of the system at 24 h and it disappeared somewhat slowly over time. When 2 days passed after the removal of the system, the skin surface in both groups looked almost normal. After 3 days after the removal of the system, the surface of the applied skin returned to the normal before the insertion of the system and all skin surfaces were rated as normal as shown in Figure 4.16. However, the skin color of group 2 at 24 h was more reddish than group 1 and the erythema ratings of group 1 and 2 over time (Figure 4.16) were different (two-way ANOVA, 95% significance, $p=0.001$). This might be caused by the different microneedle matrix material. In group 2, the mixture of CMC and trehalose was used and the dissolution of mixture microneedles may be probably faster than CMC microneedles of group 1, resulting the faster clearance of microneedles matrix material and thereby the less redness. From the result of Figure 4.16 and 4.17, dissolving microneedles made out of polysaccharide or disaccharide did not cause severe erythema or edema. Even though the skin color was somewhat noticeable at the end of the 24 hours application, it started disappearing significantly soon and returned as normal skin within 2 days. Thus, it is suggested that dissolving microneedles can be used without the unfavorable skin reaction as one of alternatives for the enhanced transdermal drug delivery.

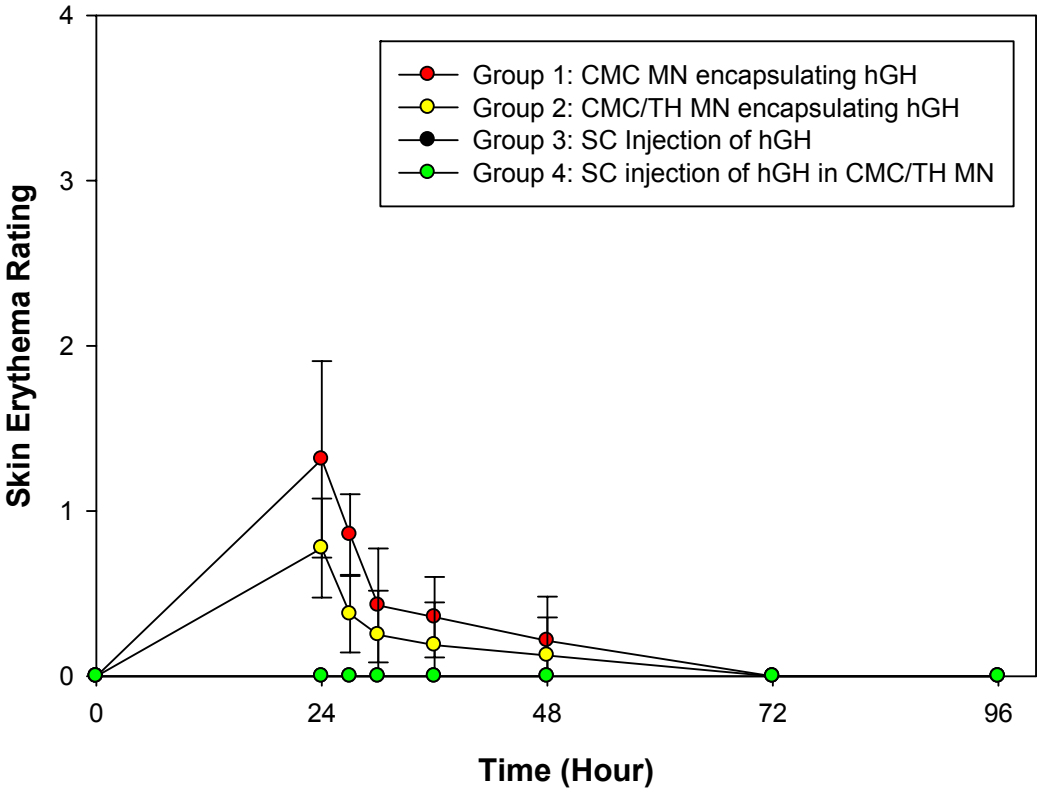

Figure 4.16 Skin erythema rating with 0-4 scale: 0-normal skin, 1-slight, 2-mild, 3-moderate, and 4-severe (very intense). For the first 24 hours, the skin and the system were occluded with the bandaging and the skin was kept unoccluded from 24 to 96 h with the removal of the system and the bandaging at 24 h. ($n \geq 4$ for up to 72 hours). Abbreviation: MN (microneedles), SC (subcutaneous), TH (trehalose), and CMC (carboxymethylcellulose).

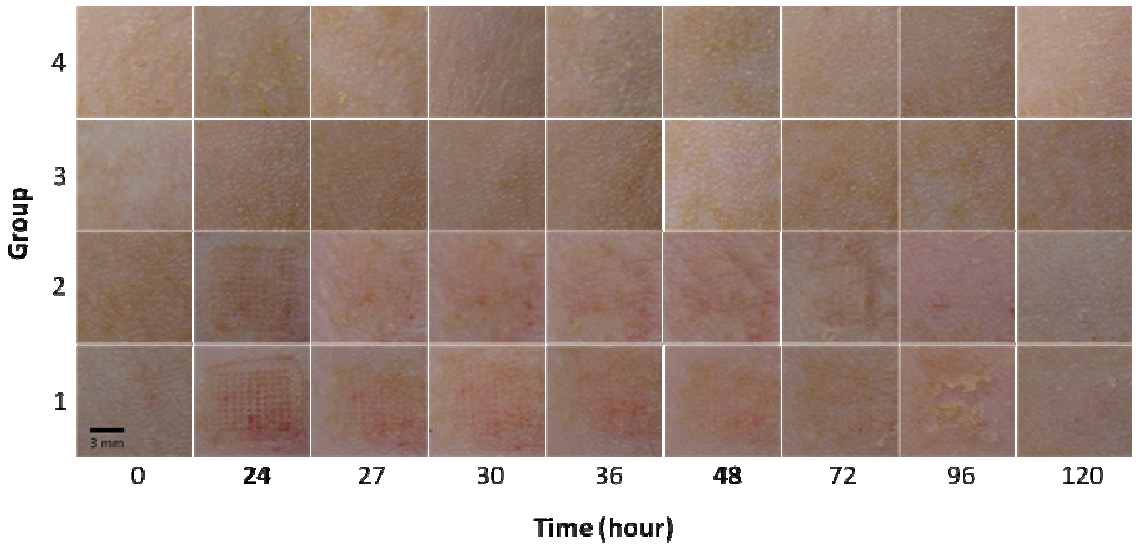

Figure 4.17 The representative image of the skin surface in the recovery progress after the administration of hGH with microneedles (group 1 and 2) or hypodermic needles (group 3 and 4). The skin was occluded with the system and the bandaging from 0 to 24 h and unoccluded after 24 h. hGH was administered through each skin with CMC microneedles (group 1), CMC/trehalose microneedles (group 2), a hypodermic needle after the reconstitution (group 3), and a hypodermic needle after the reconstitution of CMC/trehalose system (group 4).

We checked these skins by visually examining the histological images of them as shown in Figure 4.18. The skin of each group at 24 h, 48 h, and 1 week after the insertion of dissolving microneedles was sectioned, H&E stained, and viewed with the brightfield microscope. Figure 4.18 shows the histological images of the skin of group 1 and 2 at three different time points. The insertion sites in the skin at 24 h were easily found, but it was difficult to find them with the skin samples prepared for biopsy at 1 week after the insertion of microneedles, suggesting that the insertion sites were probably partially recovered at 24 h after the removal of the system. The skin samples of group 3 and 4

(subcutaneous injection) were found as the same to the untreated skin without noticeable features (data not shown), but the skin of group 1 and 2 at 24 h showed an interesting feature on the sites inserted presumably by dissolving microneedles as shown in Figure 4.18 and 19.

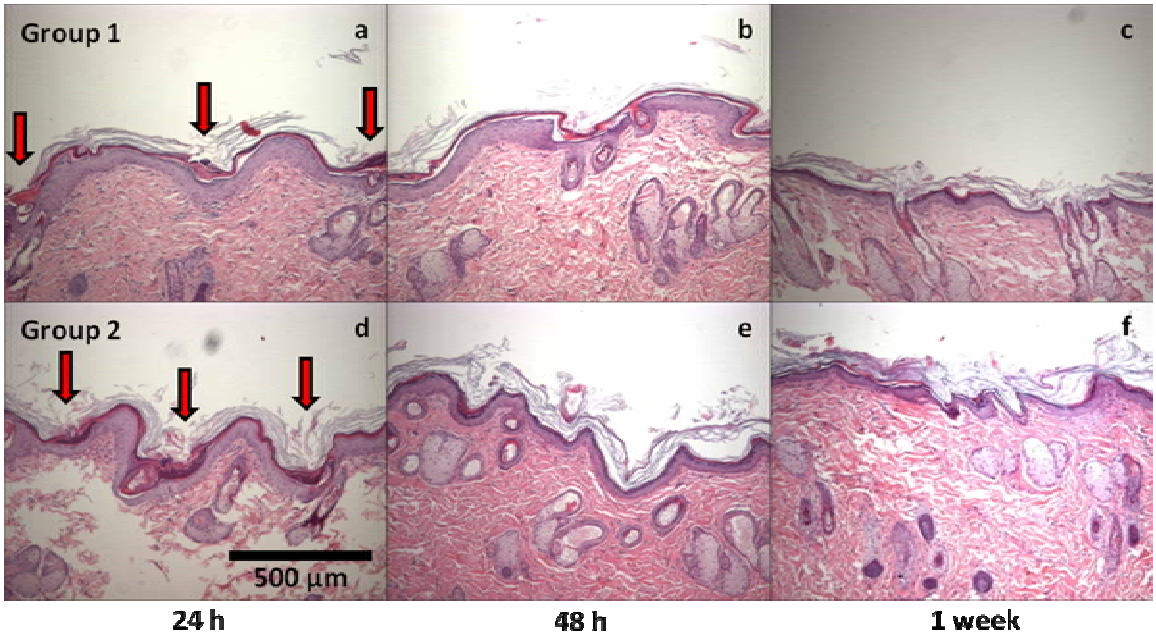

Figure 4.18 The histological images of the skin inserted by CMC microneedles (Group 1 – a, b, and c) and inserted by CMC/trehalose microneedles (Group 2 – d, e, and f) at 24 h (a and d), 48 h (b and e), and 1 week (c and f) after the insertion and the removal of dissolving microneedles 24 h.

Some features in which the processes probably related to the skin recovery were occurring intensively was found at the insertion sites of the skin at 24 h in both group 1

and 2 as shown in Figure 4.19 (g-h). A number of dark ball-shape structures were observed specifically at the site inserted with dissolving microneedles. This may probably be the cellular infiltration phenomenon which is the migration of macrophages associated with inflammations [121] to the skin sites of microneedles insertion. In Figure 4.18, it is thought that basophil granulocytes, one type of white blood cells, migrated to the insertion site and degranulated to release substances contributing to inflammation because basophils show dark blue color after H&E staining and the degranulating form at the upper layer of the damaged stratum corneum. The reddish color on the skin surface is likely to be the result of the increased flow of blood near the insertion site for the migration of basophils. Thus, it is highly probable that the inflammatory response occurred against the insertion of dissolving microneedles and would trigger the skin healing. These might be helpful features to prevent the infection problem that might happen with the application of dissolving microneedles.

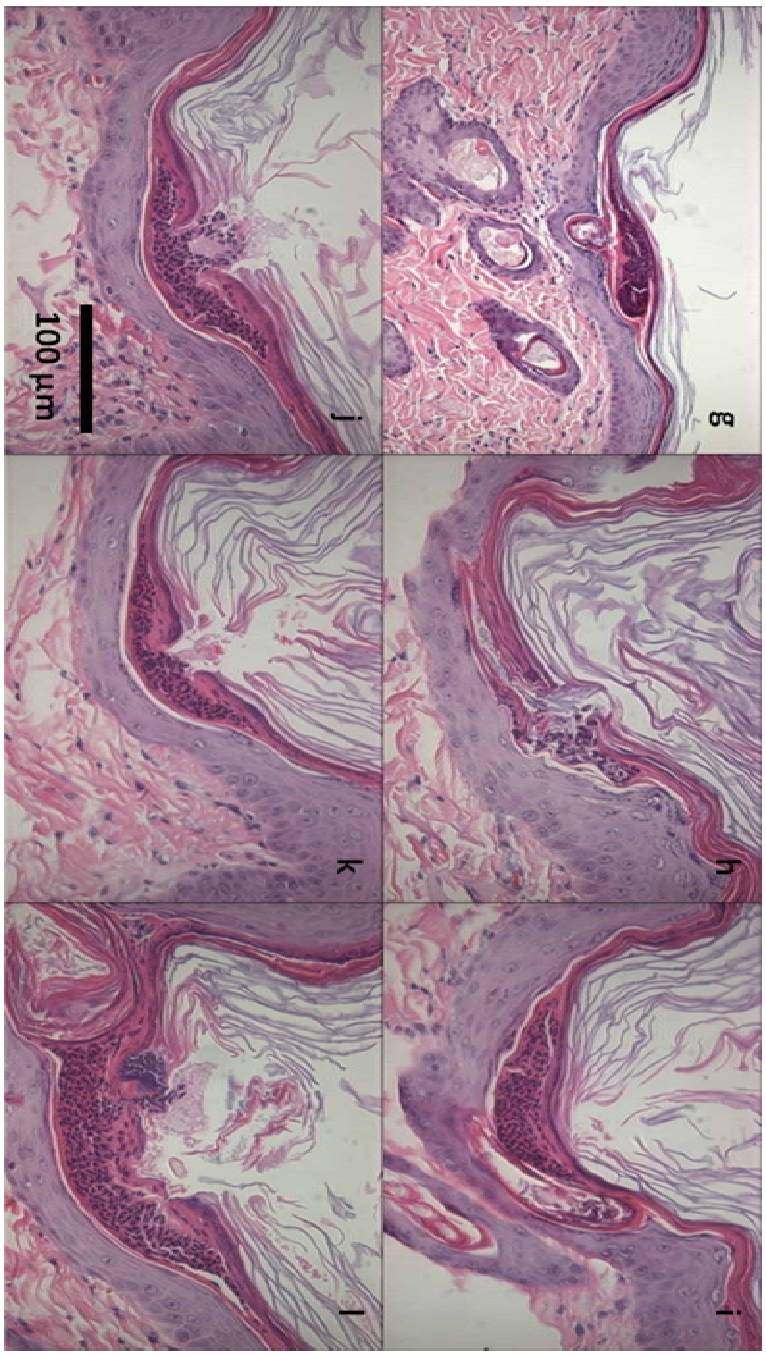

Figure 4.19 The magnified images (g-l) of the inserted sites of the skin in group 1 and 2 at 24 h

4.3 Micro skin ablation results

Various types of transdermal drug applications are designed to achieve therapeutic effects of drugs, which are not possible using the conventional transdermal patch, by disrupting integrity of the skin barrier, stratum corneum such as chemical enhancer [57], ultrasound [70], microenhancer array [24], tape stripping [89], and microneedle [20]. Thermal energy has also been used to remove stratum corneum for monitoring glucose [122] or delivering drugs [21, 91]. However, none of those based on thermal energy completely remove stratum corneum selectively and they ablate skin with the longer operation time than 1 ms.

We hypothesized that an extremely rapid pulse of thermal energy onto the skin can remove stratum corneum selectively without damaging deeper skin tissue, and allowing hydrophilic and macromolecular biotherapeutics to be delivered through the ablated skin. In this study, we (1) designed and developed the micro skin ablation (MSA) device to work on a timescale of micro second, (2) assessed the ability of the MSA to completely remove stratum corneum selectively, and (3) demonstrated increased skin permeability of hydrophilic or macro molecular compounds after treatment with the MSA.

To study this hypothesis, some important factors were considered. First, how much energy is necessary to ablate stratum corneum and at what speed should it impact the skin? The effect of thermal energy contact on skin have been reported for a long time, but most were skin burns or skin tissue damage due to a relatively long exposure to thermal energy. The rapid impact of ablation energy on skin will be the critical point in the design of the MSA device to achieve the selective removal of skin barrier.

Next, what type of energy source can be used to generate and transfer the ablation energy to the skin rapidly? This system should be able to transfer enough ablation energy to the skin within a specified amount of time to prevent deeper skin tissue damage. Using these specifications, a micro skin ablation (MSA) device based on arc discharge phenomenon was developed to generate energy impact and transfer it to the skin. When an arc is generated, it rapidly increases the temperature of the medium in which the arc occurs and a buildup of pressure follows after the discharge. Since arc discharge phenomenon can release thermal and mechanical energy very quickly [103], it is probable that enough energy to ablate stratum corneum can be sufficiently produced and then rapidly transferred to the skin.

Finally, it must be determined how much drug can be delivered using the MSA system. The MSA system will achieve therapeutic effect by passive diffusion of drug from the drug matrix into the skin in a manner similar to other conventional transdermal patch applications. The amount of diffused drug will be determined using parameters that control the rate of diffusion, including the area of diffusion, molecular weight of the drug, and the drug concentration in the matrix, but not with stratum corneum. In this study, the removal of stratum corneum by the MSA was controlled because the most important parameter will be the area of ablated skin through which drug can diffuse. Thus, it was important to control both the surface area and depth of stratum corneum removal. This could be achieved using two masking systems to guide the energy impact properly, followed by assessment of the permeation of drugs using Franz cell systems for in-vitro drug release experiments with two model compounds, sulforhodamine and Texas Red

BSA; which represent a small molecular weight drug and a high molecular weight biotherapeutic, respectively.

4.3.1 Fabrication and characterization of arc-generating device

Because the rapid impact of thermal energy on skin is a key to the success of the MSA system, arc discharge was considered to be a good model for the energy source of the MSA system. The arc generating system used to create the energy impact was fabricated by modifying the laminated gas generator actuator system [103]. The entire MSA system was designed to have two main parts; (1) a power supply circuit with the controller to provide electrical energy and (2) a microchamber to convert the provided electrical energy to ablation energy as shown in Figure 4.20. Two electrodes on the bottom and the top of the microchamber are connected to the circuit with discharging capacitors to supply electrical energy. All parts of microchamber shown in Figure 4.20 were fabricated with laser micromachining and lamination techniques so that the mass production of MSA system would be possible as a cartridge system combined with the additional electrical power supplier.

To generate the ablation energy, the microchamber was filled with PBS, which is used as the conductive medium necessary to induce arc discharge phenomenon in the microchamber, and then the electrical energy was supplied from the circuit to two electrodes. The MSA device was tested by adjusting the voltage of the charge to the capacitor in the circuit from 100 V to 200 V and 150 V was experimentally determined and optimized as the threshold voltage range to obtain the reliable energy impact so the electrical energy with around 145-150 V was charged to capacitors in the circuit. When

two electrodes in the microchamber get connected to the circuit by applying the pulse to MOSFET, arc discharge occurred between two electrodes and then the energy medium was ejected from the MSA microchamber as shown in Figure 4.20 (d).

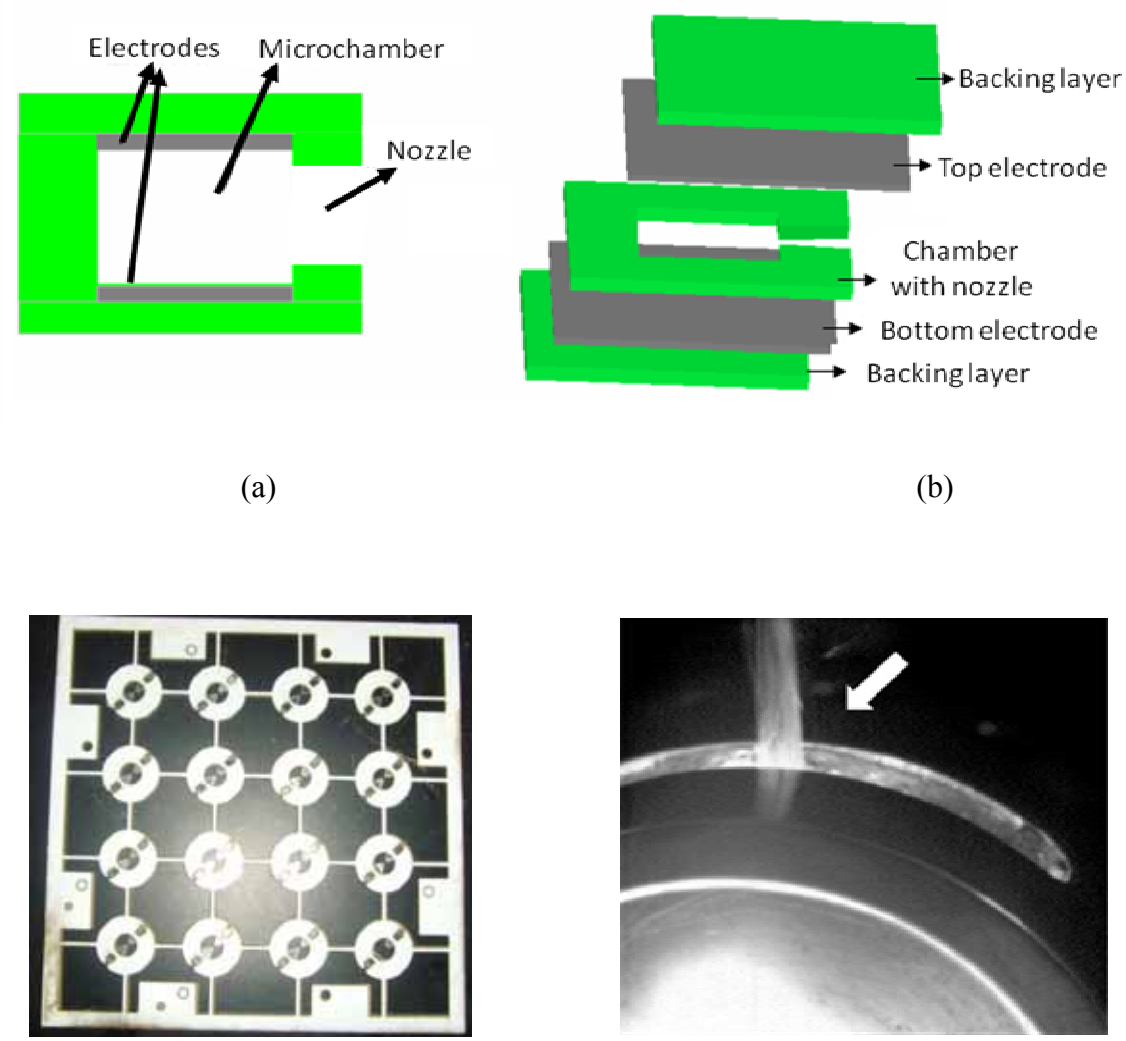

Figure 4.20 The microchamber for micro thermal ablation (MTA) in which arc discharge phenomenon occurs. (a) cross-sectional image of microchamber, (b) the disassembled parts of microchamber, (c) the laminated MSA device (backing, electrode, and chamber layers), and (d) the energy jet ejected from MSA device [104].

During arc discharge, the voltage drop across the electrodes was measured as shown in Figure 4.21, implying that the stored electrical energy to the capacitor was consumed to generate arc discharge between two electrodes. In Figure 4.21, the voltage dropped drastically within less than 0.1 ms and decreased gradually until 1.3 ms. This means that arc discharge was completed in 0.1 ms and the generation of thermal energy stopped after approximately 1.3 ms. While MOSFET in the circuit remains ON for the pulse length, 1.5 ms, the electrical energy from the capacitor was supplied to the microchamber. Even though arc discharge is completed in 0.1 ms, the MSA device still has some conductive path in the microchamber, probably due to salt particles and leakage in the circuit through which the capacitor tries to discharge, showing the gradual voltage drop. If the length of pulse applied to MOSFET is reduced like 0.5 ms, the sharp voltage drop might be seen without the gradual decrease. However, in case of the reduced pulse length, the variation from device to device was found and the discharge process did not start with the reduced length of pulse because MSA system is required to have enough time to start the discharge process. The peak voltage around 135 V in Figure 4.21 is the voltage across the microchamber, V_{high} (145 V) – V_{low} (10 V), as it has the power supply on one side and MOSFET on the other side of the microchamber (Figure 3.5 (b)).

This time characterization as shown in Figure 4.22 was supported by the measurement of force generated by jet following arc discharge phenomenon. Figure 4.22 is a sample result of the measured force according to the operation time. When the MSA device started the discharging process with MOSFET ON, the first peak of force lasted for approximately 0.1 ms and the rest part after 0.1 ms was fluctuated over time, then

became still. It is thought that the first peak of force was due to arc discharge and the force fluctuation was due to after-vibration effects from the sensor itself.

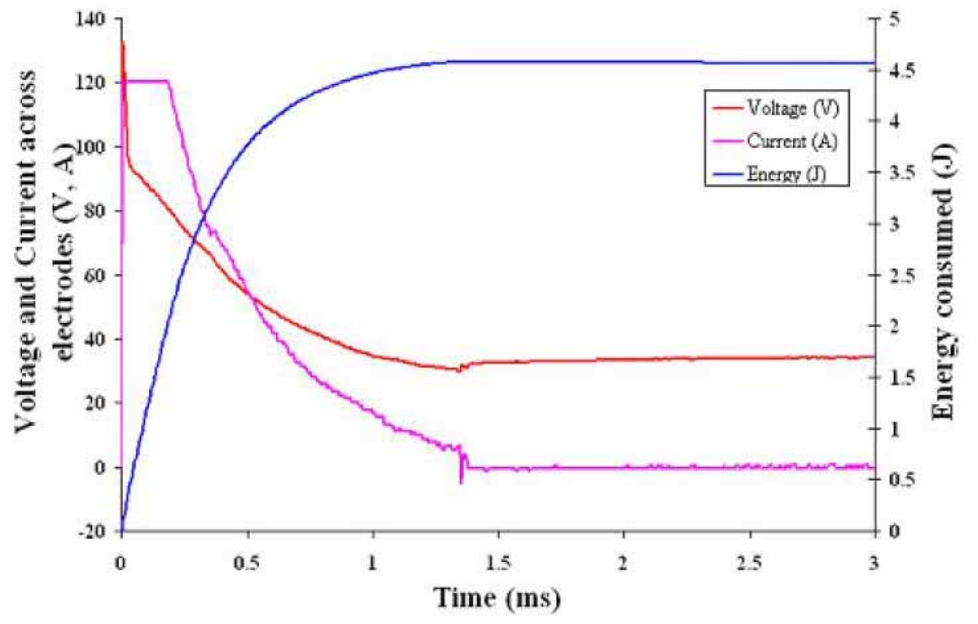

Figure 4.21 Power characteristics of MTA system during the arc generation process. The total energy (in blue) released by arc discharge is estimated with the change of voltage (in red) and current (in pink) across electrodes in the microchamber [104].

This short duration of the energy impact was the desired feature of the MSA system because the time required for the energy impact to the skin will be determined mainly by the duration of the thermal energy source. Moreover, the total power consumed by the arc discharge generating process in Figure 4.21 was calculated with the value of

approximately 2.7-3.3 kW. This energy is not all converted into the required amount of the skin ablation energy, but the power released from this system is almost 2 fold higher than the commercialized laser ablation devices using the power ranging up to around 1.5-1.8 kW [19, 90]. From the viewpoint of this, arc discharge is thought to be the appropriate choice for the energy source of the MSA system.

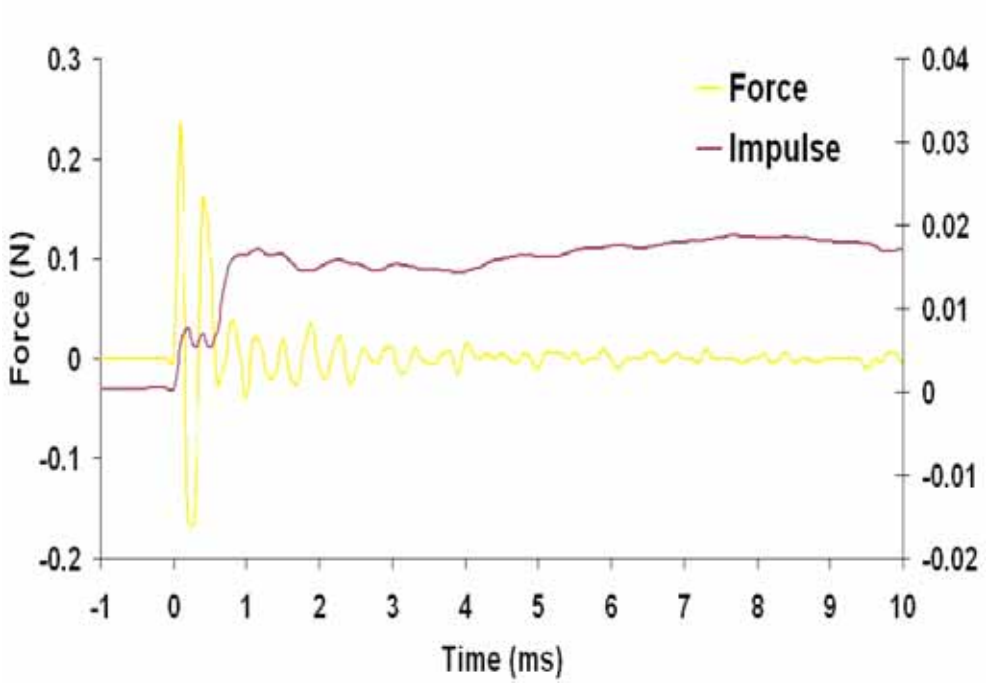

Figure 4.22 The measurement of force (in yellow) generated by arc discharge and impulse (in purple) as time integral of force [104].

4.3.2 Design of skin ablation function of arc-generating device

Guided by the rapid generation and extinction of ablation energy with arc discharge, it is believed that the function of MSA is feasible with this arc discharge generating device. Four skin ablation scenarios were designed in Table 3.1: thermo-mechanical ablation without or with the localization and thermal ablation without or with localization.

First, pig cadaver skin was exposed directly to the nozzle of the microchamber in order to examine whether the MSA system can remove stratum corneum selectively. Figure 4.23 shows histological images of pig skin samples ablated thermo-mechanically without and with the localization by using the windows mask. Both skin samples were found to have the removal of stratum corneum, implying that it was successfully selectively removed by the energy impact generated by the MSA system. Moreover, the skin sample (Figure 4.23 (b)) locally ablated with the windows mask had the multiple ablation sites while the skin sample ablated without the mask (Figure 4.23 (a)) shows a relatively larger area of skin ablation. As the purpose of the windows mask is to allow the MSA system to control the ablation area and thus achieve the minimized spots of ablation that are necessary for allowing skin to heal easily and make the treated areas cosmetically invisible.

However, arc discharge is followed by various physical phenomena due to the sudden release of high level of thermal energy. The thermal energy generated in the microchamber can be consumed to increase the temperature of medium filled in the microchamber or to melt the layer parts of the microchamber. In result, an unfavorable object might be created in the microchamber by thermal energy and it can be also ejected along the ablation energy as shown in Figure 4.23 where the black debris is deposited

onto the ablation site of the skin. Therefore, the solid masking system as shown in Figure 4.24 was designed for two issues; (1) to avoid depositing debris from the microchamber onto the skin and (2) to make mechanistic comparisons between the thermal effect or the mechanical effect.

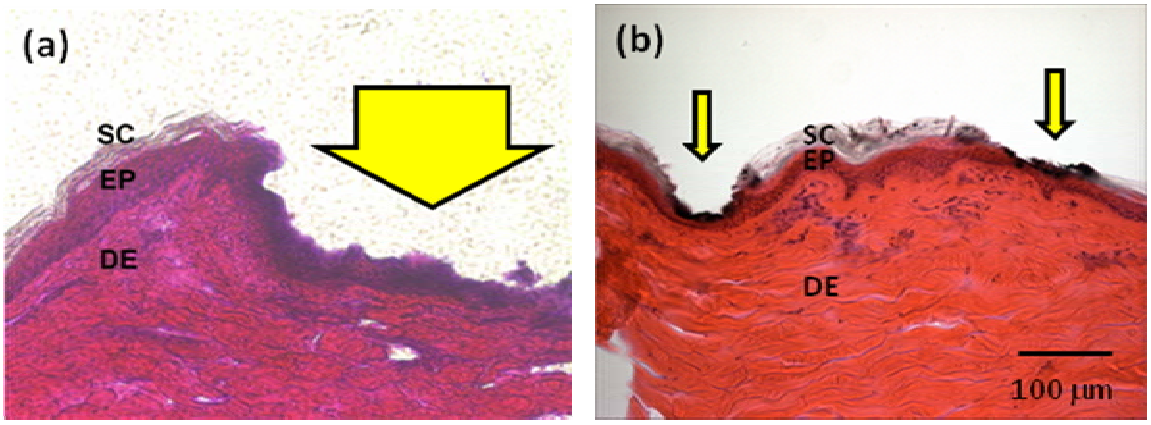

Figure 4.23 Histological images of pig cadaver skin samples ablated thermo-mechanically (a) without and (b) with the windows mask (SC: stratum corneum, EP: viable epidermis, and DE: dermis).

The solid mask is inserted between the nozzle of the microchamber and the surface of the skin as shown in Figure 4.24 (a). Any other effect of arc discharge can be blocked and only thermal energy released by arc discharge can be transferred through the solid mask. To control the ablation area, the use of the windows mask was also designed with the combination of solid mask as shown in Figure 4.24 (b). It is placed under the solid

mask to guide the impact of thermal energy through holes in the windows mask. It is expected that the area of thermal skin ablation can be controlled and localized with these solid and windows masks.

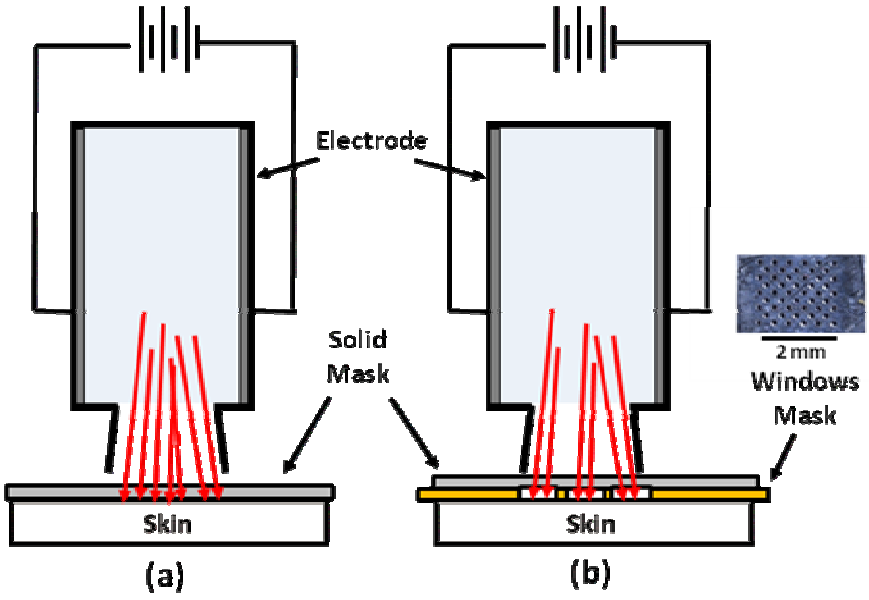

Figure 4.24 Schematic description of thermal skin ablation system with arc discharge. (a) No localization only with solid mask and (b) Localization with solid and windows mask.

4.3.3 Thermal energy characterization for thermal skin ablation

Arc discharge was found to generate relatively high level energy within 0.1 ms. It must then be determined how much energy for thermal skin ablation is generated and

transferred onto the skin. The temperature of thermal energy transferred to the skin was measured to characterize thermal energy by using temperature indicating papers described in the method section 3.3.2.1, which shows the black color of the background through the melted polymer after the contact of thermal energy at the designated temperature as shown in Figure 4.25.

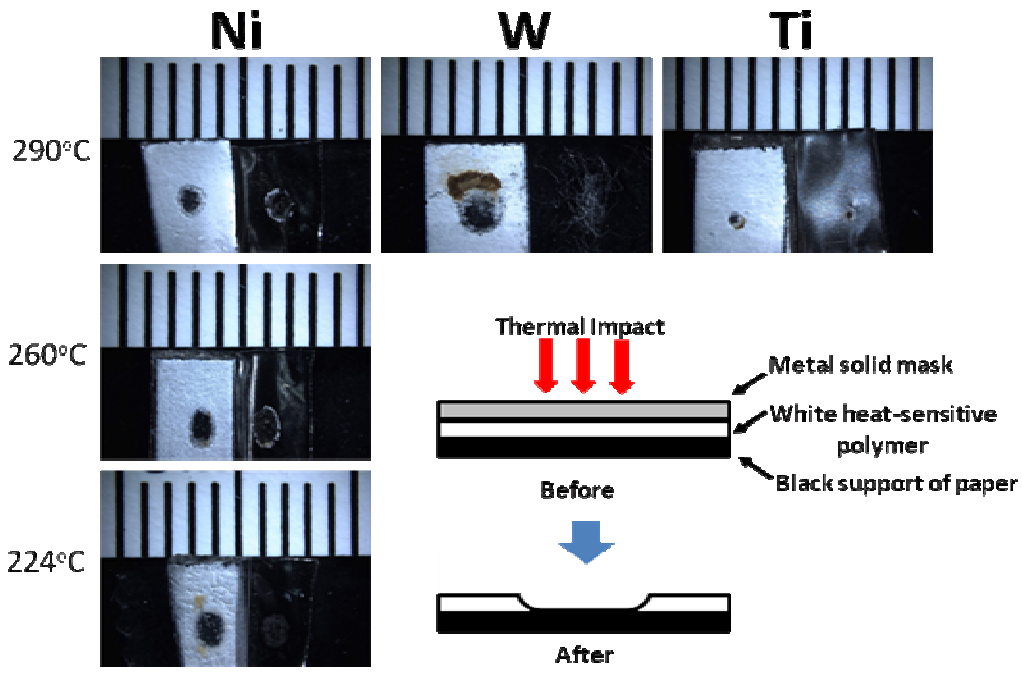

Figure 4.25 The color change of temperature indicating paper after the operation of thermal skin ablation system. The temperature measurement was performed with different kinds of metal solid masks but having the same thickness (25 μm); titanium, nickel, and tungsten, the thermal conductivity of which were 22, 91, and 173 W/m·K, respectively.

In Figure 4.25, 25 μm thickness nickel, tungsten and titanium sheets were used as the solid mask covering temperature indication paper. The available maximum temperature which can be detected was 290^{o}C. In the case of the titanium solid mask, the black color of the background support was shown, meaning that the temperature of thermal energy transferred through the titanium mask reached 290^{o}C, but it had the relatively smaller area of the black color due to low thermal conductivity. Nickel and tungsten masks showed the larger black area because they allowed a greater amount of thermal energy than the titanium mask due to higher conductivity.

According to the previous study [123] regarding the heat effect on skin permeability, the transdermal flux of drug was increased to 1000 fold higher when the skin was contacted with a hot object at approximately 300^{o}C. The temperature of thermal energy transferred through the tungsten solid mask showed the color change at 290^{o}C as shown in Figure 4.25. From these results, it was expected that the thermal energy released from arc discharge may greatly increase the transdermal flux of drugs. The temperature of the thermal energy applied to the skin surface can be controlled by the thickness and thermal conductivity of the solid metal masks. Nickel has been shown to cause skin allergies in some people; therefore, tungsten was selected for the solid mask in subsequent experiments.

Because of the limited availability of temperature indicating paper for temperatures higher than 290^{o}C, a more precise measurement of thermal energy was necessary. However, it was found that the minimum temperature of thermal energy contacting the skin was around 290^{o}C[123], which can enable a significant increase in drug flux, so we simulated the temperature profile from the outer surface of the solid mask to the

epidermis layer in order to estimate the penetration of thermal energy from arc discharge. This was especially important for determining how deeply thermal energy can penetrate into the skin during the MSA operation time of 0.1 ms.

In section 4.3.1, the amount of stored electrical energy in the system was calculated to be about 4.6 J using the measurement of voltage drop (Figure 4.21). Using the assumption that this energy was completely consumed to increase the temperature of the medium in the microchamber, the temperature of the medium was computed to be approximately 1100°C using the following equation [104].

$$E = (mC_p\Delta t)_{water} + m\Delta H_{vap} + (mC_{p,vap}\Delta t)_{vap}$$

E: 4.6 J
Mass of water in the microchamber, m: 1 mg
Δt_{water}: 75°C (from room temperature to boiling point at 1 atm)
Specific heat of water, C_p: 4.186 J/g·°C at 1 atm
Specific heat of vapor at 1 bar and 100°C, $C_{p,vap}$: 2.04 J/g·°C at 1 atm
Heat of vaporization, ΔH_{vap}: 2255 J/g at 1 atm

By using the computational result for the temperature of the ejected medium, the temperature profile of each layer from the solid mask to the epidermis layer was simulated as shown in Figure 4.26, using the assumptions that (1) the outermost surface of the layers contacts the medium at 1100°C, (2) physical properties of each layer are constant over the range of temperature, (3) each layer contacts another without any gap between layers, (4) the skin layers can maintain integrity over the range of temperatures, and (5) one-dimensional transient semi-infinite model applies.

Based on these assumptions, the temperature profile of each ablation scenario was simulated in Figure 4.26. The green and red line in three graphs (a, b, and c) of Figure

4.26 represent the temperature profile of each layer at 100 μs and 1 ms contact time with hot medium ejected from the microchamber, respectively. In the case of 100 μs contact time, the temperature at the junction of stratum corneum and viable epidermis layer was the same as body temperature, but increased to approximately 200^{o}C after 1 ms contact time as shown in Figure 4.26 (d). This means that contact times greater than 100 μs might be sufficient transfer a significant amount of thermal energy to the skinm resulting in deeper skin tissue damage. However, because it was assumed that all electrical energy is converted into thermal energy and the temperature of hot medium (1100^{o}C) is already fixed at the start of the contact time, the critical operation time without deeper skin damage might be longer in practice and the real temperature profile for all layers might be lower than the result shown in Figure 4.26.

Interestingly, stratum corneum has the lowest thermal conductivity among all layers so that the transfer of thermal energy from the microchamber is most hindered in this region and the temperature drops significantly. Therefore, if the debris is not ejected from the microchamber, it would probably ablate the skin selectively without the solid mask as shown in Figure 4.26 (a).

Comparing graphs (b) and (c) in Figure 4.26, the titanium windows mask significantly decreased the temperature of thermal energy penetrating into stratum corneum during the contacting time from 10 to 100 μs, but it became a less effective insulation mask at the longer contacting time, which was greater than 100 μs. Although the thermal conductivity of titanium is 8 fold lower than the tungsten used for the solid mask, it does not effectively perform the heat insulation function for longer times. Instead, if the polymer thin film can be used as the windows mask, the insulation function of the

windows mask will be more effective because the thermal conductivity of polymer is usually 10^3-10^4 times lower than metal [105]. However, the choice of polymer film should be considered in regard to the safety issues and/or the possible clogging of windows that may occur when polymer film is melted.

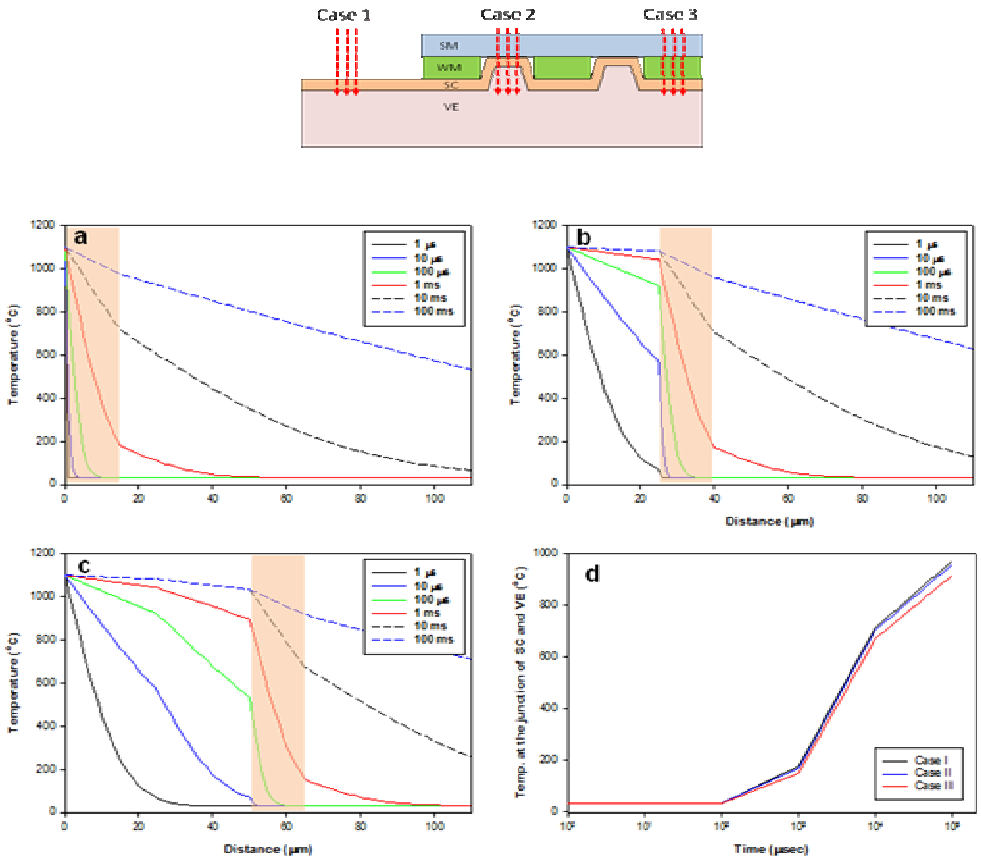

Figure 4.26 Simulation of the temperature profile from the solid mask to viable epidermis layer in each case. The upper schematic is the summarized description of each case (SM: 25 μm thick tungsten solid mask, WM: 25 μm thick titanium windows mask, SC: human stratum corneum, and VE: human viable epidermis). The shaded region in three graphs (a, b, and c) represents stratum corneum; Case 1: SC-VE (graph a), Case 2: SM-SC-VE (graph b), and Case 3: SM-WM-SC-VE (graph c). The graph (d) is the temperature at the junction of SC and VE at each case over time.

4.3.4 Selective thermal skin ablation

Guided by the energy characterization of the MSA system, the removal of stratum corneum was performed and visualized in pig cadaver skin, as described in section 4.3.2. As hypothesized, the energy impact generated by the MSA system could remove stratum corneum selectively (Figure 4.23) in a localized manner by using the windows mask. However, deposition of dark material was found on the skin and this is a critical problem during the MSA application. When the MSA operation was performed and the microchamber was viewed, the metal electrode was not intact (data not shown) indicating that the electrode melted by arc discharge. Moreover, considering the result of the temperature measurement described in Figure 4.25 and the melting point (around 260^{o}C) of the Mylar sheet used as the material of the microchamber, the deposited dark material may be the mixture of melted material created by arc discharge, most of which is probably Mylar debris.

As mentioned previously in section 4.3.2, the MSA function is the conversion of stored electrical energy in the system to thermal or mechanical energy through arc discharge phenomenon, which enables the high speed transformation of the energy. If a very hot medium at for example, 1100^{o}C, can be prepared separately and the contact of this energy medium and the skin can be mechanically controlled at the high speed, this system will also be able to ablate the skin selectively. However, these systems seem to be practically impossible and inefficient due to problems such as the length of time that the system can maintain the hot medium and the type of material that the system should use in order to survive thermal energy.

The MSA system in this study relies on rapid generation and extinction of the applied energy for the short contact time of the ablation energy. It is suggested that the energy transformation into energy impact is feasible by arc discharge phenomenon as a result of the measurements performed in this study, but it is not yet clearly explained by which mechanisms MSA function occurs; that is, thermal by heat or mechanical by jet. Therefore, the solid masking system was designed to study the mechanism of the MSA function as well as to resolve the deposition of the unfavorable dark material.

Tungsten was selected as the material for the solid mask, because it has a high melting point necessary for resisting the hot medium and good thermal conductivity for transferring thermal energy. The MSA with the solid mask was performed on pig cadaver skin samples which were viewed as shown in Figure 4.27. The surface of the untreated skin (Figure 4.27 (a)) and the skin ablated by the MSA system (Figure 4.27 (c)) looked almost the same and had no significant differences. As expected, neither the dark material nor any other debris was found in the pig skin sample ablated by MSA system using the solid mask.

To examine how the MSA system could thermally ablate the skin with the solid mask, a hydrophilic compound, sulforhodamine, was applied to the surface of each piece skin for 12 hours. After 12 h delivery of sulforhodamine, the untreated skin (Figure 4.27 (b)) did not show any color change, the MSA ablated skin showed radially decreasing intensity of purple color inside the skin (Figure 4.27 (d)). This means that sulforhodamine could not diffuse through untreated skin due to the stratum corneum, but it could diffuse into the MSA ablated skin, indicating that removal of the skin barrier could be performed by thermal energy.

To confirm the removal of stratum corneum in the MSA treated skin, cross-sections of untreated and ablated skin samples were visualized as histological sample images using fluorescence and brightfield microscopy before and after staining with H&E, a common skin stain used for histology. The brightfield and fluorescent images (Figure 4.28 (a) and (b)) of the ablated skin sample show the gradual color change of sulforhodamine from the ablated top to the deeper tissue and fluorescence due to the diffused sulforhodamine, respectively. Figure 4.28 (c) shows a cross section of the H&E stained skin samples which had intact stratum corneum of the untreated skin and which lost stratum corneum in ablated skin without epidermis damage.

According to Figure 4.27 and 4.28, it is suggested that the function of skin ablation by the MSA system could be achieved only by thermal energy to allow hydrophilic compound to diffuse into the skin. Moreover, the rapid transfer of thermal energy through the solid mask could remove stratum corneum selectively as shown in Figure 4.28 (d). This implies that thermal ablation is probably the more dominant mechanism over mechanical ablation due to the jet ejected from the microchamber. However, when hot medium is ejected, thermal energy diverges resulting in the large area of the skin ablation. For this, the second windows mask was designed to guide thermal impact for the localized and controlled removal of stratum corneum, where the heat released from arc discharge is transferred through windows and is blocked by other area of windows mask.

It was found that MSA function with arc discharge phenomenon could remove stratum corneum selectively by the impact of thermal energy. The next step is controlling the selective removal of stratum corneum. As discussed before, the localization of the skin ablation is important to control the release rate of drug by adjusting the ablated area

of the skin. To achieve this, the windows mask was designed to specify the localization of the selective removal of stratum corneum as shown in Figure 4.29. In addition to the creating localizing effect by holes in the windows mask, the windows mask should hinder the penetration of thermal energy from the solid mask, preventing damage to the deeper skin tissue as well as keep its integrity against high temperature. These features were criteria for the selection of materials for the windows mask; therefore titanium film was selected.

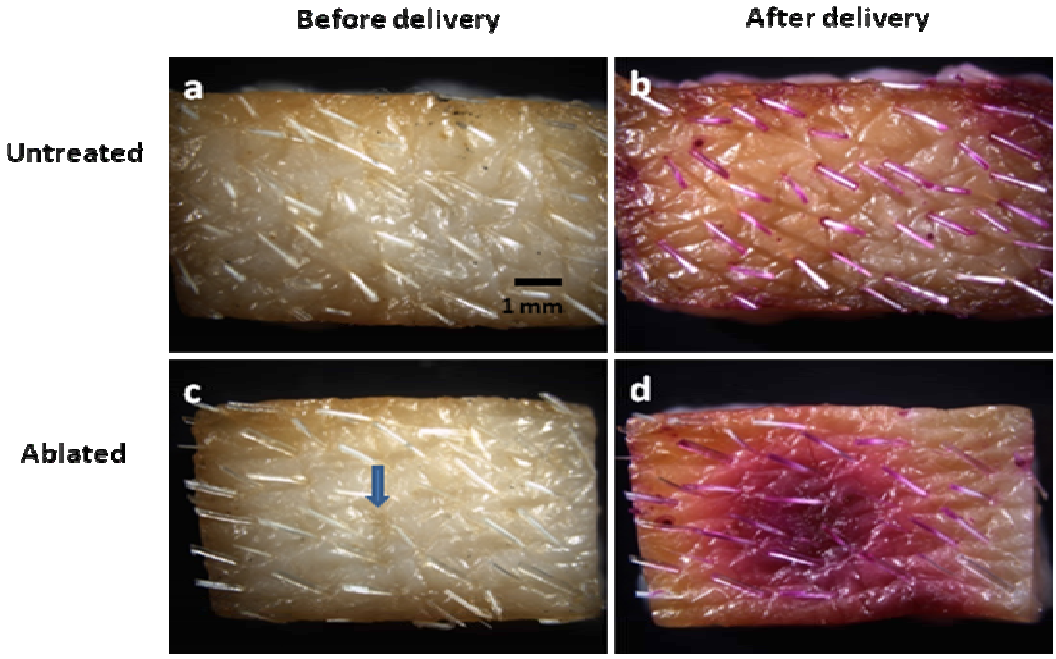

Figure 4.27 Hydrophilic drug (sulforhodamine) delivery into pig cadaver skin with thermal skin ablation system. Top views of (a) the untreated skin and (c) the skin treated with thermal ablation system before sulforhodamine delivery. Top views of (b) the untreated skin and (d) the treated skin after 12 h delivery of sulforhodamine.

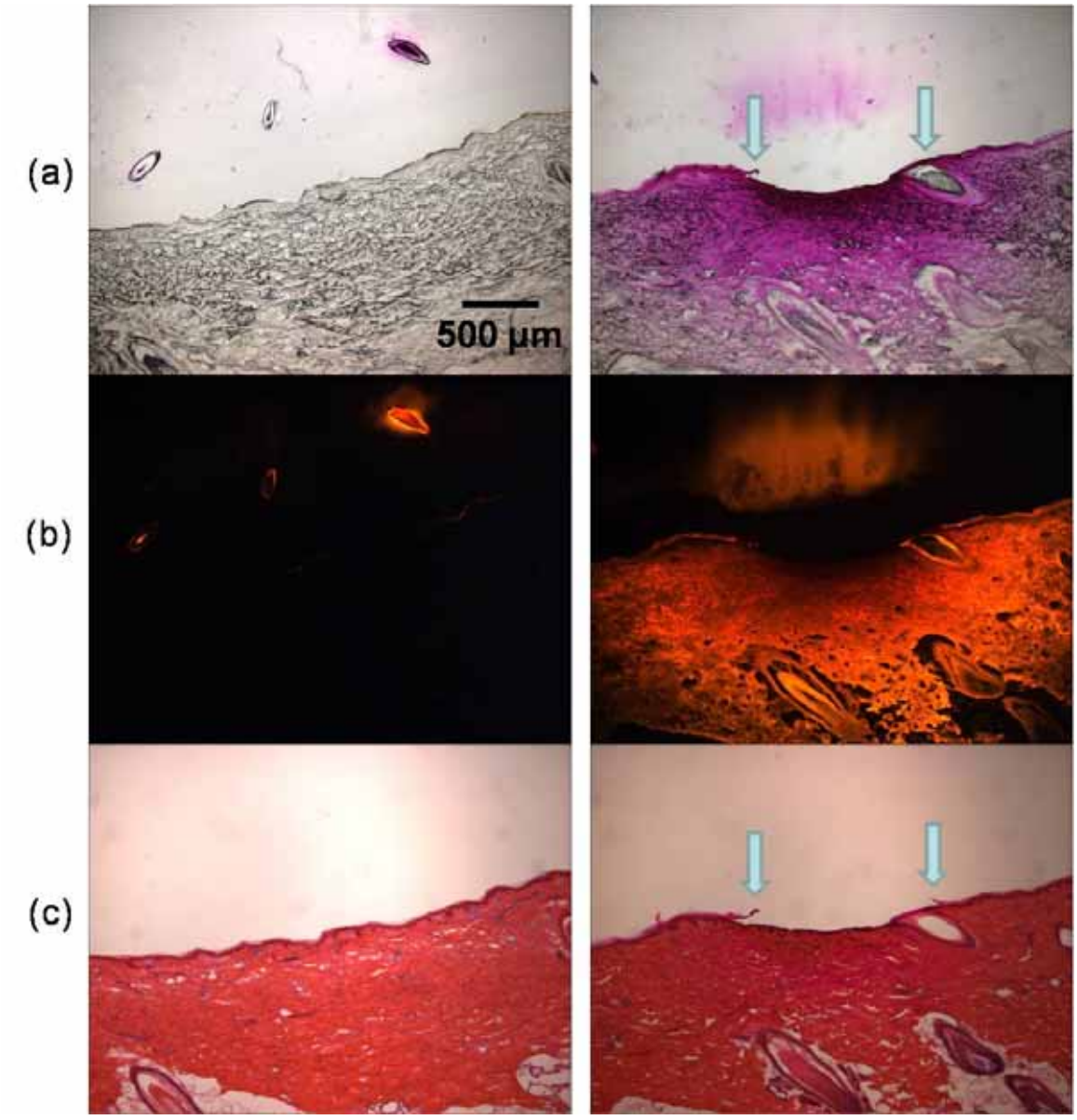

Figure 4.28 Histological images of untreated (left) and ablated (right) skin samples. (a) Brightfield, (b) Fluorescent, (c) H&E Stained, and (d) the magnified image of (c)-ablated.

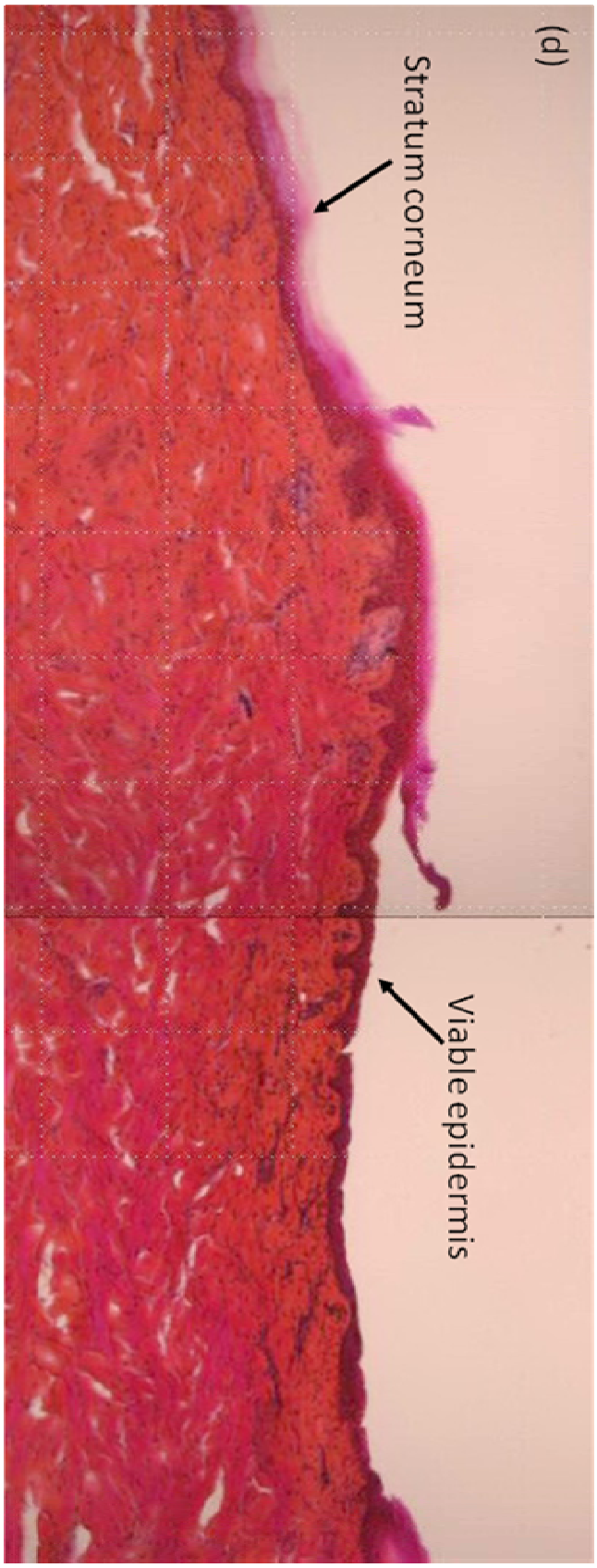
(d)
Stratum corneum
Viable epidermis

The localization of selective removal by impact of thermal energy was visualized in Figure 4.29 for a system using two masks (solid and windows mask) by the same method used to produce the images in Figure 4.27 and 4.28. After the surface of the skin treated with the two masks system (Figure 4.29 (a)), no black residue was found similar to Figure 4.27 (c). The delivery of sulforhodamine could be verified by the multiple dark pink dots in Figure 4.29 (b), which represents localized removal of stratum corneum. From the cross-sectional image of the same skin samples, the diffusion of sulforhodamine (Figure 4.29 (c)) and the localized and selective removal of stratum corneum (Figure 4.29 (d)) were confirmed. Figure 4.29 (d) shows the importance of MSA application; the technical significance of the localized and selective removal of stratum corneum by the MSA function is the control of the skin ablation in a three dimensional way. The rapid impact of thermal energy can enable the removal of the skin along the Z axis and the windows mask system control the area of the localization of the skin ablation in the X and Y planes. The Z direction of the skin ablation might be controlled by the system parameters such as MOSFET pulse width and thermal properties or thickness of material used for the solid mask. The X and Y directions of the skin ablation can be determined by the design of holes in the windows mask. By using this masking system, it is highly probable that thermal skin ablation can be controlled in three dimensions and the therapeutic rate of drug diffusing into the body might be successfully controlled by the localization of the selective thermal ablation as shown in Figure 4.30.

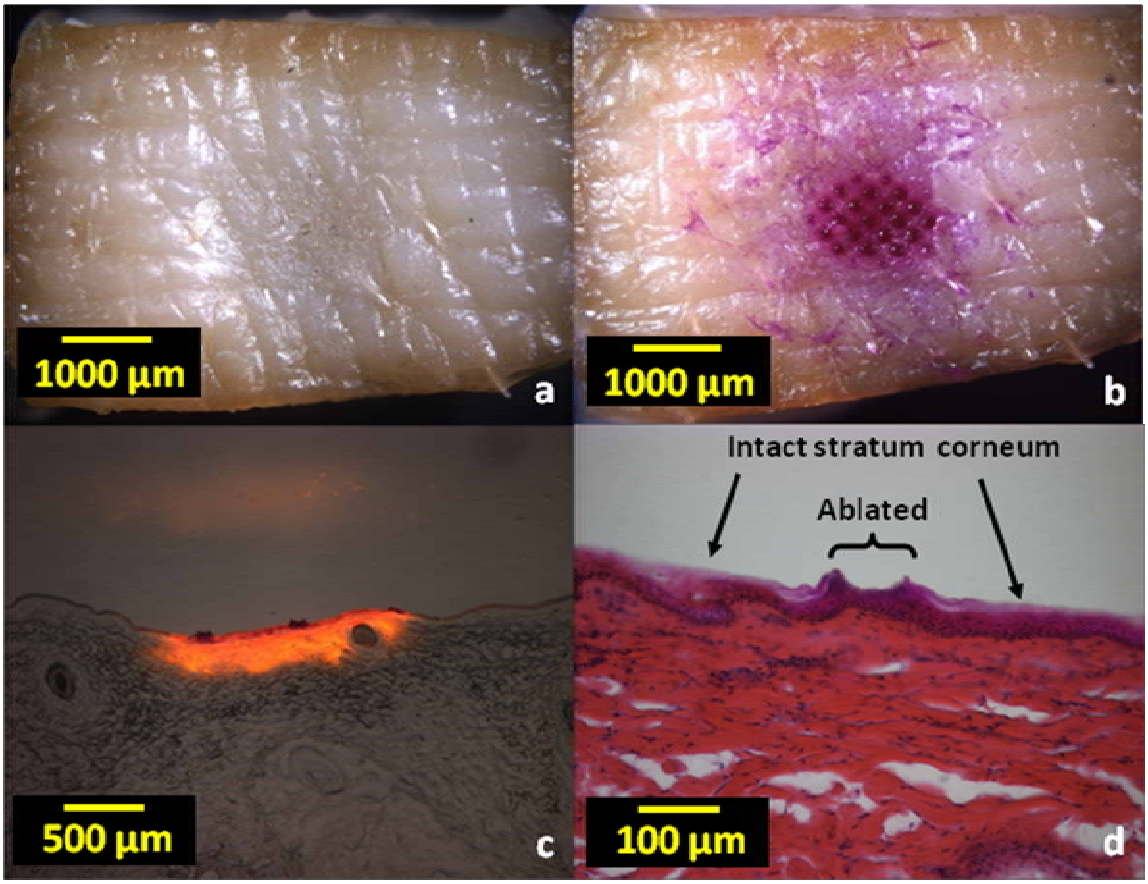

Figure 4.29 The localization of thermal skin ablation. The surface of pig cadaver skin (a) after the treatment of thermal ablation system and (b) after 30 min delivery of sulforhodamine. (c) The cross-section of the same sample imaged by the overlay of brightfield and fluorescence and (d) the magnified image of the thermally ablated stratum corneum.

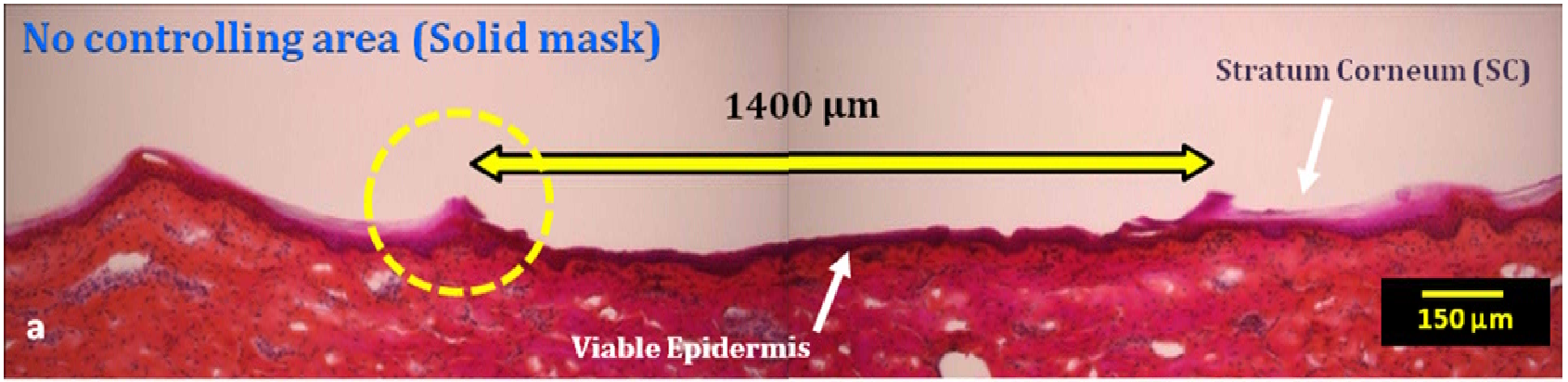
No controlling area (Solid mask)
Stratum Corneum (SC)
1400 µm
a
Viable Epidermis
150 µm

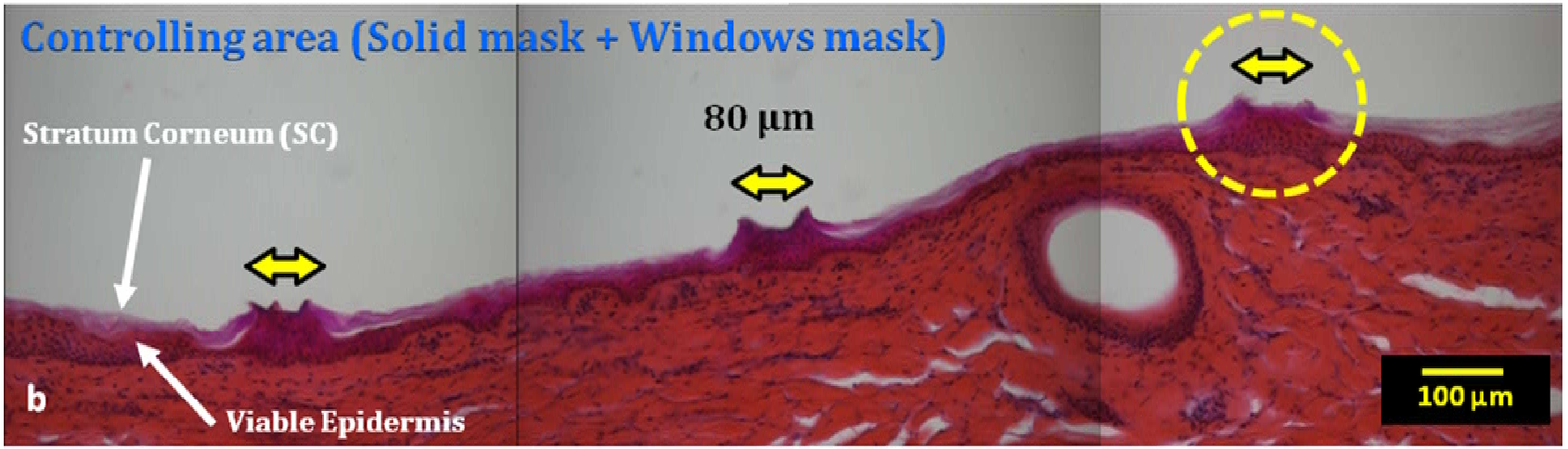
Controlling area (Solid mask + Windows mask)
Stratum Corneum (SC)
80 µm
b
Viable Epidermis
100 µm

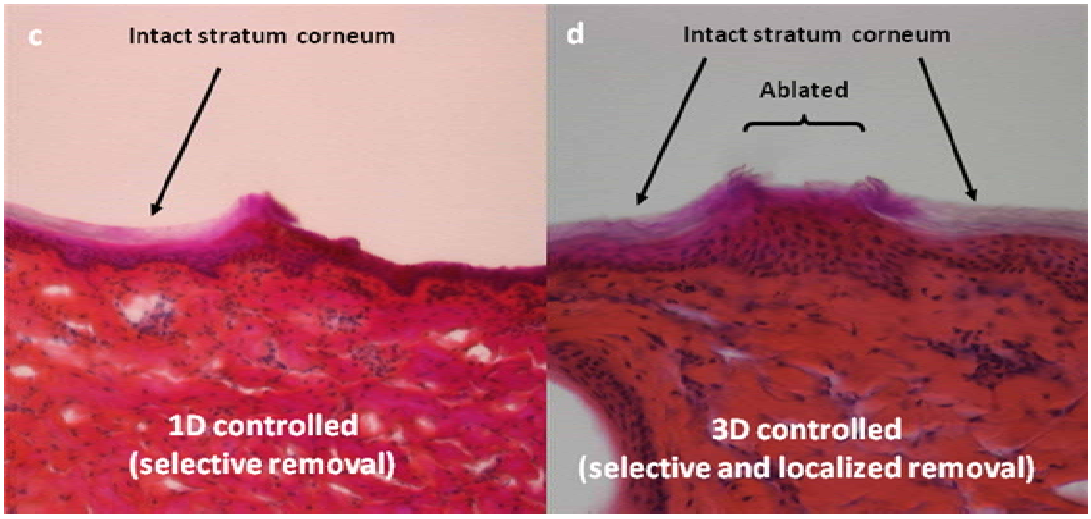

Figure 4.30 Histological images of H&E stained pig cadaver skin applied by arc-based thermal ablation system with (a) the solid mask and (b) the solid and windows masks. (c) and (d) are the magnified images of (a) and (b) (yellow dotted circle), respectively.

4.3.5 Skin permeability and transdermal flux

We expected that the localized and selective removal of stratum corneum can enhance the skin permeability of high molecular weight and hydrophilic biomolecules drugs. Even if various parameters are involved in the determination of the release rate of drug for the real applications, the flux of drug will be significantly increased by removing stratum corneum, which is the rate determining layer in most transdermal patch applications. The study of drug release using Franz cell was designed to investigate the enhanced effect of the thermal ablation system on transdermal drug delivery in human cadaver epidermis and full thickness skin using two different molecular weight compounds; sulforhodamine and Texas Red BSA.

Figure 4.31 shows the enhanced flux of molecules when human cadaver epidermis was applied by the MSA system. For each molecule, thermally ablated epidermis showed a dramatically increased flux 1000 fold higher than intact epidermis. This is definitely due to the removal of the major skin barrier, stratum corneum. The increased flux in the ablated skin in Figure 4.31 could be interpreted as the ablation effect of the MSA system. However, this increase of flux was estimated by using solely the epidermis layer, therefore it may be different from in vivo using the transdermal patch application. Holes representing fully or partially ablated epidermis were also observed (Figure 4.32).

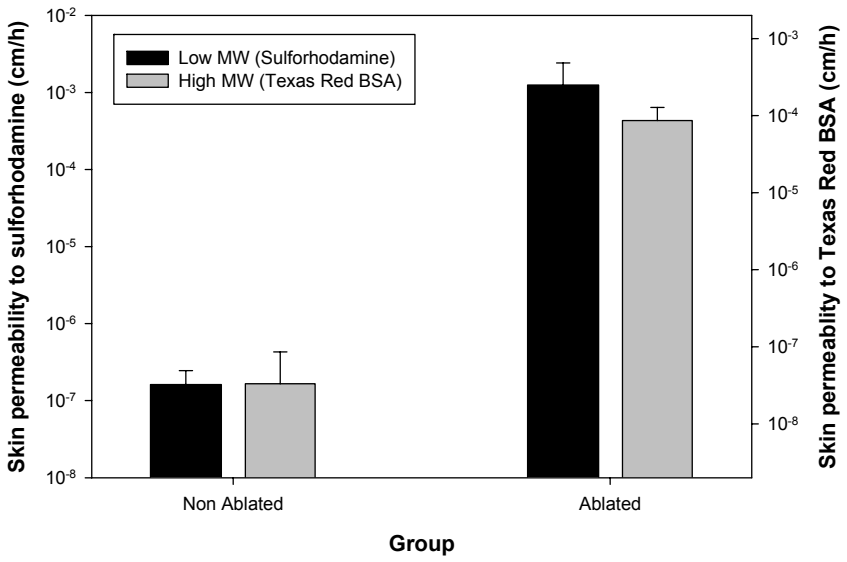

Figure 4.31 Normalized flux of low MW compound (Sulforhodamine) and high MW compound (Texas red BSA) through non-ablated (control) and thermally ablated human cadaver epidermis (n=5 for all groups, SD in error bar).

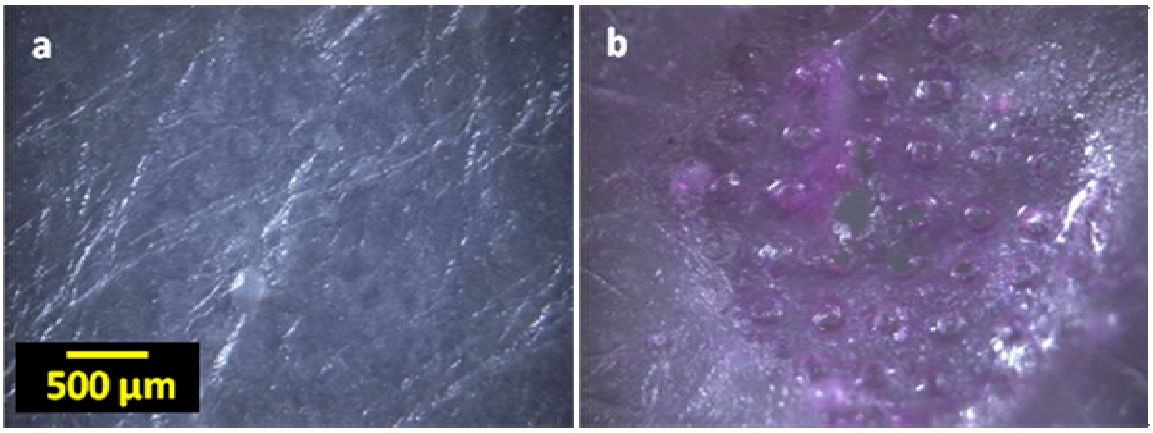

Figure 4.32 The surface of (a) intact epidermis and (b) thermally ablated epidermis used in Franz cell for the flux measurement shown in Figure 4.31.

Next, the permeability coefficient in pseudo-steady-state flux used to characterize the skin permeation of drugs [39] was measured to assess the effect of thermal skin ablation on the skin permeation of drugs and to compare the diffusion of molecules through intact (negative control), MSA ablated, and epidermis stripped human full thickness skin (positive control).

$$J = k_p C_v$$

J : flux in pseudo-steady-state flux
k_p : permeability coefficient
C_v : the concentration of drug in donor solution

The permeation profile of sulforhodamine and Texas red BSA through each type of skin is shown in Figure 4.33. As expected, the non-ablated intact skin did not allow either low or high MW drugs to diffuse through it until the end of experiment, so the flux of two compounds is zero resulting in very poor skin permeability. The thermally ablated skin samples showed a remarkable increase in the flux of each compound, reconfirming the effect of the stratum corneum removal on transdermal drug delivery. Similar to the skin permeation profile [39, 49] of small size drugs with conventional transdermal patches, the flux of the two molecules tested for this study became constant over the application time after the specific time, which is considered the lag time.

While the lag time of the traditional transdermal patch application is related to the barrier properties of stratum corneum, the lag time shown in Figure 4.33 is attributed to the barrier properties of viable epidermis and/or dermis in thermally ablated skin and epidermis stripped skin. However, the vascular structures in the dermis layer during the in vivo case will absorb drugs into the body and drive the circulation of drug, rather than function as a skin barrier. Thus, the flux profile of molecules through epidermis stripped skin in Figure 4.33 might be used to compare the diffusion barrier of the skin thermally ablated with the MSA system.

In Figure 4.33, full thickness skin ablated by MSA for each molecule showed constant flux from 6 h to 24 h for sulforhodamine (ANOVA, 95% significance, $p=0.28$) and from 18 h to 48 h for Texas Red BSA (ANOVA, 95% significance, $p=0.18$). Similarly, epidermis stripped full thickness skin also showed the almost constant flux from 6 h to 24 h for sulforhodamine (ANOVA, 95% significance, $p=0.22$) and from 18 h to 48 h for Texas Red BSA (ANOVA, 95% significance, $p=0.05$). The lag time of

sulforhodamine was 6.0 ± 2.0 (SD) hour for MSA ablated skin and 6.3 ± 1.1 (SD) hour for epidermis stripped skin, respectively; and the lag time of Texas Red BSA was 11.7 ± 4.8 (SD) hour for MSA ablated skin and 12.7 ± 3.0 (SD) hour for epidermis stripped skin, respectively. The lag time for each molecule diffused into two different types of skin was found to be the same (Students' t-test, 95% significance, p=0.78 for sulforhodamine and p=0.72 for Texas Red BSA). Furthermore, the profile for the cumulative amount per unit area for each type of skin after each lag time (12 to 24 h for sulforhodamine and 18 to 48 h for Texas Red BSA) was almost the same. (two-way ANOVA, 95% significance, p=0.27 for sulforhodamine and p=0.48 for Texas Red BSA).

When constant flux was achieved, the permeability coefficient of sulforhodamine and Texas Red BSA was calculated as 3.13 ± 0.88 (SD) $\times 10^{-2}$ and 3.63 ± 0.82 (SD) $\times 10^{-3}$ cm/h for thermally ablated skin, respectively. As expected, when the epidermis stripped full skin was tested to evaluate the permeation profile of each compound, the permeability coefficient value (3.13 ± 1.3 (SD) $\times 10^{-2}$ cm/h for sulforhodamine and 2.84 ± 0.47 (SD) $\times 10^{-3}$ cm/h for Texas Red BSA) was almost the same as the value measured using the thermally ablated full skin (Students' t-test, 95% significance, p=0.99 for sulforhodamine and p=0.1 for Texas Red BSA).

From the result of Figure 4.33, the permeability coefficient for each molecule in both MSA ablated skin and epidermis stripped skin is the same, suggesting that the difference of two skin, epidermis layer, did not affect the permeation of molecules significantly and the lag time was solely attributed to dermis layer, which is the rate controlling layer for the diffusion of molecule through each skin in this experiment. These findings may be extrapolated to show two things. (1) It is likely that once stratum

corneum is removed, the flux of molecules is less irrelevant to the area of the removed stratum corneum. Thus, localized multiple ablation sites would bring the same transdermal delivery effect as a single large ablation site equaling the same area. Furthermore, a design with multiple ablation sites will help skin healing after the ablation. (2) As described [39], the dermis layer drives the absorption of drug in the in vivo case due to vascular structure present. Therefore, since the dermis layer was the rate-controlling layer in the in-vitro experiment, the MSA function will enhance the drug diffusion probably without any hindrance effect from dermis layer.

Figure 4.34 and 4.35 show fluorescent cross-section images of each piece of full thickness skin through which the two model drugs diffused respectively. While thermally ablated and epidermis stripped skin showed a gradual increase in fluorescence intensity over time, intact skin showed no fluorescence in the skin, confirming the findings from Figure 4.33. Although the permeability coefficient of each drug has a similar value for both thermally ablated skin by the MSA system and epidermis stripped skin, the intensity of fluorescence of each image in the two groups shown in Figure 4.34 and 4.35 appears to be different. The intensity discrepancy is due to the difference in the diffusion area of each piece of skin. The applied area through epidermis stripped skin was 20 fold higher than MSA ablated skin.

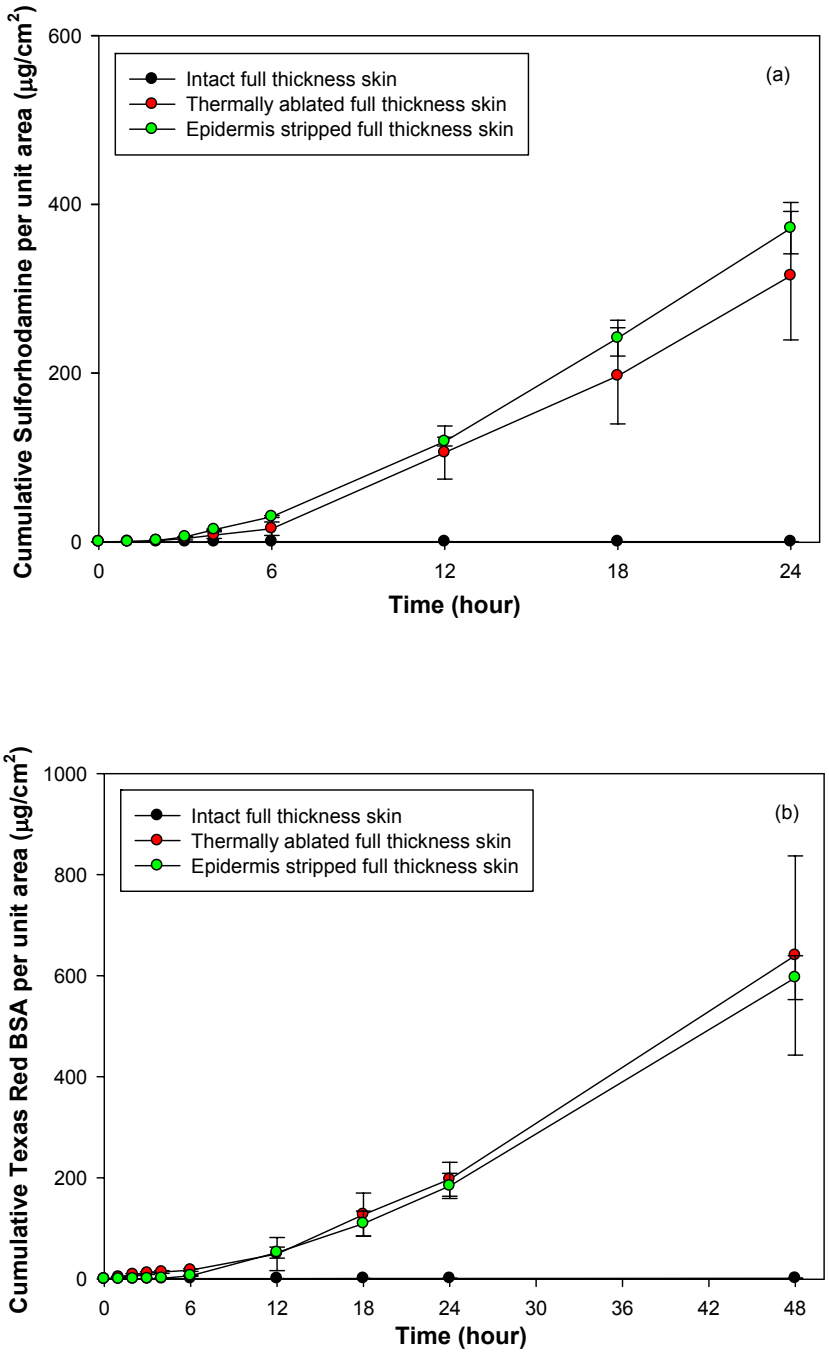

Figure 4.33 The permeation profile of (a) low molecular weight compound, sulforhodamine and (b) high molecular weight compound, Texas Red BSA with three different human cadaver full skin (n=5 for all groups, SD in error bar).

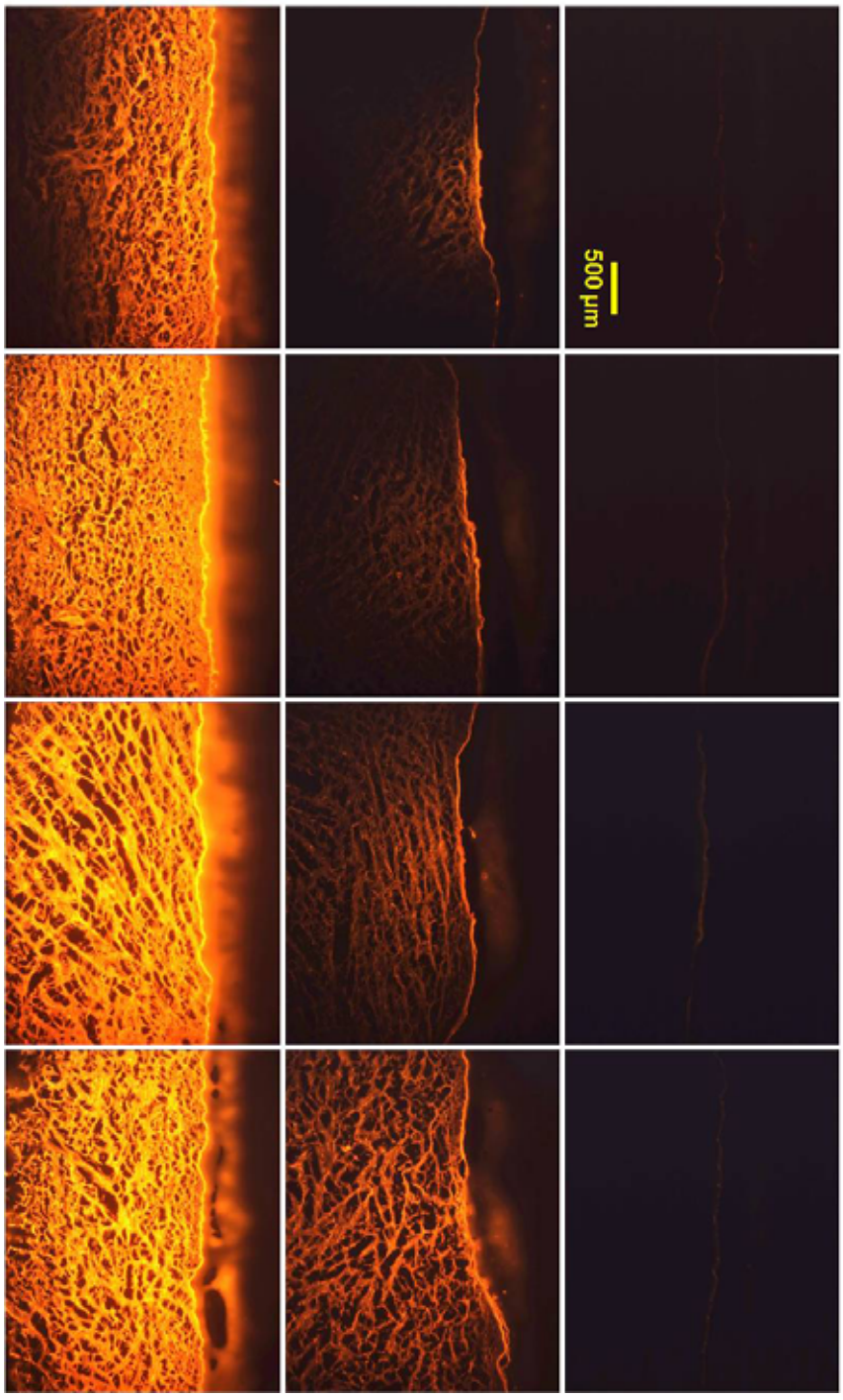

Figure 4.34 Histological image of full skin in which sulforhodamine diffused over time.

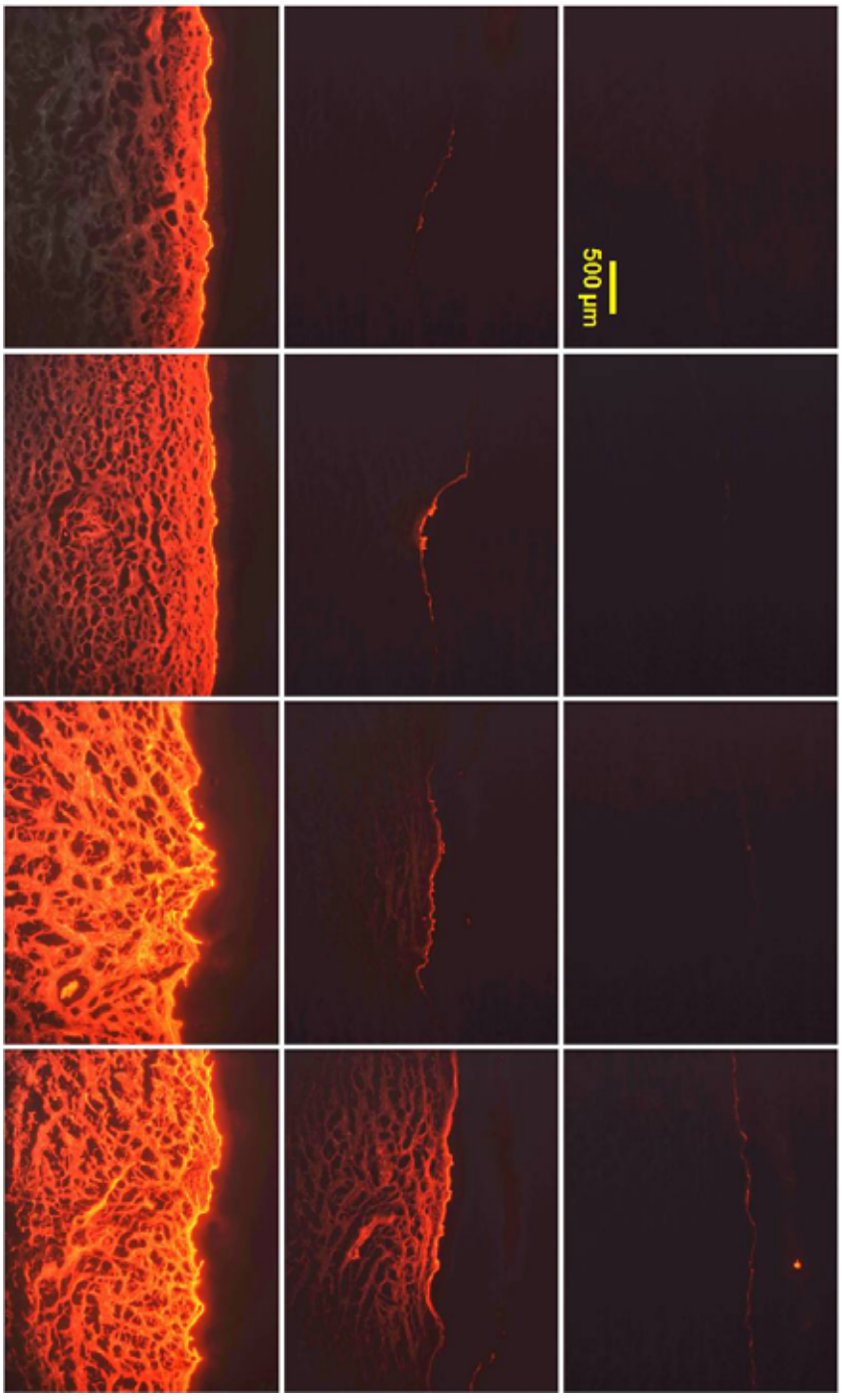

Figure 4.35 Histological image of full skin in which Texas Red BSA diffused over time.

5. Discussion

5.1 Dissolving microneedles

The dissolving microneedles designed in this study may enable (1) bolus and sustained delivery of drugs into the skin, (2) self-administration of drugs that would otherwise require a hypodermic needle and (3) elimination of dangers associated with improper needle disposal and intentional re-use, especially in the developing world.

Previous studies that have developed microneedles that dissolve or degrade in the skin have either melted polymer into a mold at high temperature [124, 125], which can damage sensitive biomolecules, or have hand assembled individual needles of millimeter dimensions [126], which is a poorly controlled and non-manufacturable process. This study has developed a well-controlled, reproducible process for fabrication under gentle conditions that designed to maintain protein integrity.

Selecting the right microneedle geometry and material were important to making functional dissolving microneedles. Most water-soluble materials are mechanically weaker than non-dissolving materials like metal or silicon. Given the many constraints, including water solubility, mechanical strength, processability, and established safety, we selected naturally occurring polysaccharides, i.e., CMC and amylopectin. However, polysaccharide microneedles having the same dimensions previously designed for metal and silicon microneedles were not strong enough. Therefore, mechanical strength was increased by reducing the microneedle aspect ratio, which permitted insertion into skin, although complete insertion of the microneedle shaft was not achieved. For adding the faster dissolution property, disaccharide, for example, trehalose was mixed with CMC for [27, 127]Another feature of our dissolving microneedles is that the backing membrane to

which microneedles are attached has been used, for the first time, as a drug reservoir for sustained drug delivery over many days. Previous approaches have encapsulated drug only within microneedle shafts [124-126] or, alternatively, coated drug onto the surface of microneedle shafts [29, 128]. These approaches have been limited to small (e.g., microgram) drug doses due to the inherently small volume and surface area of microneedles. Our use of the backing membrane as a drug reservoir may increase total doses to milligrams.

Previous studies have also pretreated skin by piercing it with microneedles and then applying a topical formulation or patch to deliver drug through the permeabilized skin [27, 127]. This two-step process may be cumbersome for patients and susceptible to mistakes. In this study, we mimicked this scenario, but accomplished it as a one-step process by using dissolving microneedles, which did not need to be removed after piercing the skin and were integrated onto the surface of a backing layer that served functionally as a transdermal patch. By controlling microneedle patch design, release kinetics was controlled over times ranging from minutes to days. Further design and formulation changes should be able to achieve a variety of different bolus and sustained release profiles.

Release from the backing layer reservoir probably occurs by a set of interacting phenomena. First, microneedles insert into the skin and dissolve, which creates channels for drug transport into skin and for interstitial fluid transport out of skin. Although drug may diffuse through a dry backing layer, drug diffusion should be enhanced by hydrating the backing layer with interstitial fluid from skin. Consistent with this expectation, the backing layer of microneedle patches was seen to swell and soften over time during sustained release delivery experiments presented in Figure 4.8. This suggests that the

patch backing layer swelled by imbibing interstitial fluid from skin through channels created by microneedles. This observation is not only relevant to understanding drug delivery mechanisms, but also suggests uses to extract interstitial fluid for diagnostic applications, such as measuring glucose concentration in diabetics or monitoring industrial toxins in at-risk populations.

We found that a model enzyme, lysozyme, was encapsulated in CMC microneedles without the significant change of its integrity even after two months storage at room temperature (Figure 4.9). The long-tem stability of biotherapeutics may be an important factor to consider due to the time associated with the distribution process of them from the manufacturer to individual patients. Contrary to small molecule drugs based on chemicals with the long expiration date, biotherapeutics are very sensitive. The protein stability seen in this study may be explained by the limited molecular mobility in the solid state that is known to enhance protein stability [32]. Additional studies are needed to determine if other proteins are similarly stable.

Based on all of these findings in vitro, additional studies were continued to assess in vivo performance of dissolving microneedles using hairless rats. For this, human growth hormone (hGH) was selected as a model drug because it should be administered multiple times a week, the formulated hGH for the injection should be kept under the specific protocol to maintain its integrity, and most patients are children who often have fear of hypodermic needles [9].

Transdermal drug delivery with dissolving microneedles is achieved for the time between the breakage and the resealing of stratum corneum. After the skin is resealed, drug will not be able to diffuse into the skin. Thus, the skin resealing time should be first

assessed with dissolving microneedles to check the available administration time. In case of the insertion of CMC microneedles, the skin was resealed slowly, suggesting that CMC dissolving microneedles can deliver hGH for bolus without the time limit given by the skin resealing process. However, the usage of CMC microneedles for the sustained release application, the skin reaction like irritation should be fully evaluated and needs to be addressed, even though microneedles were fabricated using materials found in other FDA-approved formulations.

Next to the fabrication of dissolving microneedles, the most critical issue of dissolving microneedles application is whether to maintain the integrity of drug encapsulated within microneedles. The integrity of biopharmaceuticals should be examined to determine the dose of drug in the system for the therapeutic amount of drug, bioavailability, and the storage period, all of which are cost-affecting considerations. hGH encapsulated in CMC microneedles did not lose its integrity, suggesting that the fabrication processes of CMC dissolving microneedles are compatible with the formulation of biopharmaceuticals, but hGH stored for 3 and 15 months after the fabrication without controlling the storage condition showed 15% (Nb2 cell proliferation study) and 40% (pharmacokinetics study) decreased activity, respectively. This means that hGH started degrading over time after the fabrication. To improve the quality of hGH encapsulated within microneedles for the long period, the specific protocol like the vacuum packaging or refrigerated storage might be needed.

The bolus hGH in vivo delivery experiment suggests several meaningful messages. First of all, the fabrication processes of hGH dissolving microneedles are compatible with the formulation of hGH to make the solid form which is the preferred for the storage.

Although most biopharmaceuticals are delivered with the injection of the liquid formulation, they are usually formulated as the solid form (lyophilized) and then reconstituted before the injection because biomolecules in the liquid formulation can be easily degraded during the storage. Thus, dissolving microneedles are a kind of hybrid platform combining the solid and the liquid formulation to take advantages of each formulation; the better stability and the easier administration.

We found out that carboxymethylcellulose, CMC is good material as microneedles matrix for the insertion function of microneedles and the encapsulation of hGH. However, according to the results of Figure 4.18 (in vitro release) and 4.14 (in vivo release), the dissolution of microneedles matrix can be enhanced with the mixture made out of material having the better solubility. This was supported by two findings; the same bioavailability of the reconstituted hGH (106 ± 6 %) to the unprocessed hGH (100 ± 8 %) and the higher bioavailability of hGH in CMC/trehalose (71 ± 7 %) than hGH in CMC only (13 ± 3 %). This would suggest that dissolving microneedles could be fabricated with the mixture matrix to add the specific function to the microneedles system. In this study, disaccharide, trehalose was mixed to provide the better dissolution of microneedles matrix and the faster release of hGH and thereby to increase the bioavailability of hGH.

5.2 Micro skin ablation

The ablation of stratum corneum is conceptually a very simple and straightforward method to increase the flux of molecules through the skin into the body. Previous ablation methods were impractical with the subjective manner of the ablation [24] due to longer operation times that can cause unfavorable effects [21], such as deeper skin damage.

The key point of the skin ablation method is the selective removal of the skin barrier, stratum corneum, without any damage of the deeper skin tissue. In this study, the micro skin ablation (MSA) system was developed to achieve the localized and selective removal of stratum corneum using the impact of the energy generated by arc discharge phenomenon. Because the generation and extinction of arc discharge was completed within around 100 μs, the ablation of stratum corneum is expected to be much faster than other ablation techniques [21, 91] that are performed between 1 ms and 10 ms.

The microchamber where arc discharge occurs was fabricated by laser machining and lamination technologies. These fabrication processes can enable mass production reducing fabrication cost of the MSA system. This system will be more practical if the power supplying system could be minimized enough to provide the electrical energy for the generation of arc discharge.

The energy released from arc discharge is converted into mechanical and thermal energy. Both mechanical and thermal effects could contribute to the ablation mechanism, but it was found that thermal ablation is the dominant mechanism of MSA system by using the two mask system; the solid mask to block mechanical effect and the windows mask to guide the impact of thermal energy. The thermal energy is transferred through the metal solid mask to the stratum corneum, which is heated very rapidly and causes the lipid layers encompassing corneocytes to be melted resulting in the disintegration or decomposition [123] of stratum corneum.

In previous technologies [21, 91] using thermal energy, the heating elements fabricated to generate thermal energy contact the skin directly. Thus, heating elements should be designed to optimize the way in which the thermal energy is generated rapidly, and the

contact of heating elements to the skin might be dependent on the design of heating elements. Contrary to these methods, the MSA function is composed two distinct steps; (1) the generation of thermal energy and (2) the control of the skin ablation. The significance of this mechanism is that the duration and amount of thermal energy will control the depth of the skin ablation and the masking system can control the size of the skin ablation. Therefore, the MSA system may achieve three-dimensionally controlled ablation of stratum corneum.

After localized and selective removal of stratum corneum, two molecules representing hydrophilic drugs and biotherapeutic were delivered to assess the effects of the MSA system on transdermal drug delivery. The intact skin had an extremely long lag time meaning no diffusion of molecules through the skin, while the skin ablated with the MSA showed significantly increased permeability to each molecule. Moreover, the permeation profiles of MSA ablated skin and epidermis stripped skin, as shown in Figure 4.33, suggested that the dermis became the rate determining layer after stratum corneum ablation. Because the dermis does not play the role of the skin barrier for transdermal drug delivery in the in-vivo situation, the technical meaning of Figure 4.33 is that MSA ablated skin has an extremely small practical barrier of the skin, the amount of drug diffusion will be controlled mostly by the area of the ablated skin, and the geometry of the ablation area will be the most critical criterion for delivering drugs by the MSA system.

6. Conclusion

This study presents (1) transdermal delivery of human growth hormone (hGH) with dissolving microneedles and (2) a new method of thermal ablation based on arc discharge. The dissolving microneedles system was developed with a design involving fabrication under mild conditions that may be suitable for protein delivery and amenable to mass production. It was realized by selecting FDA-approved polysaccharides and modifying a casting method with centrifugation. By using a low aspect ratio and pyramidal geometry, dissolving microneedles were formulated to have sufficient mechanical strength to insert into skin. By selectively loading microneedle shafts, microneedle patches provided bolus release of a model drug upon the dissolution of the microneedle matrix inside skin. By loading the backing layer, microneedle patches provided sustained release probably due to drug diffusion and swelling of the backing layer over time. Model drug release rate was controlled by altering microneedle formulation. A model protein (i.e., lysozyme) maintained structural and functional integrity after encapsulation and release from dissolving microneedles, even after two months storage at room temperature. Overall, dissolving microneedles may be useful as a method for patients to self-administer drugs without the pain or hazards of hypodermic needles.

Guided by the development of dissolving microneedles, transdermal delivery of hGH was demonstrated with the fabrication of dissolving microneedles encapsulating hGH. By using SDS-PAGE and Nb2 cell proliferation to examine the integrity of the processed hGH, it was found that the integrity of hGH encapsulated in microneedles was not damaged during the fabrication processes, but it was partially degraded (approximately 15%) after three months storage at room temperature. By measuring the

impedance of the skin inserted with CMC dissolving microneedles, CMC microneedles was determined to be possibly applied for at least 1 day. From the pharmacokinetics of hGH administered into hairless rats with microneedles or a hypodermic needle, the bioavailability of hGH dissolving microneedles was determined up to 71 % with the comparison of the subcutaneously injected hGH, but the minimum 17 % of the total amount of hGH remained in microneedles because of the imperfect insertion with the viscoelastic properties of skin.

The micro skin ablation (MSA) system was designed for the localized and selective removal of stratum corneum on the basis of the impact of energy on skin with arc discharge phenomenon. The microchamber for generating arc discharge was fabricated in a way that can enable the mass production of the device. The dominant mechanism of MSA function was thought to be based on thermal effect rather than mechanical effect. The thermal energy from arc discharge was impacted on the skin surface for around 100 μs with the guidance of the masking system which enabled localized and selective removal of stratum corneum, implying the possibility of three-dimensionally controlled skin ablation. The skin ablated by the MSA system showed significantly increased skin permeability to two molecules, sulforhodamine and Texas Red BSA, suggesting the capability of transdermal delivery of biopharmaceuticals using the MSA system.

7. Recommendation

Based on the results of this thesis, I would recommend three further studies. Regarding the bioavailability of drug delivered with the dissolving microneedles system, the geometry of dissolving microneedles may be modified to have the more perfect delivery of drug into the body to reduce the amount of drug remaining in the system. The geometry of dissolving microneedles was designed to have a low aspect ratio, thus providing better mechanical properties for the insertion of these microneedles, which were made of the mechanically poor material. If the geometry of microneedles is designed to give better good mechanical property and the improved delivery of drug into the body without loss, it will probably result in higher bioavailability of drug.

In addition, the reason for the missing portion of the total amount of drug encapsulated within microneedles was figured out to be the slower absorbing rate of drug from the microneedles matrix to the circulation system, by comparing the administration of the reconstituted drug using the injection. To prove this, multiple microneedles systems with the same total amount of drug as that in a single microneedle system can be used to examine the effect of absorbing rate from the system into the body on the bioavailability.

The MSA system showed localized and selective removal of stratum corneum after the impact of thermal energy. By using human cadaver skin, the in vitro permeation profile of the MSA treated skin showed remarkably increased delivery of molecules across skin. If the entire system, including the microchamber and the external power supplying system, is fabricated with the integrated and portable size used for in vivo experiments, the actual skin permeability of biopharmaceuticals delivered by this method

can be estimated. Also, optimization of parameters related to the masking system and the energy supplying system will be helpful for understanding the MSA system in detail.

References

1. Walsh, G. Biopharmaceuticals: recent approvals and likely directions. *Trends in Biotechnology* **23**, 553-558 (2005).

2. Walsh, G. Biopharmaceutical benchmarks 2006. *Nature Biotechnology* **24**, 769-U5 (2006).

3. Rader, R.A. (Re)defining biopharmaceutical. *Nature Biotechnology* **26**, 743-751 (2008).

4. Lawrence, S. Biotech drug market steadily expands. *Nature Biotechnology* **23**, 1466-1466 (2005).

5. Pavlou, A.K. & Reichert, J.M. Recombinant protein therapeutics - success rates, market trends and values to 2010. *Nature Biotechnology* **22**, 1513-1519 (2004).

6. Ashton, G. Growing pains for biopharmaceuticals. *Nature Biotechnology* **19**, 307-311 (2001).

7. Mahato, R.I., Narang, A.S., Thoma, L. & Miller, D.D. Emerging trends in oral delivery of peptide and protein drugs. *Critical Reviews in Therapeutic Drug Carrier Systems* **20**, 153-214 (2003).

8. Deacon, B. & Abramowitz, J. Fear of needles and vasovagal reactions among phlebotomy patients. *Journal of Anxiety Disorders* **20**, 946-960 (2006).

9. Hanas, R. Reducing injection pain in children and adolescents with diabetes: a review of indwelling catheters. *Pediatric Diabetes* **5**, 102-111 (2004).

10. Siekmeier, R. & Scheuch, G. Inhaled Insulin - Does It Become Reality? *Journal of Physiology and Pharmacology* **59**, 81-113 (2008).

11. Siekmeier, R. & Scheuch, G. Systemic Treatment by Inhalation of Macromolecules - Principles, Problems, and Examples. *Journal of Physiology and Pharmacology* **59**, 53-79 (2008).

12. Yang, W., Peters, J.I. & Williams, R.O. Inhaled nanoparticles - A current review. *International Journal of Pharmaceutics* **356**, 239-247 (2008).

13. Blank, I.H. & Gould, E. Penetration of Anionic Surfactants into Skin .2. Study of Mechanisms Which Impede the Penetration of Synthetic Anionic Surfactants into Skin. *Journal of Investigative Dermatology* **37**, 311-315 (1961).

14. Fredriksson, T. Interchangeable Collimators in Measurements of Percutaneous Absorption of Labelled Compounds. *Acta Dermato-Venereologica* **42**, 405-& (1962).

15. Matoltsy, A.G., Schragger, A. & Matoltsy, M.N. Observations on Regeneration of the Skin Barrier. *Journal of Investigative Dermatology* **38**, 251-253 (1962).

16. Scheuple.Rj & Blank, I.H. Permeability of Skin. *Physiological Reviews* **51**, 702-& (1971).

17. Tsai, J.C., Sheu, H.M., Hung, P.L. & Cheng, C.L. Effect of barrier disruption by acetone treatment on the permeability of compounds with various lipophilicities: Implications for the permeability of compromised skin. *Journal of Pharmaceutical Sciences* **90**, 1242-1254 (2001).

18. Lanke, S.S.S., Kolli, C.S., Strom, J.G. & Banga, A.K. Enhanced transdermal delivery of low molecular weight heparin by barrier perturbation. *International Journal of Pharmaceutics* **365**, 26-33 (2009).

19. Jacques, S.L., Mcauliffe, D.J., Blank, I.H. & Parrish, J.A. Controlled Removal of Human Stratum-Corneum by Pulsed Laser. *Journal of Investigative Dermatology* **88**, 88-93 (1987).

20. Henry, S., McAllister, D.V., Allen, M.G. & Prausnitz, M.R. Microfabricated microneedles: A novel approach to transdermal drug delivery. *Journal of Pharmaceutical Sciences* **87**, 922-925 (1998).

21. Sintov, A.C. et al. Radiofrequency-driven skin microchanneling as a new way for electrically assisted transdermal delivery of hydrophilic drugs. *Journal of Controlled Release* **89**, 311-320 (2003).

22. Mitragotri, S. Synergistic effect of enhancers for transdermal drug delivery. *Pharmaceutical Research* **17**, 1354-1359 (2000).

23. Bronaugh, R.L. & Stewart, R.F. Methods for Invitro Percutaneous-Absorption Studies .5. Permeation through Damaged Skin. *Journal of Pharmaceutical Sciences* **74**, 1062-1066 (1985).

24. Mikszta, J.A. et al. Improved genetic immunization via micromechanical disruption of skin-barrier function and targeted epidermal delivery. *Nature Medicine* **8**, 415-419 (2002).

25. Gerstel, M.S. (Alza Corporation, USA, 1976).

26. Prausnitz, M.R. Microneedles for transdermal drug delivery. *Advanced Drug Delivery Reviews* **56**, 581-587 (2004).

27. McAllister, D.V. et al. Microfabricated needles for transdermal delivery of macromolecules and nanoparticles: Fabrication methods and transport studies. *Proceedings of the National Academy of Sciences of the United States of America* **100**, 13755-13760 (2003).

28. Park, J.H., Allen, M.G. & Prausnitz, M.R. Biodegradable polymer microneedles: Fabrication, mechanics and transdermal drug delivery. *Journal of Controlled Release* **104**, 51-66 (2005).

29. Gill, H.S. & Prausnitz, M.R. Coated microneedles for transdermal delivery. *Journal of Controlled Release* **117**, 227-237 (2007).

30. Martanto, W. et al. Transdermal delivery of insulin using microneedles in vivo. *Pharmaceutical Research* **21**, 947-952 (2004).

31. Davis, S.P., Martanto, W., Allen, M.G. & Prausnitz, M.R. Hollow metal microneedles for insulin delivery to diabetic rats. *Ieee Transactions on Biomedical Engineering* **52**, 909-915 (2005).

32. McNally, E.J. Protein formulation and delivery / edited by Eugene J. McNally (New York M. Dekker, c2000., 2000).

33. Singh, R., Singh, S. & Lillard, J.W. Past, present, and future technologies for oral delivery of therapeutic proteins. *Journal of Pharmaceutical Sciences* **97**, 2497-2523 (2008).

34. Shaji, J. & Patole, V. Protein and Peptide Drug Delivery: Oral Approaches. *Indian Journal of Pharmaceutical Sciences* **70**, 269-277 (2008).

35. Vadokas, V. Long-term intrathecal application of baclofen in the treatment of spinal and cerebral spasticity. *Journal of Neurologic Rehabilitation* **11**, 61-64 (1997).

36. Husseini, G.A. & Pitt, W.G. Ultrasonic-Activated Micellar Drug Delivery for Cancer Treatment. *Journal of Pharmaceutical Sciences* **98**, 795-811 (2009).

37. Schaefer, H. & Redelmeier, T.E. Skin Barrier: Principles of Percutaneous Absorption (Karger, New York, 1996).

38. Kydonieus, A.F. & Wille, J.J. Biochemical Modulation of Skin Reacions: Transdermals, Topicals, Cosmetics (CRC Press, New Yotk, 2000).

39. Williams, A.C. Trasndermal and Topical Drug Delivery (Pharmaceutical Press, London, 2003).

40. Lampe, M.A. et al. Human Stratum-Corneum Lipids - Characterization and Regional Variations. *Journal of Lipid Research* **24**, 120-130 (1983).

41. Elias, P.M. Epidermal Lipids, Membranes, and Keratinization. *International Journal of Dermatology* **20**, 1-19 (1981).

42. Wertz, P.W., Miethke, M.C., Long, S.A., Strauss, J.S. & Downing, D.T. The Composition of the Ceramides from Human Stratum-Corneum and from Comedones. *Journal of Investigative Dermatology* **84**, 410-412 (1985).

43. Michaels, A.S., Chandrasekaran, S.K. & Shaw, J.E. Drug Permeation through Human Skin - Theory and Invitro Experimental Measurement. *Aiche Journal* **21**, 985-996 (1975).

44. Roberts, M.S., Pugh, W.J. & Hadgraft, J. Epidermal permeability: Penetrant structure relationships .2. The effect of H-bonding groups in penetrants on their diffusion through the stratum corneum. *International Journal of Pharmaceutics* **132**, 23-32 (1996).

45. Abraham, M.H., Chadha, H.S. & Mitchell, R.C. The Factors That Influence Skin Penetration of Solutes. *Journal of Pharmacy and Pharmacology* **47**, 8-16 (1995).

46. Prausnitz, M.R., Mitragotri, S. & Langer, R. Current status and future potential of transdermal drug delivery. *Nature Reviews Drug Discovery* **3**, 115-124 (2004).

47. Prausnitz, M.R. & Langer, R. Transdermal drug delivery. *Nature Biotechnology* **26**, 1261-1268 (2008).

48. B.W., B. Dermatological Formulations: Percutaneous Absorption (Marcel Dekker, New York, 1983).

49. Chien, Y.W. Novel Drug Delivery Systems (Marcel Dekker, New York, 1992).

50. Blank, I.H. Further Observations on Factors Which Influence the Water Content of the Stratum Corneum. *Journal of Investigative Dermatology* **21**, 259-271 (1953).

51. Winsor, T. & Burch, G.E. Differential roles of layers of human epigastric skin on diffusion rate of water. *Archives of Internal Medicine* **74**, 428-436 (1944).

52. Blank, I.H., Gould, E. & Theobald, A. Penetration of Cationic Surfactants into Skin. *Journal of Investigative Dermatology* **42**, 363-366 (1964).

53. Scheuple.Rj. Mechanism of Percutaneous Absorption .2. Transient Diffusion and Relative Importance of Various Routes of Skin Penetration. *Journal of Investigative Dermatology* **48**, 79-& (1967).

54. Benson, H.A.E. & Namjosh, S. Proteins and peptides: Strategies for delivery to and across the skin. *Journal of Pharmaceutical Sciences* **97**, 3591-3610 (2008).

55. Hajare, A.A., Dange, A.S. & Shetty, Y.T. Therapeutic protein production and delivery: An overview. *Indian Journal of Pharmaceutical Education and Research* **42**, 104-112 (2008).

56. Jain, A.K., Thomas, N.S. & Panchagnula, R. Transdermal drug delivery of imipramine hydrochloride. I. Effect of terpenes. *Journal of Controlled Release* **79**, 93-101 (2002).

57. Kligman, A.M. Topical Pharmacology and Toxicology of Dimethyl Sulfoxide .I. *Journal of the American Medical Association* **193**, 796-& (1965).

58. Machet, L. & Boucaud, A. Phonophoresis: efficiency, mechanisms and skin tolerance. *International Journal of Pharmaceutics* **243**, 1-15 (2002).

59. Burnette, R.R. & Marrero, D. Comparison between the Iontophoretic and Passive Transport of Thyrotropin-Releasing-Hormone across Excised Nude-Mouse Skin. *Journal of Pharmaceutical Sciences* **75**, 738-743 (1986).

60. Prausnitz, M.R., Bose, V.G., Langer, R. & Weaver, J.C. Electroporation of Mammalian Skin - a Mechanism to Enhance Transdermal Drug-Delivery. *Proceedings of the National Academy of Sciences of the United States of America* **90**, 10504-10508 (1993).

61. Drabick, J.J., Glasspool-Malone, J., Somiari, S., King, A. & Malone, R.W. Cutaneous transfection and immune responses to intradermal nucleic acid vaccination are significantly enhanced by in vivo electropermeabilization. *Molecular Therapy* **3**, 249-255 (2001).

62. Lahm, K. & Lee, G. Penetration of crystalline powder particles into excised human skin membranes and model gels from a supersonic powder injector. *Journal of Pharmaceutical Sciences* **95**, 1511-1526 (2006).

63. Clements, C.J., Larsen, G. & Jodar, L. Technologies that make administration of vaccines safer. *Vaccine* **22**, 2054-2058 (2004).

64. Nelson, J.S. et al. Midinfrared Laser Ablation of Stratum-Corneum Enhances Invitro Percutaneous Transport of Drugs. *Journal of Investigative Dermatology* **97**, 874-879 (1991).

65. Chen, Y.P. et al. Transdermal protein delivery by a coadministered peptide identified via phage display. *Nature Biotechnology* **24**, 455-460 (2006).

66. Scheuplein, R. The skin as a barrier. In: The Physiology and Pathophysiology of Skin (Academic Press, London, 1978).

67. Dyson, M., J.B., P., Woodward, B. & Broadbent, J. The production of red blood cell stasis and endothelial damage in the blood vessels of chik embryo heated with ultrasound as a stationary wave field. *Ultrasound in medicin and biology* **1**, 133-148 (1974).

68. Williams, A.R., Rosenfeld, E.H. & Williams, K.A. Gel-Sectioning Technique to Evaluate Phonophoresis Invitro. *Ultrasonics* **28**, 132-136 (1990).

69. Mitragotri, S., Blankschtein, D. & Langer, R. Transdermal drug delivery using low-frequency sonophoresis. *Pharmaceutical Research* **13**, 411-420 (1996).

70. Mitragotri, S., Edwards, D.A., Blankschtein, D. & Langer, R. Mechanistic Study of Ultrasonically-Enhanced Transdermal Drug-Delivery. *Journal of Pharmaceutical Sciences* **84**, 697-706 (1995).

71. Lenart, I. & Auslander, D. The Effect of Ultrasound on Diffusion through Membranes. *Ultrasonics* **18**, 216-218 (1980).

72. Guy, R.H. & Hadgraft, J. Transdermal Drug Delivery (Marcel Dekker, New York, 2003).

73. Padmanabhan, R.H., Phipps, J.B., Lattin, G.A. & Sawchuk, R.J. In vitro and in vivo evaluation of transdermal iontophoretic delivery of hydromorphone. *Journal of Controlled Release* **11**, 123-135 (1990).

74. Gupta, S.K., Southam, M., Sathyan, G. & Klausner, M. Effect of current density on pharmacokinetics following continuous or intermittent input from a fentanyl electrotransport system. *Journal of Pharmaceutical Sciences* **87**, 976-981 (1998).

75. Green, P.G. Iontophoretic delivery of peptide drugs. *Journal of Controlled Release* **41**, 33-48 (1996).

76. Heit, M.C., Williams, P.L., Jayes, F.L., Chang, S.K. & Riviere, J.E. Transdermal Iontophoretic Peptide Delivery - Invitro and Invivo Studies with Luteinizing-Hormone-Releasing Hormone (Vol 82, Pg 240, 1993). *Journal of Pharmaceutical Sciences* **82**, U554-U558 (1993).

77. Langkjaer, L., Brange, J., Grodsky, G.M. & Guy, R.H. Iontophoresis of monomeric insulin analogues in vitro: effects of insulin charge and skin pretreatment. *Journal of Controlled Release* **51**, 47-56 (1998).

78. Lombry, C., Dujardin, N. & Preat, V. Transdermal delivery of macromolecules using skin electroporation. *Pharmaceutical Research* **17**, 32-37 (2000).

79. Zewert, T.E., Pliquett, U.F., Langer, R. & Weaver, J.C. Transdermal Transport of DNA Antisense Oligonucleotides by Electroporation. *Biochemical and Biophysical Research Communications* **212**, 286-292 (1995).

80. Pliquett, U. Mechanistic studies of molecular transdermal transport due to skin electroporation. *Advanced Drug Delivery Reviews* **35**, 41-60 (1999).

81. Pliquett, U., Gift, E.A. & Weaver, J.C. Determination of the electric field and anomalous heating caused by exponential pulses with aluminum electrodes in electroporation experiments. *Bioelectrochemistry and Bioenergetics* **39**, 39-53 (1996).

82. Jiang, J., Moore, J.S., Edelhauser, H.F. & Prausnitz, M.R. Intrascleral Drug Delivery to the Eye Using Hollow Microneedles. *Pharmaceutical Research* **26**, 395-403 (2009).

83. Sivamani, R.K., Liepmann, D. & Malbach, H.I. Microneedles and transdermal applications. *Expert Opinion on Drug Delivery* **4**, 19-25 (2007).

84. Vandervoort, J. & Ludwig, A. Microneedles for transdermal drug delivery: a minireview. *Frontiers in Bioscience* **13**, 1711-1715 (2008).

85. Hanson, K.J., Simons, J.K. & Peterson, T.A. in AAPS National Biotech Conference (Toronto, 2008).

86. Scherer, R.P. (1949).

87. McNally, E.J. & Hastedt, J.E. Protein Formulation and Delivery (Informa Healthcare, New York, 2008).

88. Singer, A.J. et al. Cutaneous tape stripping to accelerate the anesthetic effects of EMLA cream: A randomized, controlled trial. *Academic Emergency Medicine* **5**, 1051-1056 (1998).

89. Tsai, J.C., Weiner, N.D., Flynn, G.L. & Ferry, J. Properties of Adhesive Tapes Used for Stratum-Corneum Stripping. *International Journal of Pharmaceutics* **72**, 227-231 (1991).

90. Shapiro, H., Harris, L., Hetzel, F.W. & Bar-Or, D. Laser assisted delivery of topical anesthesia for intramuscular needle insertion in adults. *Lasers in Surgery and Medicine* **31**, 252-256 (2002).

91. Badkar, A.V., Smith, A.M., Eppstein, J.A. & Banga, A.K. Transdermal delivery of interferon alpha-2B using microporation and iontophoresis in hairless rats. *Pharmaceutical Research* **24**, 1389-1395 (2007).

92. Birchall, J. et al. Cutaneous gene expression of plasmid DNA in excised human skin following delivery via microchannels created by radio frequency ablation. *International Journal of Pharmaceutics* **312**, 15-23 (2006).

93. Levin, G. et al. Transdermal delivery of human growth hormone through RF-microchannels. *Pharmaceutical Research* **22**, 550-555 (2005).

94. Park, J.H., Yoon, Y.K., Choi, S.O., Prausnitz, M.R. & Allen, M.G. Tapered conical polymer microneedles fabricated using an integrated lens technique for transdermal drug delivery. *IEEE Transactions on Biomedical Engineering* **54**, 903-913 (2007).

95. Davis, S.P., Landis, B.J., Adams, Z.H., Allen, M.G. & Prausnitz, M.R. Insertion of microneedles into skin: measurement and prediction of insertion force and needle fracture force. *Journal of Biomechanics* **37**, 1155-1163 (2004).

96. Smith, W.G. Analytic solutions for tapered column buckling. *Computers & Structures* **28**, 677-681 (1988).

97. Kligman, A.M. & Christophel, E. Preparation of isolated sheets of human stratum corneum. *Archives of Dermatology* **88**, 702-& (1963).

98. Bollag, D.M., Rozycki, M.D. & Edelstein, S.J. Protein Methods (Wiley-Liss, New York, 1996).

99. Masschalck, B., Van Houdt, R., Van Haver, E.G.R. & Michiels, C.W. Inactivation of gram-negative bacteria by lysozyme, denatured lysozyme, and lysozyme-derived peptides under high hydrostatic pressure. *Applied and Environmental Microbiology* **67**, 339-344 (2001).

100. Gout, P.W., Beer, C.T. & Noble, R.L. Prolactin-stimulated growth of cell cultures established from malignant Nb rat lymphomas. *Cancer Research* **40**, 2433-2436 (1980).

101. Tanaka, T. et al. A new sensitive and specific bioassay for lactogenic hormones: measuremnt of prolactin and growth hormone in human serum. *Journal of Clinical Endocrinology and Metabolism* **51**, 1058-1063 (1980).

102. Barry, B.W. & Woodford, R. Comparative Bio-Availability of Proprietary Topical Corticosteroid Preparations - Vasoconstrictor Assays on 30 Creams and Gels. *British Journal of Dermatology* **91**, 323-338 (1974).

103. English, B.A. in School of Electrical and Computer Engineering (Georgia Institute of Technology, Atlanta, 2006).

104. Gadiraju, P.D. in School of Electrical and Computer Engineering (Georgia Institute of Technology, Atlnata, 2008).

105. Incropera, F.P., Dewitt, D.P., Bergman, T.L. & Lavine, A.S. Fundamentals of Heat and Mass Transfer (John Wiley & Sons, Inc., Hoboken, 2007).

106. Eppstein, J.A., Hatch, M.R. & Yang, D. (SpectRx, Inc. Technologies, Inc., USA, 2000).

107. Appel, R.A., Dmochowski, R.R. & Herschorn, S. Urethal injection for female stress incontinence. *BJU International* **98**, 27-30 (2006).

108. Crookes, B.A. et al. Building a better fluid for emergency resuscitation of traumatic brain injury. *Journal of Trauma-Injury Infection and Critical Care* **57**, 547-554 (2004).

109. Feng, X.H., Pelton, R. & Leduc, M. Mechanical properties of polyelectrolyte complex films based on polyvinylamine and carboxymethyl cellulose. *Industrial & Engineering Chemistry Research* **45**, 6665-6671 (2006).

110. Kalichevsky, M.T., Jaroszkiewicz, E.M., Ablett, S., Blanshard, J.M.V. & Lillford, P.J. The glass-transition of amylopectin measured by DSC, DMTA and NMR. *Carbohydrate Polymers* **18**, 77-88 (1992).

111. Dumitriu, S. Polysaccharides in medicinal applications (M. Dekker, New York, 1996).

112. Arion, H. Carboxy-methyl cellulose hydrogels used to fill breast implants: 15 years of experience. *European Journal of Plastic Surgery* **24**, 172-175 (2001).

113. Martanto, W., Moore, J.S., Couse, T. & Prausnitz, M.R. Mechanism of fluid infusion during microneedle insertion and retraction. *Journal of Controlled Release* **112**, 357-361 (2006).

114. Leveque, J.L. Cutaneous Investigation in Health and Disease (Marcel Dekker, New York, 1989).

115. Cunningham, B.C., Mulkerrin, M.G. & Wells, J.A. Dimerization of Human Growth-Hormone by Zinc. *Science* **253**, 545-548 (1991).

116. Brostedt, P. & Roos, P. Isolation of Dimeric Forms of Human Pituitary Growth-Hormone. *Preparative Biochemistry* **19**, 217-229 (1989).

117. Nagatomi, Y. et al. Reversible dimerization of 20 kilodalton human growth hormone (hGH). *Growth Hormone & Igf Research* **10**, 207-214 (2000).

118. Wang, Y.J. & Pearlman, R. Stability and Characterization of Protein and Peptide Drugs (Plenum Publishing Corporation, New York, 1993).

119. Pikal, M.J., Dellerman, K.M., Roy, M.L. & Riggin, R.M. The effects of formulation variables on the stability of freeze-dried human grwoth hormone. *Pharmaceutical Research* **8**, 427-436 (1991).

120. Zurcher, K. & Krebs, A. Cutaneous Drug Reactions: An integral synopsis of today's systemic drugs with drug tables and sign/symptom tables (S. Karger, Basel, 1992).

121. Babiuk, S. et al. Needle-free topical electroporation improves gene expression from plasmids administered in porcine skin. *Molecular Therapy* **8**, 992-998 (2003).

122. Burdick, J. et al. Optimization of the SpectRx continuous glucose monitoring system (SCGMS) in pediatric patients with type I diabetes. *Diabetes* **52**, A90-A91 (2003).

123. Park, J.H., Lee, J.W., Kim, Y.C. & Prausnitz, M.R. The effect of heat on skin permeability. *International Journal of Pharmaceutics* **359**, 94-103 (2008).

124. Miyano, T. et al. Sugar micro needles as transdermic drug delivery system. *Biomedical Microdevices* **7**, 185-188 (2005).

125. Park, J.H., Allen, M.G. & Prausnitz, M.R. Polymer microneedles for controlled-release drug delivery. *Pharmaceutical Research* **23**, 1008-1019 (2006).

126. Ito, Y., Yoshimitsu, J.I., Shiroyama, K., Sugioka, N. & Takada, K. Self-dissolving microneedles for the percutaneous absorption of EPO in mice. *Journal of Drug Targeting* **14**, 255-261 (2006).

127. Teo, M.A.L., Shearwood, C., Ng, K.C., Lu, J. & Moochhala, S. In vitro and in vivo characterization of MEMS microneedles. *Biomedical Microdevices* **7**, 47-52 (2005).

128. Matriano, J.A. et al. Macroflux (R) microprojection array patch technology: A new and efficient approach for intracutaneous immunization. *Pharmaceutical Research* **19**, 63-70 (2002).